

**CHARACTERIZATION OF SUBTYPES  
OF PRECURSOR CELLS IN THE DEVELOPING  
CENTRAL NERVOUS SYSTEM**

**DISSERTATION**

ZUR ERLANGUNG DES DOKTORGRADES  
DER NATURWISSENSCHAFTEN (DR.RER.NAT)  
DER FAKULTÄT FÜR BIOLOGIE  
DER LUDWIG-MAXIMILIANS UNIVERSITÄT MÜNCHEN

ANGEFERTIGT AM MAX-PLANCK-INSTITUT FÜR NEUROBIOLOGIE  
IN DER ARBEITSGRUPPE NEURONALE SPEZIFIZIERUNG

**EVA HARTFUSS  
MÜNCHEN, FEBRUAR 2003**

1. Gutachter: PD Dr. Magdalena Götz
2. Gutachter: Prof.Dr.Dr.h.c. Gerhard Neuweiler

eingereicht am 26. Februar 2003

Tag der mündlichen Prüfung: 30.September 2003

The search for truth begins with the doubt  
of all 'truths' in which one has previously believed.

Friedrich Nietzsche (1844 – 1900)

## TABLE OF CONTENTS

<b>1.</b>	<b>Abstract</b> .....	<b>7</b>
<b>2.</b>	<b>Introduction</b> .....	<b>8</b>
2.1	The history of radial glia discovery.....	8
2.2	Radial glial cells in the developing cerebral cortex .....	9
2.3	Immunohistochemistry on radial glial cells .....	12
2.3.1	Radial cell 2 (RC2).....	13
2.3.2	Glutamate astrocyte-specific transporter (GLAST) .....	14
2.3.3	Brain lipid-binding protein (BLBP).....	15
2.4	Radial glial cells as CNS precursors.....	16
2.5	Factors regulating radial glial cells .....	17
2.5.1	The <i>reeler</i> mouse.....	18
2.5.2	The Reelin-signalling pathway.....	20
<b>3.</b>	<b>Abbreviations</b> .....	<b>23</b>
<b>4.</b>	<b>Material &amp; Methods</b> .....	<b>24</b>
4.1	Animals .....	24
4.1.1	Strains .....	24
4.1.2	Genotyping of mutant and transgenic mice .....	24
4.2	Histology.....	26
4.2.1	Vibratome sections .....	26
4.2.2	Cryosections .....	27
4.3	Tissue culture .....	27
4.3.1	Acutely dissociated cells and cell culture.....	27
4.3.2	Adult and embryonic neurosphere cultures .....	28
4.3.3	Astrocyte preparation .....	29
4.3.4	Fluorescent activated cell sorting (FACS) .....	29
4.3.5	Viral infection - BAG-retrovirus .....	30
4.3.6	Cell-lines and conditioned medium .....	30
4.4	Time-lapse video-microscopy .....	31
4.4.1	Cell culture and viral infection.....	31
4.4.2	Slice preparation and viral infection.....	31
4.4.3	Image acquisition.....	32
4.5	Immunochemistry.....	32
4.5.1	Immunocytochemistry .....	32
4.5.2	Immunohistochemistry .....	33
4.5.3	Negative controls .....	33
4.5.4	Antibodies .....	34
4.6	BrdU Labelling .....	36
4.6.1	BrdU Pulse Labelling .....	36
4.6.2	Cumulative BrdU Labelling .....	36
4.6.3	BrdU-labelling in cultures with conditioned medium .....	37
4.7	Tracing experiments .....	37

4.7.1	Live tracing of precursors by Dil or Beads.....	37
4.7.2	DiI-labelling from the ventricular surface in fixative and 3D-reconstruction .	38
4.8	DNA-labelling.....	38
4.9	In-situ hybridisation.....	39
4.9.1	Plasmid preparation and <i>in vitro</i> transcription.....	39
4.9.2	Non-radioactive in-situ hybridisation.....	40
4.10	Westernblotting .....	41
4.11	LightCycler real-time RT-PCR .....	42
4.11.1	RNA extraction.....	42
4.11.2	LightCycler RT-PCR.....	42
4.11.3	Quantitative analysis of the LightCycler data .....	43
4.12	Data analysis.....	44
4.12.1	Double-staining in sections .....	44
4.12.2	Triple-staining in cell cultures.....	44
4.12.3	Clonal analysis .....	45
4.12.4	Analysis of the orientation of cell division .....	45
4.12.5	3D-analysis of DiI-labelled ventricular zone cells .....	46
4.12.6	Statistics.....	46
4.13	Material.....	47
4.13.1	Microscopy.....	47
4.13.2	Complex media, buffers and solutions .....	48
4.13.3	Product list .....	52
4.13.4	Consumables.....	55
4.13.5	Instruments .....	56
<b>5.</b>	<b>Results.....</b>	<b>57</b>
5.1	Immunohistochemical analysis in sections of the telencephalon.....	57
5.2	Immunocytochemical analysis of acutely dissociated cells .....	59
5.2.1	Characterization of acutely dissociated cells .....	59
5.2.2	Co-localization of RC2, GLAST and BLBP in acutely dissociated cells .....	61
5.2.3	Analysis of the precursor pool .....	63
5.3	Antigenic profile of identified precursor populations .....	65
5.3.1	Precursors with specific progeny.....	65
5.3.2	Precursors identified by transcription factors .....	68
5.3.3	Subventricular zone (SVZ) precursor cells .....	69
5.4	Cell cycle parameters of precursor cell subpopulations .....	71
5.5	Morphology of precursor cells.....	73
5.5.1	Morphologically identified precursors .....	73
5.5.2	3D-reconstruction of ventricular zone (VZ) precursor morphology.....	75
5.6	Process retraction or maintenance during radial glial cell division .....	77
5.6.1	Process length and soma-position during interkinetic nuclear migration.....	77
5.6.2	Time-lapse video microscopy of dividing radial glial cells <i>in vitro</i> .....	78
5.6.3	Visualization of radial glial cells during M-Phase.....	81
5.7	The <i>reeler</i> mouse.....	84
5.7.1	Precursor cell subtypes in the <i>reeler</i> telencephalon .....	85
5.7.2	Radial glial morphology is impaired in the <i>reeler</i> cortex, but not in the GE..	88

---

5.7.3	In-situ hybridisation analysis of the Notch pathway in the <i>reeler</i> .....	90
5.7.4	Proliferation in the <i>reeler</i> telencephalon .....	92
5.7.5	Neuronal differentiation and cell fate analysis in the <i>reeler</i> cortex.....	93
5.7.6	Reelin signalling affects radial glial identity <i>in vitro</i> .....	96
5.7.7	Reelin signals directly to radial glial cells .....	100
5.7.8	Expression of Reelin-receptors in radial glial cells by real-time RT-PCR..	102
<b>6.</b>	<b>Short Summary .....</b>	<b>103</b>
<b>7.</b>	<b>Discussion.....</b>	<b>104</b>
7.1	Radial glial cells as a major precursor subtype .....	104
7.1.1	Contribution of radial glial cells to the progenitor pool.....	104
7.1.2	Proliferation of precursor cells and radial glia .....	105
7.2	Heterogeneity of the precursor pool .....	106
7.2.1	Subtypes of precursor cells .....	106
7.2.2	Molecular markers for distinct sets of precursor cells .....	107
7.2.3	Cell cycle differences among the novel precursor subtypes .....	107
7.2.4	Specific precursor subtypes express bHLH transcription factors .....	108
7.2.5	Precursor subtypes are correlated to distinct progenies .....	108
7.3	Role of BLBP in radial glial subsets .....	110
7.3.1	Alteration of precursor subtypes in the <i>reeler</i> cerebral cortex.....	110
7.3.2	Role of BLBP in differentiation and proliferation.....	111
7.3.3	Radial glial defects in the <i>reeler</i> cerebral cortex.....	112
7.3.4	Reelin signals directly to radial glial cells .....	114
7.3.5	Factors regulating radial glial identity .....	116
<b>8.</b>	<b>References.....</b>	<b>118</b>
<b>9.</b>	<b>Thanks &amp; Acknowledgements .....</b>	<b>131</b>
<b>10.</b>	<b>Curriculum Vitae .....</b>	<b>132</b>

## 1. ABSTRACT

The role of radial glial cells as guides for migrating neurons is well established, whereas their role as precursor cells is less understood. Here we examined the composition of radial glial cells and their proliferation in the mouse telencephalon during development. We found that almost all radial glial cells proliferate throughout neurogenesis. They consist of distinct subsets identified by the differential co-localization of the antigens RC2, the astrocyte-specific glutamate transporter (GLAST) and the brain lipid-binding protein (BLBP). In addition, from on late neurogenesis GLAST- and BLBP-antisera label precursor cells with non-radial, but stellate morphology and thereby cover almost the entire progenitor pool in the developing cerebral cortex. The subsets identified by differential expression of these antigens differ in their transcription factor expression and cell cycle characteristics.

Moreover, we could show by morphologically tracing ventricular zone precursor cells, that cells with a radial morphology constitute the majority of precursor cells in the CNS during neurogenesis. Furthermore, we here present indications showing that radial glial cells divide without retracting their processes during M-phase, suggesting that radial glial cells can proliferate and guide migrating neurons at a time.

The molecular signals regulating this crucial morphology of radial glial cells, however, are largely unknown. Here we show that radial morphology is impaired in the Reelin-deficient cerebral cortex of the *reeler* mouse correlated to a decrease in the content of BLBP in radial glial cells. These defects were restricted to the cerebral cortex, but did not occur in the basal ganglia that exhibit normal migration and radial glial cell differentiation in the *reeler* mouse. These defects could be rescued *in vitro* by addition of Reelin. Even in cultures of radial glial cells isolated by fluorescent-activated cell sorting Reelin lead to an increase in BLBP. These data therefore demonstrate a direct signalling of Reelin to radial glial cells, thereby regulating their bipolar morphology - most likely involving BLBP - in a region-specific manner.

## 2. INTRODUCTION

### 2.1 The history of radial glia discovery

Radial glial cells are a widespread cell type throughout the developing central nervous system (CNS) of vertebrates. While in most vertebrates they persist into adulthood, in the case of mammals they transform in most CNS regions into astrocytes (Margotta and Morelli 1997). Radial glial cells are characterized by their morphology with a distinctive long radial process reaching the basal surface of the brain as well as by their astroglial properties. Since the 1970s, the dual role of radial glia as guiding cables for neuronal migration and as astrocyte precursors has been established (Rakic 1971a; Rakic 1971b; Rakic 1972; Levitt and Rakic 1980; Levitt *et al.* 1981; Voigt 1989). However, they were first described as early as the 19<sup>th</sup> century. Radial glial cells were first fully visualized through Golgi impregnation in the chicken spinal cord in the late 1870s by Camillo Golgi and were published a few years later as “cylindrical cells ... that traverse radially the entire plane of the section of the spinal cord, reaching its extreme peripheral border towards the pia mater. Here the filiform extremities of the individual cylindrical cells terminate, forming a conic swelling or a tenous expansion, through which the filaments are inserted within the pia mater ... These features result in an elegant and dense irradiation of fibers which extend from the entire border of the central canal to the periphery of the spinal cord” (Golgi 1885). Later Kölliker examined the main stages of cortical layering during development and noted the appearance of elongated, fusiform cells in the pseudostratified epithelium lining the ventricles (Kölliker 1879; Kölliker 1882; Kölliker 1896). These initial observations suggested that these long radial cells were epithelial or ependymal cells. Several other investigators like Vignal, His, Cajal and Magini became interested in these long cells and the developing cerebral cortex (Vignal 1888a; Vignal 1888b; Magini 1888b; Ramon y Cajal 1897). His observed two morphologically distinct cell types in the ventricular epithelium, germinal cells, which are round and highly proliferative and spongioblasts, which are elongated cells that form a syncytium (His 1887; His 1888; His 1889a; His 1889b; His 1904). The round germinal cells were proposed as neuronal precursors, whereas the spongioblasts were allocated to the astroglial lineage. On the contrary, Schaper hypothesized, that these morphological differences do not reflect lineage relationship but reflect different

phases of the cell cycle (Schaper 1897), which was later confirmed by Sauer with his model of interkinetic nuclear migration (Sauer 1935).

In the late 19<sup>th</sup> century, scientists were concentrating not only on the morphology of radial glia, but their glial properties and their function as a scaffold for migrating neuroblasts were also hypothesized at this time (Lenhossek 1893). Guiseppe Magini described 1888 that “these filaments bear ... numerous varicosities or swellings” (Magini 1888a), but only 1951 – more than 60 years later – these varicosities were proven to be migrating neuroblasts (Godina 1951). Then for several decades, these early investigations on the nature of radial glial cells were suspended, and only with the establishment of electron microscopy, radial glial cells were again the topic of exact inspections. Pasco Rakic published in the 1970s a series of articles about these characteristic cells in the fetal monkey neocortex, which he then finally named radial glial cells (Rakic 1971a; Rakic 1971b; Rakic 1972). He was the first to visualize migrating neuroblasts by electron microscopy attached to the radial scaffold in the cerebral cortex, which nearly seem to ‘embrace’ the radial processes during their migration (Rakic 1972). The glial characteristics of radial glial cells were highly debated until the 1980s. At that time immunohistochemistry in the developing cerebral cortex of primates revealed that both mature astrocytes and as well radial glial cells contain the glial fibrillary acidic protein (GFAP), which is the major protein of glial intermediate filaments (Levitt and Rakic 1980; Levitt *et al.* 1981). This discovery finally closed the dispute about the glial character of radial glial cells.

## **2.2 Radial glial cells in the developing cerebral cortex**

From the first discovery of radial glial cells in the late 19<sup>th</sup> century until today, a more complete view of what radial glial cells are and which function they fulfil during CNS development has been achieved. At the beginning of neurogenesis radial glial cells differentiate from neuroepithelial cells, which are precursor cells spanning the entire thickness of the telencephalon until embryonic day 12 (E12; stages refer to mouse embryogenesis; Fig. 2.1, left panel). Neuroepithelial cells themselves originate from the neuroectoderm and have many epithelial characteristics, for example their polarity. Polarity is generated by differences in the biochemical nature of the apical and basal pole of the cell and a polarized architecture of epithelial cells and tissues is a fundamental determinant of animal anatomy and physiology and plays an important role in various morphogenetic processes e.g. cell division of

precursor cells. At the neuroepithelial cell stage, cells divide mostly symmetrically i.e. cells distribute their protein content symmetrically to both daughter cells, resulting in two identical precursors and thereby exponentially amplifying their population (Chenn and McConnell 1995; Qian *et al.* 1998; Qian *et al.* 2000).

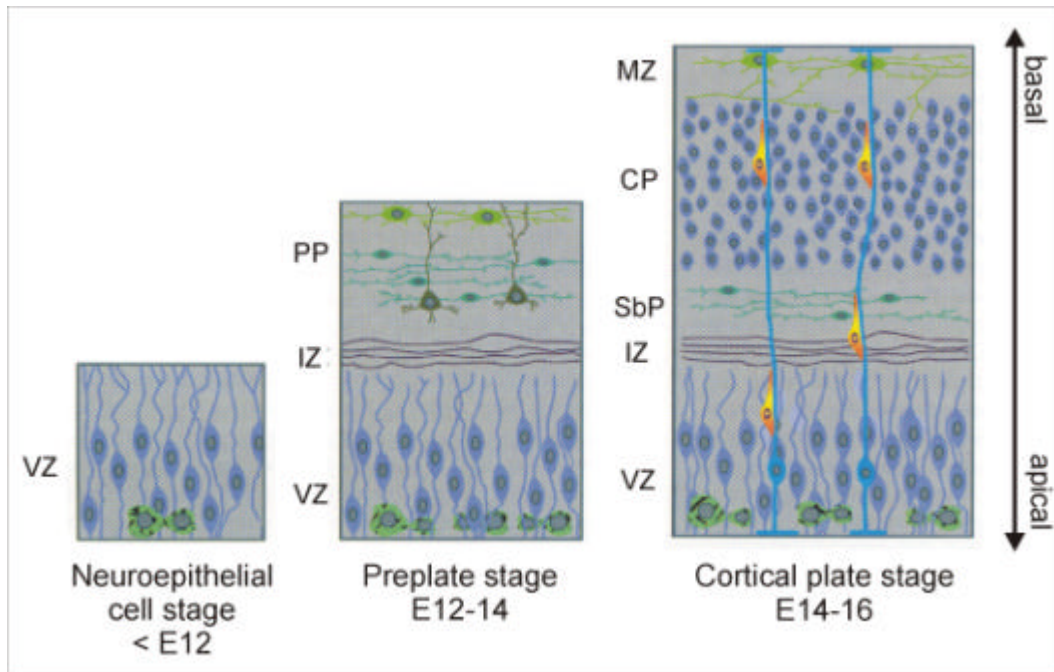


**Figure 2.1 Histogenesis of the cerebral cortex** (for details, see text; adapted from Zigmond *et al.* 1999; VZ: ventricular zone; IZ: intermediately positioned zone; PP: preplate; SbP: subplate; CP: cortical plate; MZ: marginal zone.)

With the onset of neurogenesis, the mode of cell division changes and cells divide mostly asymmetrically thereby generating two different daughters; at this stage one basally situated neuroblast, which then differentiates into a neuron, and one apically positioned un-destined precursor cell (Qian *et al.* 1998). While the young neurons radially migrate away from the ventricular zone and settle underneath the pial surface, building the so-called preplate (PP), the precursors remain at apical positions in the ventricular zone (VZ; Fig. 2.1, middle panel). During the different phases of the cell cycle, neuroepithelial cells undergo a nuclear translocation called interkinetic nuclear migration (Sauer 1935). In this process the cell soma moves up from the ventricle to the pial surface during G1 and S-Phase and down again to the ventricular surface during G2 and M-phase (see Fig. 5.15). After the neuroepithelial cell stage, due to the progressive thickening of the cerebral cortex during neurogenesis, the to-and-fro movement of interkinetic nuclear migration is confined to the cortical VZ. Most neuroepithelial cells are thought to lose their basal contacts and only some keep attached to the pial surface by long processes. The so-called

'short precursors', which have lost their pial contacts, were thought to constitute the population of neuronal precursor cells, whereas the 'long precursors', the radial glial cells, serve as substrate for neuronal migration. Some of the neuroepithelial cells not only lose their basal processes but as well their apical contacts to the ventricular surface and build the second proliferative layer, the subventricular zone (SVZ), a specialized subset of progenitors above the VZ (Boulder Committee 1970; Smart 1976).

Around this time, neurons start to migrate into the PP splitting it into the cortical marginal zone (MZ) underneath the pial surface (layer 1 neurons) and the subplate (SbP; Fig. 2.1, right panel). The following neurons bypass their predecessors and settle in an inside-out manner thereby building the cortical plate (CP; layer 2-6 neurons; (Angevine and Sidman 1961; Bayer and Altman 1991; Marin-Padilla 1998). Only with the end of neurogenesis, when all neurons have settled and have established their major contacts, does the glial system develop. The mode of cell division changes again with the beginning of gliogenesis and progenitors divide mostly symmetrically, resulting in two identical glioblasts, which differentiate into mature glial cells (Qian *et al.* 1998; Qian *et al.* 2000). The very first macroglia, in this case astrocytes, appear around E16 and only around birth are the first oligodendrocytes detectable. However, the vast majority of both cell types are produced during the first postnatal month (see e.g. Cameron and Rakic 1991). Additionally with the beginning of gliogenesis, radial glial cells were shown to transform into astrocytes and finally disappear in the cerebral cortex (Choi and Lapham 1978; Schmechel and Rakic 1979; Levitt and Rakic 1980; Voigt 1989).

This view, of how the neocortex develops and the role that radial glial cells play therein, was accepted for a long time even in the presence of contradictory evidence. By now, radial glial cells are best known for their role in guiding migrating neurons (Rakic 1972; Hatten 1999). In contrast, their role as precursor cells is less clear. For example, there is good evidence that radial glial cells divide not only during gliogenesis but also during neurogenesis, since they incorporate S-phase markers, such as  $^3\text{H}$ -Thymidine during this time (Levitt *et al.* 1981; Misson *et al.* 1988b). Moreover, radial glial cells have been labelled by retroviral vectors, which require a breakdown of the nuclear membrane that only happens during the G2/M-phase of the cell cycle (Gray and Sanes 1992; Halliday and Cepko 1992; Gaiano *et al.* 2000). However, surprisingly few radial glial cells have been observed in retroviral lineage

analysis. Moreover, in the primate monkey neocortex radial glial cells have been shown to even arrest their proliferation during midneurogenesis and exclusively serve as guiding scaffold for neurons (Schmechel and Rakic 1979). Conversely, in the rodent brain such a silence-phase has never been described. It is therefore not clear, to which extent radial glial cells divide in the developing rodent telencephalon and how radial glial cells combine proliferation with their role as static guiding scaffold, since cells had classically been thought to retract their processes and round up at the ventricular surface during the M-phase of the cell cycle (Hinds and Ruffett 1971).

Furthermore, even if radial glial cells have many astroglial characteristics such as GFAP-immunoreactivity in the primate cortex (Levitt and Rakic 1980; Choi 1981) or glycogen granule content (Choi and Lapham 1978), they are not only astrocyte precursors. Recently it has been shown by isolating radial glial cells that they act as neuronal precursors during neurogenesis, whereas only after neurogenesis has completed do they become glial progenitors (Malatesta *et al.* 2000). This is particularly interesting in the light of recent data suggesting that astrocytes, which are closely linked to radial glial cells (Barres 1999), may be multipotent stem cells in the adult telencephalon (Doetsch *et al.* 1999). However, it is still not known, whether radial glial cells are a homogenous cell population and all express glial antigens or whether subsets of radial glial cells exist, which might share the dual function of providing a static scaffold and being an actively dividing precursor cell.

The general aim of this thesis was therefore to identify putative subpopulations of radial glial cells and to characterize the role of these subpopulations in I) the multiple functions of radial glial cells during development, II) the cell fate of radial glia, and III) the function of the protein Reelin in regulating the different radial glial properties and fates.

### **2.3 Immunohistochemistry on radial glial cells**

In order to characterize radial glial cells we first aimed to identify putative subpopulations that might coordinate the dual function of radial glial cells. Several antibodies were previously described to stain radial glial cells. GFAP, the glial fibrillary acidic protein, was the first radial glia marker developed. It indeed labels radial glial cells, but only in the primate monkey neocortex not in rodents. GFAP in rodents is only expressed in mature astrocytes and it was therefore not suitable for our analysis (Bignami and Dahl 1974; Antanitus *et al.* 1976; Levitt and Rakic 1980;

Eng 1985). The monoclonal antisera RC1/2 (Radial Cell 1/2; Misson *et al.* 1988a; Misson *et al.* 1988b; Edwards *et al.* 1990) are most frequently used for radial glial stainings. However, the antisera against the brain lipid-binding protein (BLBP; Feng *et al.* 1994; Kurtz *et al.* 1994) and against the glutamate astrocyte-specific transporter (GLAST; Shibata *et al.* 1997) also stain radial glial processes and co-localize with the RC2-antigen and nestin, an intermediate filament present in CNS precursor cells (Frederiksen and McKay 1988; Feng *et al.* 1994; Kurtz *et al.* 1994). These reports, however, did not clarify whether the described antisera all label the same radial glial cells or whether they could be used to discriminate between putative radial glial subtypes. We therefore addressed the co-localization of these radial glial markers at a cellular level during neuro- and gliogenesis in the mouse telencephalon using the antibodies RC2, anti-GLAST and anti-BLBP.

### 2.3.1 Radial cell 2 (RC2)

The monoclonal mouse antibody RC2 (Radial Cell 2) that we used is considered one of the best markers for studies of radial glial cells because of the lack of specificity of other radial glial antigens. RC1, for example embryonically co-localizes with RC2, but it also postnatally detects Bergmann glia in the cerebellum as well as mature astrocytes, Müller glia, ependymal cells, tanocytes and a specialized glia-type in the hippocampus-formation (Misson *et al.* 1988a; Misson *et al.* 1988b; Edwards *et al.* 1990; Misson *et al.* 1991).

For long time it was not possible to further characterise the antigen detected by RC2 and it was speculated that RC2 detects an epitope shared by at least two different protein-species and a ganglioside, which might be correlated to carbohydrate-structures of precursor cells (Misson *et al.* 1988a). It was shown only recently that RC2 labels a 295kD intermediate filament-associated protein (IFAP) existing in radial glial cells and developing muscle cells. Further characterisation of this IFAP finally suggested that RC2 detects a different posttranslational modified form of the IFAP nestin (Chanas-Sacré *et al.* 2000), which exclusively exists in the CNS in radial glial cells.

RC2-immunoreactivity is detectable as early as E9 in bipolar cells of the mouse CNS (Misson *et al.* 1988a; Misson *et al.* 1991) and remains in radial glial cells until their postnatal transformation into astrocytes. During the period of radial glial transformation, multipolar premature astrocytes are also detectable with RC2-

antiserum, but mature astrocytes are RC2-negative. Only the cerebellar radial glial cells, the Bergmann glia, which persist during adulthood and do not transform into astrocytes, remain RC2-positive for the first two postnatal weeks when they also lose their RC2-immunoreactivity. RC2-immunoreactivity follows a caudal to rostral sequence during development, in line with the general progression of neurogenesis and the overall maturation gradient in the CNS. Although RC2 is already detectable in radial glia of the spinal cord at E9, only between E10 and E11 does RC2 stain at more rostral levels. In the cerebral cortex, RC2-immunoreactivity only starts with the beginning of neurogenesis (E12) and progressively increases until E16. After reaching its peak, RC2-immunoreactivity decreases, in conjunction with the transformation of radial glial cells into astrocytes (Misson *et al.* 1988a).

### 2.3.2 Glutamate astrocyte-specific transporter (GLAST)

Another important marker for the examination of radial glial cells is the astrocyte-specific glutamate transporter (GLAST; Storck *et al.* 1992; Shibata *et al.* 1997). This glutamate transporter is specifically expressed on astroglia and their precursors. Glutamate is the most important excitatory neurotransmitter in the CNS of mammals. Sodium-dependent glutamate-transporter proteins are needed to minimize the extracellular glutamate concentration in the nervous tissue thereby stopping glutamate receptor activity and protecting neurons against glutamate-excitotoxicity (Hertz 1979; Choi 1992). Four sub-classes of glutamate-transporters are known so far, two astroglial and two neuronal glutamate-transporters. GLAST, otherwise known as EAAT1/GLuT-1, and EAAT2/GLT-1 are astroglial transporters, and EAAT3/EAAC1 and EAAT4 are neuron-specific. Both astroglial glutamate-transporters exist predominantly in the telencephalon and the cerebellum (Rothstein *et al.* 1994; Chaudhry *et al.* 1995; Shibata *et al.* 1996; Furuta *et al.* 1997; Ullensvang *et al.* 1997). Whereas GLAST is already expressed during embryonic stages and persisting into adulthood, EAAT2/GLT-1 is only expressed in mature astrocytes.

GLAST-expression in the mouse CNS starts at the spinal cord level in a ventral to dorsal gradient and further expression follows the caudal to rostral maturation sequence. With the beginning of neurogenesis, it is first detectable in the neocortex (E12; Shibata *et al.* 1997; Furuta *et al.* 1997) and during ongoing development GLAST-expression expands, but is mainly detectable in radial glial cells. Highest GLAST-expression however is detectable at postnatal stages on mature astrocytes.

In the adult CNS, astrocytes are the main regulators of the extracellular glutamate-concentration in the brain but in the embryonic CNS, neurons take over this role. It has been shown that in early brain development, before neuronal synaptic connections are established, neurotransmitters and their receptors play an important role in directed neuronal migration (Komuro and Rakic 1998). Therefore GLAST, by modulating glutamate-concentration, could influence neuronal migration, since its expression during embryonic brain development is highly correlated with neuronal migration on radial glial processes (Shibata *et al.* 1997; Swanson *et al.* 1997).

### 2.3.3 Brain lipid-binding protein (BLBP)

The third antiserum, which has played a key role in this work, is BLBP, brain lipid-binding protein (Feng *et al.* 1994; Kurtz *et al.* 1994). It is a brain-specific member of the family of fatty acid-binding proteins (FABPs). The members of this protein family bind hydrophobic ligands, like fatty acids, eicosanoids and retinoids (Xu *et al.* 1996) and play an important role in signal-transduction in the CNS. For example CRABP (cellular retinoic acid-binding protein), a member of the FABP-family, which is expressed in the developing nervous system and as well craniofacial region and limb bud plays an important role in tissue morphogenesis by transporting hydrophobic signalling molecules between cellular compartments (Dolle *et al.* 1989; Maden and Holder 1991; Kurtz *et al.* 1994).

BLBP is expressed in a caudal to rostral sequence starting from E10 in the spinal cord, the dorsal root ganglia, the hindbrain, the midbrain, and the trigeminal ganglion. In the forebrain, BLBP-expression is first detectable in the ganglionic eminence around E12, and expands into dorsal regions at around E14 (Kurtz *et al.* 1994). Previously, it has been suggested that postnatal BLBP-expression vanishes increasingly during the first postnatal weeks and is not detectable anymore in the adult (Feng *et al.* 1994).

Immunohistochemical examinations have shown that BLBP is also expressed in radial glial cells in the embryonic cortex. On the cellular level BLBP-expression is detectable in the cytoplasm as well as in the nucleus, but is not associated with mitochondria or other cytoplasmic organelles. This cellular distribution is a first hint that BLBP, consistent with the other members of the FAB-protein family, might be involved in signal-transduction in the CNS. The expression-pattern of BLBP is strictly correlated to neuronal differentiation and migration on radial glial processes. BLBP

has been shown to mediate signalling between neurons and glial cells and is required for neuronal attachment onto cerebellar radial glia *in vitro* (Feng *et al.* 1994). In the absence of BLBP, migration of cerebellar granule cells is impaired without affecting the adhesive properties of radial glial cells (Feng *et al.* 1994). Furthermore, it has also been shown *in vitro* that the BLBP-content of radial glial cells is affected by neurons, attaching to radial glial cells (Feng *et al.* 1994; Anton *et al.* 1997). This suggests, that BLBP-content in radial glial cells and neuronal migration are directly correlated, but the consequences of this for radial glial cell biology are not clear, even if an influence of BLBP on bipolar morphology has been proposed (Anton *et al.* 1997).

## 2.4 Radial glial cells as CNS precursors

We were not only interested in a putative heterogeneity of the radial glia population itself but also in their contribution to both the neuronal and glial precursor cell pool. The morphology of radial glial cells is one of their most prominent characteristics; they have long radial processes connecting the ventricular surface with the basement membrane. Neuronal precursors, on the other hand, were thought to have only short processes, if at all, and consequently lack basal connectivity to the pial surface. However, recently radial glial cells have as well been implicated in the neuronal cell lineage (Malatesta *et al.* 2000; Noctor *et al.* 2001). An evolving question then is whether two distinct lines of neuronal precursors exist that differ in their morphology. Hence, we wanted to examine the morphology of precursor cells in the developing cerebral cortex and quantify the portion of radial glial cells to the entire progenitor population.

Furthermore, we aimed to clarify how radial glial cells coordinate both proliferation and neuronal migration along their radial processes. Already Sauer suggested in his model of interkinetic nuclear migration (see Fig. 5.15), that during neurogenesis ventricular zone cells round up completely undergoing mitosis (Sauer 1935) and Hinds and Ruffet described in an extensive electron microscopic study that ventricular zone cells retract their processes before metaphase of mitosis. In the mitotic anaphase, the cell divides and with late telophase it starts to grow out its basal process again (Hinds and Ruffett 1971). Other studies, however, suggested that the nuclei of ventricular zone cells might undergo mitotic divisions while retaining elongated processes (Berry and Rogers 1965; Morest 1970; Wolf *et al.* 1997).

Nevertheless, to date it has not been shown how radial glial cells divide and it is not clear what might happen to the migrating neurons, if cycling radial glial cells retract their processes during M-phase. One possible explanation could be that cells are not synchronized in their cell cycle and hence only some would retract their processes at a given moment. The migrating neurons might then simply switch to the adjacent radial fiber on their way outwards. Indeed, migrating neurons that change radial glial fibers occasionally were observed using time-lapse video microscopy (O'Rourke *et al.* 1992; O'Rourke *et al.* 1995). Surprisingly, however, there were no *in vivo* reports of retracting radial processes, neither when imaging neuronal migration in the intermediate zone or cortical plate nor in images of cell divisions in the ventricular zone. We therefore wanted to assess *in vivo* with time-lapse video microscopy whether the processes of radial glial cells are maintained during cell proliferation or if they are retracted.

## 2.5 Factors regulating radial glial cells

Since radial glial cells play so many crucial roles in the developing CNS (for review see Campbell and Götz 2002), it is important to identify factors regulating their phenotypic characteristics such as their morphology, gene expression, cell proliferation and cell fate. One such factor has already been identified. It is the homeobox transcription factor Pax6, which regulates region-specific differences in radial glial cell morphology, in their cell cycle (Götz *et al.* 1998) and in their neurogenic potential (Heins *et al.* 2002). However, in the Pax6-deficient cerebral cortex, radial glial cells still have their bipolar processes attached to the pial surface (Götz *et al.* 1998; P.Malatesta, N.Haubst and M.Götz - unpublished observations by electron microscopy) and their BLBP-immunoreactivity is not affected. In our search for molecular regulators of the characteristic radial glial morphology with a potential link to BLBP, we examined Reelin as a possible regulator of radial glial cells. Reelin is a large extracellular matrix glycoprotein of approximately 385kD. It is expressed in and secreted from neurons in the marginal zone (MZ), the region where the specialized basal processes of radial glial cells, the endfeet, terminate (D'Arcangelo *et al.* 1995; Ogawa *et al.* 1995; Alcantara *et al.* 1998).

### 2.5.1 The *reeler* mouse

In the mouse mutant *reeler*, a spontaneous 150kb deletion amputates the 3' end of the reelin gene (D'Arcangelo *et al.* 1995; Bar *et al.* 1995) thereby leading to a complete loss of Reelin expression in the CNS. The absence of Reelin in the *reeler* mouse has profound effects on neuronal migration in the cerebral cortex and cerebellum, but not the basal ganglia (Fig. 2.2; for review see e.g. Lambert de Rouvroit and Goffinet 1998). In the developing *reeler* cortex neurons do not penetrate the preplate (PP), thereby forming the marginal zone (MZ) and the subplate (SbP), but pile up underneath (Goffinet 1979; Pinto-Lord *et al.* 1982; Caviness, Jr. 1982; Hoffarth *et al.* 1995; Ogawa *et al.* 1995; Caviness, Jr. *et al.* 1995; Sheppard and Pearlman 1997). This evolving neuronal structure is called the superplate (SpP). Because neurons are not able to bypass their predecessors, the SpP shows an outside-in positioning in contrary to the perfectly defined inside-out-formed 6-layered normal cortex (Caviness, Jr. and Sidman 1973a). Despite the severe positioning defects, all major cell classes are present in the *reeler* cortex (Caviness, Jr. and Sidman 1973b). The disorganized SpP contains Cajal-Retzius cells, SbP neurons and a few CP neurons (Caviness, Jr. 1982; Derer 1985). It is important to note that the CP does form in the *reeler* and neurons do migrate on radial glial cells.

A possible explanation for the obstructed positioning might be, that neurons are not able to break their tight contacts to the radial processes and therefore are impeded in their migration to the MZ (Pinto-Lord *et al.* 1982). Furthermore, some morphological aberrations of radial glial cells, such as a decreased branching of subpial endfeet have already been detected (Pinto-Lord *et al.* 1982; Hunter-Schaedle 1997), suggesting a putative link between Reelin-signalling and radial glial cell morphology. It remains unclear how Reelin affects the positioning of neurons. Several models exist hypothesizing Reelin on the one hand as a chemo-attractant for migrating neurons to bypass the predecessors or as a repellent for subplate-neurons, thereby facilitating the invasion of the CP. On the other hand Reelin is speculated as an inhibitory or detachment signal, releasing migrating neurons from the glial scaffold or as a stop signal (for review see: (Caviness, Jr. and Rakic 1978; Lambert de Rouvroit and Goffinet 1998; Curran and D'Arcangelo 1998). However, none of these models has yet been confirmed. Recently it has been shown, that mis-expressing Reelin in cortical ventricular zone precursor cells is able to rescue most of the defects

apparent in the *reeler* (Magdaleno *et al.* 2002). Since all of the proposed models are based on the fact, that Reelin-signalling only affects neurons close to the MZ these data show no evidence for any of them.

However, radial glial cells span the entire thickness of the cerebral cortex with a basal contact in the MZ and an apical contact in the VZ. Therefore, radial glial cells could function as a mediator of Reelin-signalling to deeper cortical layers. We therefore aimed to examine the influence of Reelin on radial glial cells and furthermore whether radial glial cells could play a direct role in Reelin-signalling

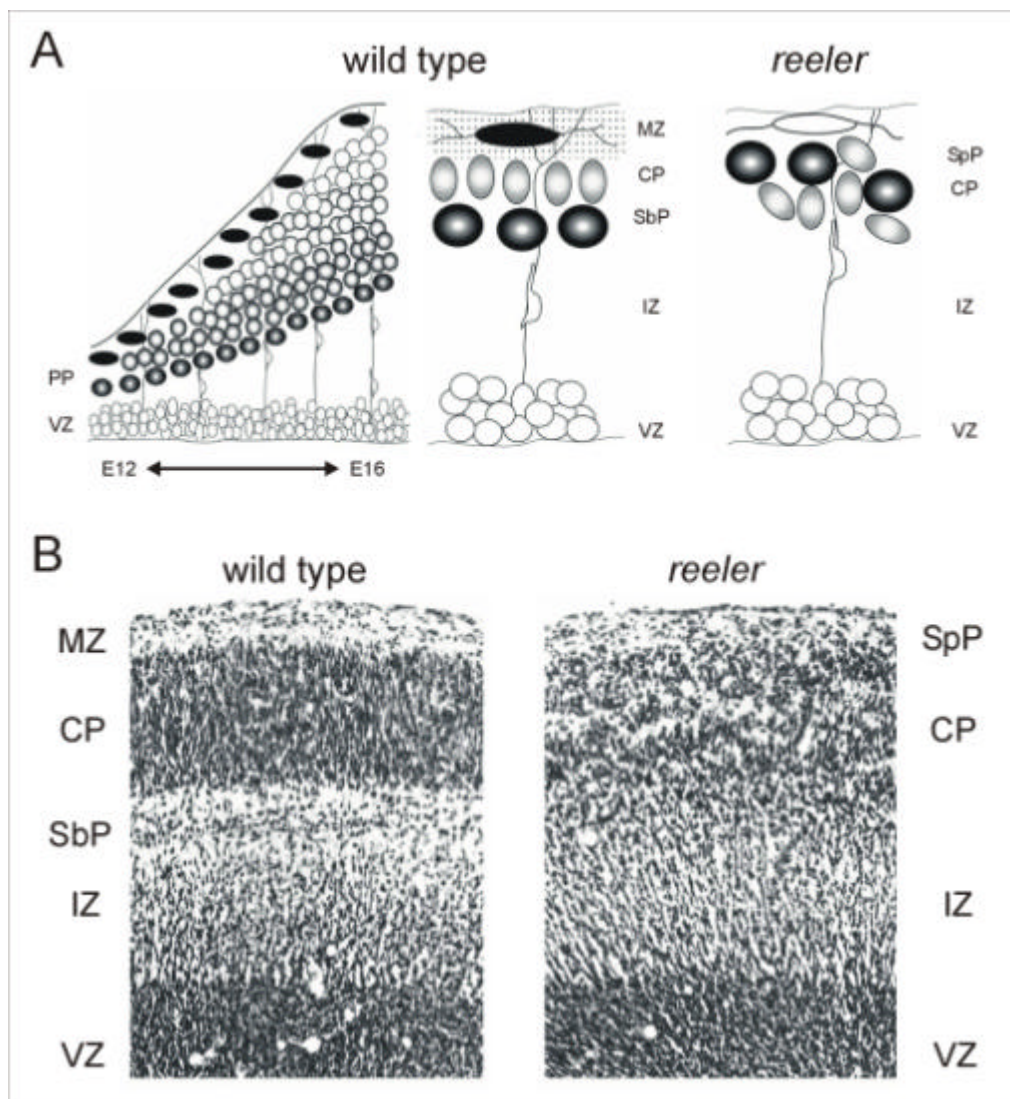


**Figure 2.2 Migrational defects in the *reeler* cerebral cortex**

A) Corticogenesis in the WT cerebral cortex (left and middle panel; for details see text). In the *reeler* cerebral cortex the preplate fails to split into MZ and SbP resulting in the disorganized SpP (right panel). B) Histological sections of a WT, compared to a *reeler* cerebral cortex at E16. (adapted from Rice and Curran 2001).

## 2.5.2 The Reelin-signalling pathway

However, the recent progress in the Reelin-signalling pathway has focussed on the signalling cascade in neurons (Fig. 2.3; for review see Rice and Curran 2001). Reelin binds to the lipoprotein-receptors apolipoprotein receptor 2 (ApoER2) and the very low-density lipoprotein receptor (VLDLR; Trommsdorff *et al.* 1999; Hiesberger *et al.* 1999), and has been suggested to also act via the adhesion molecules  $\beta$ 1-class integrin (Dulabon *et al.* 2000; Magdaleno and Curran 2001; Förster *et al.* 2002) and Cadherin-related neuronal receptors (CNRs; Senzaki *et al.* 1999; Gilmore and Herrup 2000). Lipoprotein receptors have previously been considered as the resources supplying cells with lipids for metabolism and membrane synthesis. Nevertheless, it turned out that some members of this receptor family, such as VLDLR and ApoER2, are not expressed in the liver, suggesting an alternative role than systemic lipid transport. The identical phenotype of mice lacking both ApoER2 and VLDLR and the *reeler* mice confirmed *in vivo* that Reelin acts via these receptors (Trommsdorff *et al.* 1999; Hiesberger *et al.* 1999; for review see Herz and Bock 2002).

Both receptors bind the cytosolic adapter protein mouse Disabled 1 (mDab1). mDab1 encodes a cytoplasmic protein containing a motif known as a protein interaction/phosphotyrosine-binding domain (PI/PTB), which is required for binding of tyrosine-phosphorylated proteins (for review see Margolis 1996). One important binding site of the PI/PTB domain of mDab1 is the peptide sequence Asn-Pro-x-Tyr (NPxY). This NPxY-motif was first discovered in members of the low-density lipoprotein receptors (LDLR; Chen *et al.* 1990) and so it was shown, that the mDab1 PI/PTB-domain interacts with the VLDLR- and ApoER2-cytoplasmic tails via the NPxY-motif (Trommsdorff *et al.* 1998; Hiesberger *et al.* 1999). Binding of Reelin to lipoprotein receptors results in phosphorylation of mDab1 at several tyrosine residues (Fig. 2.3; Howell *et al.* 1999; Keshvara *et al.* 2001), however, the LDLR-family itself does not have intrinsic tyrosine kinase activity. Therefore, it is suggested that binding of mDab1 to the cytoplasmic NPxY-motif, which is important for clathrin-mediated endocytosis and receptor cycling (Chen *et al.* 1990) leads to the internalisation of receptor-bound Reelin and endocytosis then might recruit a tyrosine kinase to mDab1 in vesicles (D'Arcangelo *et al.* 1999).

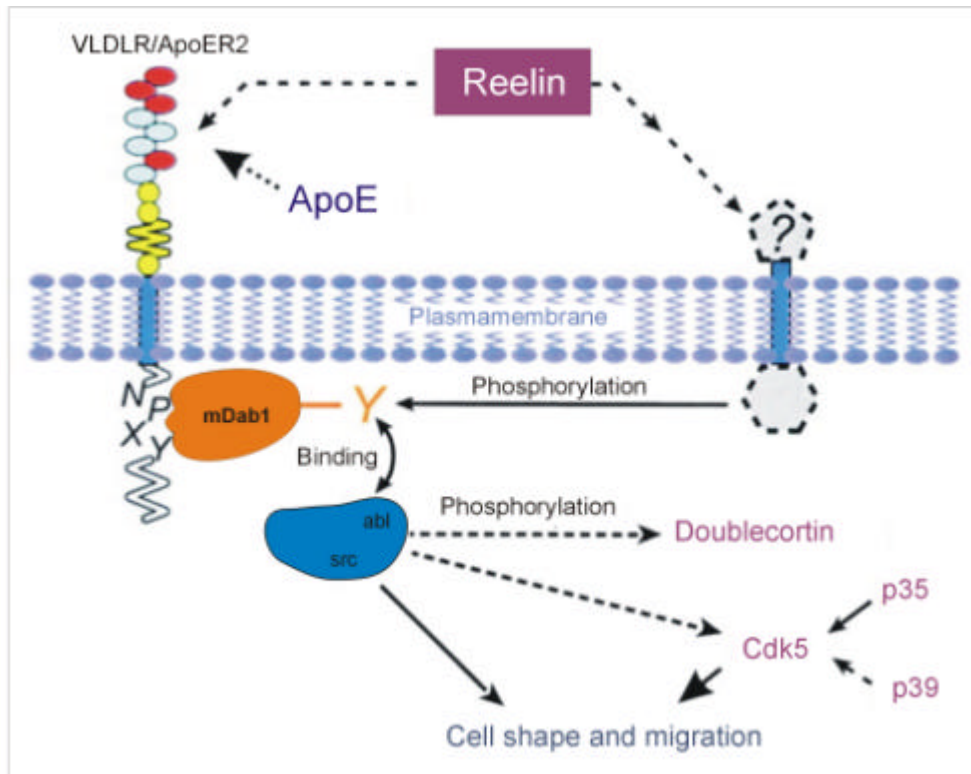


**Figure 2.3 Hypothetical pathway of Reelin-signalling**

Reelin binds to the putative Reelin-receptors VLDLR and ApoER2 on the neuronal surface. mDab1 then is recruited to the cell-surface and binds to the cytoplasmic NPXY-motif of both receptors. Binding to the receptors leads to tyrosine phosphorylation of mDab1 through interaction with extracellular components, probably Reelin itself or alternatively by a membrane tyrosine kinase activated by Reelin. Tyrosine phosphorylation of mDab1 then leads to recruitment and activation of non-receptor tyrosine kinases of the Src and Abl-family, which act on downstream targets of the pathway (adapted from Trommsdorff *et al.* 1999).

In an alternative strategy, Reelin might also bind to co-receptors with associated kinase activity, expressed on migrating neurons, like e.g. CNR or  $\beta$ 1-class integrin, which have been shown to trigger tyrosine kinase activity such as Fyn or Fak and Syk respectively (Clark and Brugge 1995; Senzaki *et al.* 1999). Interestingly, the cytoplasmic tail of  $\beta$ 1-class integrin contains two NPXY motifs, one of which has been suggested to function in cell migration (Vignoud *et al.* 1994; Vignoud *et al.* 1997). Tyrosine phosphorylation of mDab1 promotes interaction with several non-receptor tyrosine kinases, including Src, Fyn and Abl through their SH2 domains, implying mDab1-functions in kinase signalling cascades during development. Downstream signalling of phosphorylated mDab1 affects the cytoskeletal organization thereby influencing neuronal migration (Howell *et al.* 1997; Rice *et al.* 1998; Hammond *et al.* 2001). E.g. the cyclin-dependent kinase 5 (Cdk5), a member of the family of serine/threonine kinases and its regulatory subunits p35 and p39, all of which are widely expressed in postmitotic neurons, phosphorylates a variety of substrates associated with the cytoskeleton (Tsai *et al.* 1993; Cai *et al.* 1997b). It has been

shown *in vitro* that mDab1 is a substrate of Cdk5 and it is therefore speculated that the Reelin-signalling pathway might be a modulator of Cdk5-activity (Homayouni *et al.* 1999).

This signalling pathway is also supported *in vivo* by the identical defects of the mDab1-deficient mice *scrambler* and *yotari* and the *reeler* mice (Sweet *et al.* 1996; Goldowitz *et al.* 1997; Gonzalez *et al.* 1997; Sheldon *et al.* 1997; Ware *et al.* 1997; Yoneshima *et al.* 1997): I.e. invasion of neurons into the cell-sparse MZ, failure of the split of the PP into MZ and SbP and the inverted neuronal layering in the neocortex. Notably, these defects are not observed in the  $\beta$ 1-class integrin-deficient mice (Graus-Porta *et al.* 2001). Importantly, ventricular zone cells express high amounts of ApoER2, VLDLR and mDab1 (Sheldon *et al.* 1997; Trommsdorff *et al.* 1999; Magdaleno *et al.* 2002; Förster *et al.* 2002; Luque *et al.* 2003) and hence have the prerequisite proteins to perceive Reelin-signals. Consistent with the idea that Reelin profoundly influences radial glia, it was recently shown that radial glial cells from the hippocampus depend on Reelin and preferentially adhere and extend on a Reelin-containing substrate (Förster *et al.* 2002).

We therefore further examined the role of Reelin signalling to radial glial cells in a combination of a loss-of-function analysis using *reeler* mice and gain-of-function experiments by addition of Reelin to isolated radial glial cells *in vitro*. This analysis should elucidate, whether Reelin is a direct modulator of radial glial identity in the developing mouse cerebral cortex.

### 3. ABBREVIATIONS

<b>3D</b>	3-dimensional	<b>LV</b>	Lateral ventricle
<b>AB</b>	Antibody	<b>mAB</b>	Monoclonal antibody
<b>B</b>	Cortico-striatal boundary	<b>MGE</b>	Medial ganglionic eminence
<b>BLBP</b>	Brain lipid-binding protein	<b>MI</b>	Maximum intensity
<b>CB</b>	Cerebellum	<b>M-phase</b>	Mitosis phase of the cell cycle
<b>CLSM</b>	Confocal laser scanning microscopy	<b>MZ</b>	Marginal zone
<b>CNS</b>	Central nervous system	<b>n</b>	Sample number
<b>CP</b>	Cortical plate	<b>OB</b>	Olfactory bulb
<b>Ctx</b>	Cortex	<b>P</b>	Postnatal day
<b>DIV</b>	Days <i>in vitro</i>	<b>P</b>	Pial surface
<b>E</b>	Embryonic day	<b>pAB</b>	Polyclonal antibody
<b>FACS</b>	Fluorescent activated cell sorting	<b>PP</b>	Preplate
<b>G1-phase</b>	Gap phase 1 of the cell cycle	<b>RC2</b>	Radial cell 2
<b>G2-phase</b>	Gap phase 2 of the cell cycle	<b>Rln</b>	Reelin
<b>GC</b>	Growth cone	<b>RMS</b>	Rostral migratory stream
<b>GE</b>	Ganglionic eminence	<b>RT</b>	Room temperature
<b>GFAP</b>	Glial fibrillary acidic protein	<b>SbP</b>	Subplate
<b>GFP</b>	Green fluorescent protein	<b>SEM</b>	Standard error of the mean
<b>GLAST</b>	Glutamate astrocyte-specific transporter	<b>SOSI</b>	Single optical section image
<b>HC</b>	Hippocampus	<b>S-phase</b>	DNA synthesis phase of the cell-cycle
<b>IFAP</b>	Intermediate filament associated protein	<b>SpP</b>	Super plate
<b>Ig</b>	Immunoglobulin	<b>STDEV</b>	Standard deviation
<b>IZ</b>	Intermediate zone	<b>SVZ</b>	Subventricular zone
<b>LGE</b>	Lateral ganglionic eminence	<b>VZ</b>	Ventricular zone
<b>LI</b>	Labelling index	<b>WT</b>	Wildtype

## 4. MATERIAL & METHODS

### 4.1 Animals

#### 4.1.1 Strains

The inbred mouse strain C57BL6/J and occasionally CD-1 albino mice were used. The day of vaginal plug was considered as embryonic day 0 (E0), the day of birth as postnatal day 0 (P0). Cortical cells for feeder layers were isolated from wistar rats (rats only: the day of sperm detection was considered as E1).

*Reeler* mice (B6C3Fe *a/a-ReI<sup>n</sup>*<sup>r/+</sup>, stock number 000235, The Jackson Laboratory; backcrossed to C57BL6/J), the transgenic mouse lines hGFAP-GFP(94-4) (Zhuo *et al.* 1997; generously given by A. Messing, University of Wisconsin, Madison, USA), hGFAP-eGFP (Nolte *et al.* 2001; generously given by F.Kirchhoff, Max-Planck-Institute of Experimental Medicine, Göttingen, Germany) and Tau::GFP-knockin mice (Tucker *et al.* 2001; generously given by Y. A. Barde, Friedrich-Miescher-Institute for Biomedical Research, Basel, Switzerland) were used. WT and homozygous *reeler* littermates were obtained by heterozygous crossings. Genotyping was performed by PCR on tail DNA as described below. The hGFAP-GFP(94-4), hGFAP-eGFP and Tau::GFP embryos were genotyped by visualization of green fluorescence at the fluorescent stereo microscope.

#### 4.1.2 Genotyping of mutant and transgenic mice

Genotyping was performed by PCR on tail DNA. DNA was obtained following the protocol by Laird *et al.* (1991): Tail biopsies of less than 5mm length were transferred in 0.5ml lysis buffer and incubated rotating for several hours or overnight at 55°C in a modified hybridisation oven. Following complete lysis, hairs and tissue residues were removed by centrifugation in an Eppendorf centrifuge at maximal speed ( $13.1 \times 10^3$ rpm ~ 16.000 xg) for 10-20 minutes. The supernatant was poured into 0.5ml isopropanol and mixed well. DNA-precipitates were transferred in 300-500µl TE-buffer. To solve the DNA, tubes were again rotated at 55°C for several hours.

#### 4.1.2.1 *Reeler* PCR protocol

The PCR protocol for *reeler* genotyping was adapted from D'Arcangelo *et al.* (1996). PCR was carried out using approximately 80ng of genomic DNA (~2µl) and 0.6µM each of the primers RIn-pA, RIn-pB and RIn-pC (see Table 4.1) in a 30µl reaction containing 0.2mM dNTPs, 1.5 U of HotstarTaq-polymerase, 3µl 10xPCR-buffer and 3µl 5xQ-solution. Cycling conditions were: 15-20 minutes at 94°C for HotStarTaq-activation and 10 cycles at 94°C for 30 seconds and a touchdown of 0.5°C each cycle from 55°C at the beginning to 50°C at the 10<sup>th</sup> cycle for 30 seconds to prevent mis-annealing of primers and therefore to maximize the yield of specific products (Don *et al.* 1991). Then 35 cycles at 94°C for 30 seconds, at 48°C for 30 seconds and at 72°C for 1 minute followed. Finally, amplicons were extended at 72°C for 10 minutes. 15µl of each PCR-product was analysed on a 1.8% agarose-TBE-gel. The amplicon obtained from normal WT-DNA (RIn-pA / RIn-pB) is 266bp long, whereas the amplicon from *reeler*-DNA (RIn-pA / RIn-pC) is 363bp long (Fig 4.1).

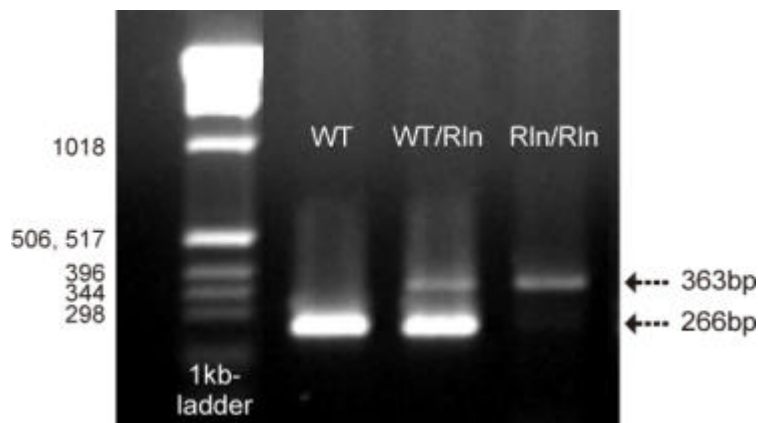


**Figure 4.1**

PCR of genomic DNA from WT, heterozygous (WT/RIn) and *reeler* (RIn/RIn) mice. PCR-products were analysed on a 1.8% agarose gel. The amplicon obtained from normal WT-DNA (RIn-pA / RIn-pB) is 266bp long, whereas the amplicon from *reeler*-DNA (RIn-pA / RIn-pC) is 363bp long. Numbers on the right indicate molecular weight standards (1kb DNA ladder).

#### 4.1.2.2 hGFAP-GFP(94-4) and hGFAP-eGFP PCR protocol

The PCR protocol for genotyping of the hGFAP-GFP(94-4) and the hGFAP-eGFP mouse line was adapted from Zhuo *et al.* (1997) and Nolte *et al.* (2001). PCR was carried out using about 40ng of genomic DNA (~1µl) and 0.4µM of the primers GFAP-LZ1 and GFP-2 (see Table 4.1) in a 30µl reaction containing 0.2mM dNTPs, 1.5 U of Taq-DNA-polymerase, 3µl 10xPCR-buffer and 3µl 5xQ-solution. Cycling conditions were: 4 minutes at 94°C, followed by 30 cycles at 94°C for 30 seconds, at 61.5°C for 30 seconds and at 72°C for 1 minute. Finally, amplicons were extended at 72°C for 5 minutes. 15µl of each PCR-product was analysed on a 1 % agarose-TBE-gel. The amplicon obtained from transgenic animals is 498bp long.

**Table 4.1 PCR-Primers**

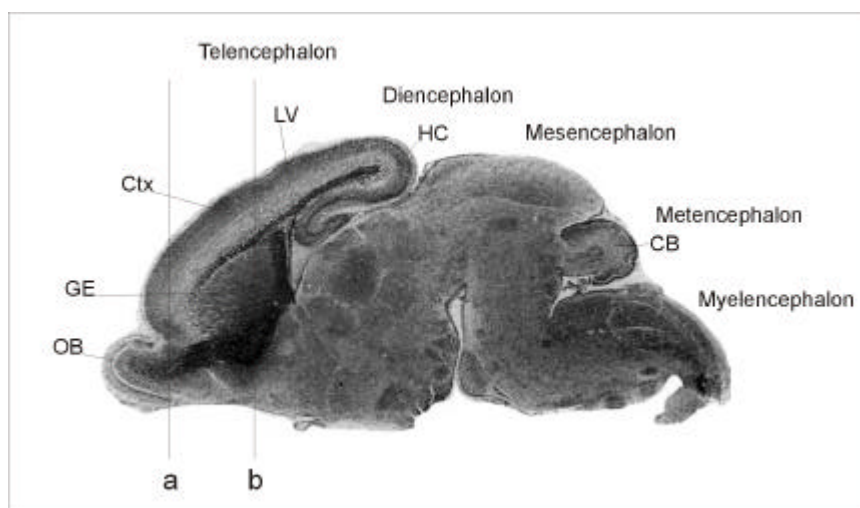
Primer name	Primer sequence
RIn-pA	5'-TAATCTgTCCTCACTCTgCC-3'
RIn-pB	5'-CAgTTgACATACCTTAAT-3'
RIn-pC	5'-TgCATTAATgTgCAgTgT-3'
GFAP-LZ1	5'-ACTCCTTCATAAAgCCCTCg-3'
GFP-2	5'-AAgTCgATgCCCTTCAgCTC-3'

## 4.2 Histology

Pregnant animals were sacrificed with diethylether or increasing CO<sub>2</sub> concentrations followed by cervical dislocation. Embryos were removed by hysterectomy and transferred to Hanks buffered salt solution (HBSS) with 10mM HEPES. Embryonic brains were removed and fixed as described below.

### 4.2.1 Vibratome sections

Brains were fixed for 6 hours in 2% paraformaldehyde (PFA) in phosphate-buffered saline (PBS) at 4°C, washed in PBS, and embedded in 3% agarose in H<sub>2</sub>O. Animals from postnatal stages P0 to P6 were anaesthetized with ether on ice and transcardially perfused with isotonic NaCl, followed by 2% PFA-PBS for fixation. The brains were removed and postfixed with 2% PFA-PBS at 4°C for further 2-4 hours. Vibratome sections were cut frontally, sagittally or horizontally at 100-150 µm thickness and processed for immunohistochemistry (Fig. 4.2 and see below).

**Figure 4.2**

Nissle stained sagittal section of an E18 mouse-brain (Schambra *et al.* 1992). Lines a and b mark the region, where frontal sections were taken from.

#### 4.2.2 Cryosections

Brains were either fixed for 2-4 hours in 4% PFA-PBS at 4°C, cryo-protected in 30% sucrose in PBS overnight, embedded in TissueTek on dry ice and stored at -20°C. Cryosections were cut frontally at 8-12 µm thickness, mounted on glass slides and processed for immunohistochemistry. Sections of unfixed brains were fixed prior to immunohistochemistry with 4% PFA-PBS for 15 minutes and washed with PBS.

For in-situ hybridisation, brains were fixed and cryo-protected in fresh sterile PFA-PBS and sucrose respectively. Sections for in-situ hybridisation were mounted on Superfrost®-Plus slides.

### 4.3 Tissue culture

#### 4.3.1 Acutely dissociated cells and cell culture

Embryonic brains (E12-E18) were isolated as described above. The meninges were removed, the telencephalic hemispheres separated, and the hippocampus and the olfactory bulbs removed. The cerebral cortex and the ganglionic eminence (GE) were dissected (Fig. 4.3) and were collected in separate vials in HEPES-HBSS on ice.

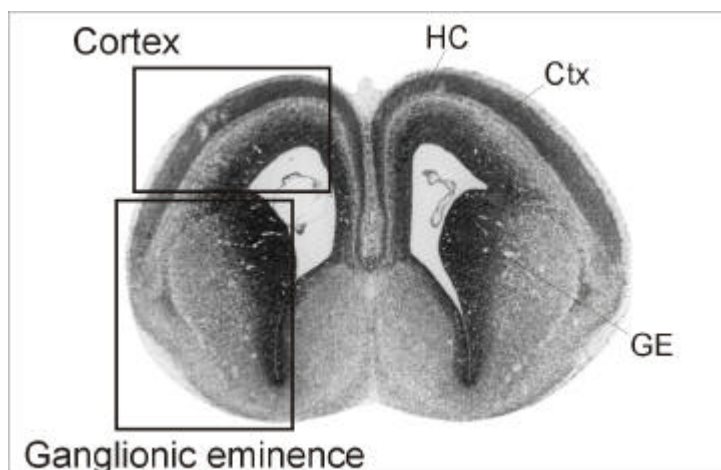


**Figure 4.3**

Nissle stained frontal section of an E16 mouse-brain (Schambra *et al.* 1992). Rectangles schematically mark regions that were used for the acutely dissociated cell preparations.

Cells were digested for 15 minutes in trypsin-EDTA at 37°C. The enzyme activity was stopped by addition of Dulbecco's modified eagle medium (DMEM) supplemented with 10% fetal calf serum (FCS) and 1% penicillin/streptomycin (PS). The tissue was dissociated mechanically with a fire-polished and medium-coated Pasteur pipette. After centrifugation for 5 minutes at 172x g the pellet was resuspended in FCS-PS-DMEM. Washes were repeated twice. Cells were then

plated at a density of  $1 \times 10^6$  cells/ml onto poly-D-lysine-coated (PDL) glass coverslips, incubated at 37°C and 5% CO<sub>2</sub> for 2 hours. Acutely dissociated cells were fixed after 2 hours with 4% PFA-PBS for 15 minutes to avoid any influence of *in vitro* differentiation. Control experiments where the cells had been allowed to adhere for up to 8 hours showed no obvious differences in the cell type composition except a tendency towards an increased number of neurons after longer plating times. Long-term cell cultures were maintained in SATO-medium, which was changed every second day. Long-term cultures were fixed after 5-7 days *in vitro* (DIV) with 4% PFA-PBS for 15 minutes. After three washes with PBS at room temperature (RT), cells were processed for immunocytochemistry.

#### 4.3.2 Adult and embryonic neurosphere cultures

Adult neurosphere cultures (generously given by R.Galli, Institute of Stem Cell Research DIBIT, Hospital San Raffaele, Milan, Italy) were obtained following the procedure described in Gritti *et al.* (1996). Briefly, subependyma were isolated from the telencephalic periventricular region of adult mice following coronal sectioning and cutting into 1mm<sup>3</sup> pieces. Pieces were transferred into ACSF-digestion medium and incubated under continuous oxygenation and stirring for 90 minutes at 32-34°C. Tissue sections were then transferred to neurosphere ovomucoid-medium and were carefully triturated with a fire-polished Pasteur pipette. Cells were collected by centrifugation and were resuspended in adult neurosphere complete-medium and plated onto 10mm tissue culture dishes. For serial propagation, cells were plated at  $8 \times 10^3$  cells/cm<sup>2</sup>. Spheres, formed after 8-10 DIV were harvested, collected by centrifugation (10 minutes at 150x g), mechanically dissociated to a single cell suspension, and re-plated at  $8 \times 10^3$  cells/cm<sup>2</sup> in complete medium. This procedure was repeated every 8-10 DIV. For immunocytochemistry embryonic- or adult neurospheres were dissociated and plated at a density of  $1 \times 10^6$  cells/ml onto PDL-coated glass coverslips and fixed after 2-6 hours as described above.

Embryonic neurosphere cultures were prepared from E14 telencephalon as described for the acutely dissociated cell preparation with the exception that these cells were dissociated mechanically without enzymatic digestion. Dissociated cells were then cultured in embryonic neurosphere complete-medium. Cells were cultured at a density of  $1 \times 10^5$  cells/ml in 25cm<sup>2</sup> or 75cm<sup>2</sup> tissue culture flasks at 37°C and 5% CO<sub>2</sub> for 5 to 6 days. Neurospheres were passaged up to 5 times by centrifugation

at 172x g for 10 minutes, chopping with a tissue chopper followed by re-dissociation and replating as described above.

#### 4.3.3 Astrocyte preparation

Brains were isolated from P3-10 mice and the cortex was dissected as described for the acutely dissociated cell preparation. Cortices of 3-5 animals were collected in HEPES-HBSS on ice and cut up into small pieces. The tissue was dissociated mechanically into single cells with a plastic pipette. After centrifugation for 5 minutes at 172x g the pellet was resuspended in 1ml FCS-PS-DMEM per brain. Cells were cultured in 75cm<sup>2</sup> tissue culture flasks at 37°C and 5% CO<sub>2</sub>. After 3 DIV half of the medium was replaced by fresh FCS-PS-DMEM. Every 7 DIV cells were passaged and after the third passage hardly any oligodendrocytes were present. Cells were then plated at a density of  $1.7 \times 10^5$  cells/ml onto 10cm tissue culture dishes and fixed after further 3-5 DIV with 4% PFA-PBS for 15 minutes. After three washes with PBS at RT, cells were processed for immunocytochemistry as described above.

#### 4.3.4 Fluorescent activated cell sorting (FACS)

Primary cortical cells from GFP-transgenic animals were prepared as described above. Fluorescent and non-fluorescent cells were analysed and separated using a FACSVantage or FACSsort in the single cell mode at the appropriate sort rate (e.g. below 100 cells per second with the FACSsort). A negative control of non-fluorescent cells was used to determine the background fluorescence in order to include less than 1% of non-fluorescent cells in the sort gate. The composition of sorted cells was re-examined by FACS and by analysing plated cells as soon as they were adherent on PDL-coated coverslips (1-2 hours after plating). Cells were either analysed for their GFP-fluorescence and/or stained with cell-type-specific antibodies.

For cell lineage analysis, E14 sorted cells were plated onto a rat feeder layer at a density of about 50 cells per coverslip to minimize the likelihood of clonal superimposition (see Williams et al 1991). Rat feeder layer was prepared from E15-E16 rat brain. Cells were dissected from E15-E16 cortices as described above and were plated about 1-2 hours before plating FACS-sorted mouse cells. Cells were cultured for 5-7 DIV at 37°C and 5%CO<sub>2</sub> in SATO-medium. BrdU was added each day to the culture medium at a final concentration of 10µM to ensure, that only sorted

precursors were included in the analysis. After 5-7 DIV, cells were fixed and stained as described above.

#### 4.3.5 Viral infection - BAG-retrovirus

Primary cortical cell cultures from E14 *reeler* and WT embryos were prepared as described above. Cells were infected 2 hours after plating with a BAG retrovirus (Price *et al.* 1987), which expresses LacZ, encoding for  $\beta$ galactosidase from the long terminal repeat (LTR) promoter and simultaneously co-expresses a neomycin resistance gene from the simian virus 40 (SV40) early promoter. Such virus concentration was used, that a maximum of 40 clones per coverslip was obtained to minimize the likelihood of clonal superimposition (Williams *et al.* 1991). Cells were cultured for 5-7 DIV, fixed and stained as described below.



#### 4.3.6 Cell-lines and conditioned medium

HEK-293 cells expressing either Reelin or GFP (clone pCrl, for further information see D'Arcangelo *et al.* 1995; Förster *et al.* 2002; kindly provided by T.Curran, St.Jude Childrens Hospital, Memphis Tennessee, USA) were cultured in FCS-PS-DMEM at 37°C and 5% CO<sub>2</sub>. Cells were passaged after reaching 80% confluence (each 2-4 days) 1:7 to 1:10. Stably transfected clones were selected with the antibiotic geneticin (G418).

Medium was collected from GFP or Reelin containing cells 2 days after incubation in G418 free medium, either FCS-PS-DMEM or chemically defined SATO-medium, filtered (0,45  $\mu$ m) and stored at 4°C. The high content of Reelin protein in medium collected from Reelin-transfected but not from GFP-transfected cells was confirmed by Western blotting using the mAb E4 directed against Reelin (see below; Fig. 4.4).

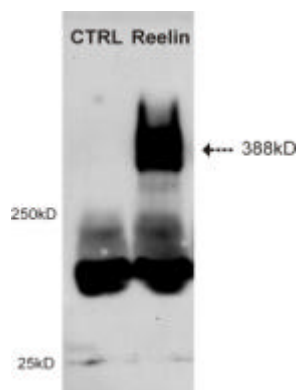


**Figure 4.4**

A western blot (for details see text) is depicted showing the presence of Reelin-protein (388kD) in Reelin-conditioned medium but not in control medium.

## 4.4 Time-lapse video-microscopy

### 4.4.1 Cell culture and viral infection

Either human embryonic kidney (HEK-293) cells (see 4.3.6), mouse fibroblast (NIH-3T3) or mouse primary cortical cells (E14), prepared as described above, were plated in cell culture dishes of 3cm diameter at a density of about  $1 \times 10^6$  cells/ml . Mouse cells were infected immediately after plating with the GFP-retrovirus (depicted below) expressing GFP under the LTR-promoter and the neomycin-resistance gene under the SV40-promotor (Flügel *et al.* 1999; provided by Alexander Flügel, MPIN, Martinsried, Germany). Cells were cultured in FCS-PS-DMEM-medium overnight at 37°C and 5%CO<sub>2</sub> before they were used in time-lapse video-microscopy (see Results 5.6.2).



### 4.4.2 Slice preparation and viral infection

Brains were isolated from E14 mouse embryos as described above. Hemispheres were separated and the meninges and the hippocampus removed. Hemispheres were then frontally with a tissue-chopper at 300µm thickness and were transferred in HEPES-HBSS. Separated slices were laid on permeable filter membrane inserts and cultured in time-lapse (TL) medium at 37°C and 5%CO<sub>2</sub>. Slices were injected with a replication incompetent adenovirus expressing eGFP under the control of the CMV-promoter (generously provided by Annette Gärtner, UCL London, UK; Chapouton *et al.* 1999). Injections with the eGFP-adenovirus were performed immediately after slice preparation. The eGFP adenovirus was pressure injected focally in the cortical ventricular zone of the slice through a glass electrode with a 10µm-opening diameter, using a pneumatic picopump. Thereafter, slices were incubated in TL-medium overnight at 37°C and 5%CO<sub>2</sub>.



### 4.4.3 Image acquisition

The used inverted microscope employs conventional wide-field optics and a cooled CCD-camera for image detection. Image acquisition has been automated and controlled by a computer system running MetaVue imaging software. The used lenses were long distance objectives to allow accurate focussing through the entire thickness of the 300 $\mu$ m forebrain slices. Used exposure times and time-intervals are described in the Results (see 5.6.2).

Time lapse set-up	
AxioVert 10	Zeiss
MicroMax Camera and Controller	Princeton Instruments
Objective LD-Achroplan 20x/0,40 korr (Phase 2)	Zeiss
Objective LD-A Plan 40x/0,50 (Phase 2)	Zeiss
MetaVue imaging program	Visitron Systems
CO <sub>2</sub> regulator	MPI-Workshop
Temperature regulator	MPI-Workshop
Incubation chamber	MPI-Workshop

## 4.5 Immunochemistry

### 4.5.1 Immunocytochemistry

As primary antibodies (see Table 4.2), we used the monoclonal mouse antibody (mAb) RC2 (IgM; 1:500 in 0.5% Triton X-100), the polyclonal antibody (pAb) directed against GLAST (guinea pig; Watanabe: 1:200-100; commercial: 1:8000-500 in 0.1% Triton X-100), the pAb against BLBP (1:1500 in 0.5% Triton X-100) and the mAb E4 against Reelin (IgG1; 1:500 in 0.5% Triton X-100). For the analysis of transcription factors, we used the mAb against Mash1 (IgG1; 1:2 in 0.1% NP40). In order to stain proliferating cells, we used the pAb (rabbit) anti-Ki67 (1:10 in 0.5% Triton X-100), the rat mAb TEC-3 anti Ki-67 (IgG; 1:25 in 0.5% Triton X-100), the mAb anti-nestin (IgG1; 1:3 in PBS) and the pAb (rabbit) anti-nestin (1:1000 in PBS). For the analysis of cells in M-phase we used the pAb against phosphorylated histone H3 (PH3; 1:200 in 0.5% Triton X-100) and the mAb 4A4, which recognizes a cdc2-Kinase phosphorylated form of vimentin (IgG2b, 1:100 in PBS; special fixation: 3.7% formalin 10 minutes on ice, wash 2x PBS on ice, 100% MeOH 10 minutes at -20°C, wash 3x PBS on ice). For S-phase-analysis by BrdU-labelling methods (for details see 4.6) the

mAb anti-BrdU (IgG1; 1:10 in PBS) was used. As a marker for postmitotic neurons, we used the mouse mAb against  $\beta$ -tubulin-III (IgG2b; 1:50 in PBS) and the mAb against NeuN (IgG1; 1:50 in 0.5% Triton X-100), for astrocytes the mAb directed against GFAP (IgG1, 1:200 in PBS), and for oligodendrocyte precursors the mAb AN2 (rat IgG1, 1:50 in PBS). For clonal analysis of mouse neural precursor cells plated on a feeder layer from rat forebrain (for details see 4.3.4 and 4.12.3) cells were stained with the pAb (rat) M2 and M6 (1:200-10 in PBS). BAG-infected clones were detected by the pAb (rabbit) against anti- $\beta$ -galactosidase (1:500 in PBS; pre-treatment: incubation in 1% Triton X-100 for 5 minutes at RT). Intermediate filament stainings like anti-nestin-, anti- $\beta$ -tubulin-III- and anti-GFAP-staining required a special pre-treatment for better visualization of intermediate filaments before application of the primary antibodies. Therefore, cells were incubated in EtOH-glacial acetic acid for 15 minutes at -20°C followed by three washes in PBS for 10 minutes at RT. Acutely dissociated cells and long term cell cultures were incubated in the primary antibody at the appropriate dilution. After several washes in PBS cells were incubated in the secondary antibody for 45 minutes at RT.

Secondary subclass-specific FITC- or TRIC-coupled antisera were used at a dilution of 1:50, and Cy2- or Cy3-coupled antisera at 1:100. For triple-stainings, we used biotinylated secondary antibodies (dilution 1:50) followed by incubation in Streptavidin-AMCA at a 1:50 dilution. After three further washes, the glass coverslips were mounted in Aqua Poly/Mount, a glycerol-based mounting medium.

#### 4.5.2 Immunohistochemistry

Vibratome sections were incubated free floating in primary antibody always containing 0.5% Triton X-100 and 10% normal goat serum (NGS) overnight at 4°C rocking. Special pre-treatment as for anti-nestin, anti- $\beta$ -tubulin-III or anti-GFAP was discarded to avoid any damage of the slices. After primary and secondary antibody staining slices were mounted in Aqua Poly/Mount mounting medium on glass slides. Cryostate sections were stained as described in the immunocytochemistry section.

#### 4.5.3 Negative controls

To rule out any unspecific binding of the secondary antisera, control experiments were performed by either leaving out the primary antibody or by using a primary antibody against an antigen that is not present in the respective tissue or at the respective developmental stage.

## 4.5.4 Antibodies

**Table 4.2 Primary antibodies (alphabetical order)**

<b>Name</b>	<b>Host-animal</b>	<b>Marker</b>	<b>Supplier</b>	<b>Reference</b>
4A4	Mouse, monoclonal IgG2b	Mitotic radial glial cells	Naoyuki Inagaki, Nara Institute of Science and Technology, Ikoma, Japan	Kamei <i>et al.</i> 1998
AN2	Rat, monoclonal IgG	Migratory oligodendrocyte precursors	Jacqueline Trotter, University of Heidelberg, Germany	Niehaus <i>et al.</i> 1999
Anti- $\beta$ - galactosidase O3G / O3H	Rabbit	Marker gene	Jack Price, Kings College, Institute of Psychiatry, London, UK	Williams and Price 1995
Anti- $\beta$ -tubulin- III	Mouse, monoclonal IgG2b	Postmitotic neurons	Sigma	Lee <i>et al.</i> 1990
Anti-BLBP	Rabbit	Precursor cell subtypes	Nathaniel Heintz, Howard Hughes Medical Institute, Rockefeller University, New York, USA	Feng <i>et al.</i> 1994; Kurtz <i>et</i> <i>al.</i> 1994
Anti-BrdU	Mouse, monoclonal IgG1	S-Phase marker	Bio-Science Products	Götz <i>et al.</i> 1998
Anti-GFAP	Mouse, monoclonal IgG1	Astrocytes	Sigma	Bignami <i>et al.</i> 1972; Uyeda <i>et</i> <i>al.</i> 1972
Anti-GLAST	Guinea pig	Precursor cell subtypes	?? Masahiko Watanabe, Hokkaido University, Sapporo, Japan ?? Chemicon	Shibata <i>et al.</i> 1997
Anti-Ki67	Rabbit	Precursor cells	Dianova Immundiagnosics	Gerdes <i>et al.</i> 1997
Anti-Ki67 (TEC-3)	Rat	Precursor cells	Dianova Immundiagnosics	Steiner <i>et al.</i> 1999
Anti-Mash1	Mouse, Monoclonal IgG1	bHLH-transcription factor	David Anderson, California Institute of Technology, Pasadena, CA, USA	Lo <i>et al.</i> 1991; Torii <i>et al.</i> 1999

Anti-Nestin	Mouse, monoclonal IgG1	Precursor cells	Developmental Studies Hybridoma Bank	Frederiksen and McKay 1988
Anti-Nestin	Rabbit	Precursor cells	Masato Nakafuku, Graduate School of Medicine, University of Tokyo, Japan	Frederiksen and McKay 1988
Anti-NeuN	Mouse, Monoclonal IgG1	Postmitotic neurons	Chemicon	Mullen <i>et al.</i> 1992
Anti-PH3	Rabbit	M-Phase marker	Upstate Biotech	Hendzel <i>et al.</i> 1997
Anti-Reelin (E4)	Mouse, monoclonal IgG1	Cajal-Retzius-cells in the cerebral cortex	André Goffinet, University of Louvain, Medical School, Brussels, Belgium	de Bergueyck <i>et al.</i> 1998
M2	Rat	Mouse precursor cells and glial cells	Carl F. Lagenaur, University of Pittsburgh, PA, USA	Lagenaur and Schachner 1981
M6	Rat	Mouse neurons	Carl F. Lagenaur, University of Pittsburgh, PA, USA	Lund <i>et al.</i> 1985
RC2	Mouse, monoclonal IgM	Precursor cell subtypes	Pierre Leprince, Laboratory of Experimental Neuropathology, University of Liege, Belgium	Misson <i>et al.</i> 1988a

**Table 4.3 Secondary antibodies (alphabetical order)**

<b>Name</b>	<b>Supplier</b>
Anti-rabbit Ig FITC / TRIC / biotinylated	Boehringer Ingelheim
Anti-rabbit Ig Cy2 / Cy3	(Vector Laboratories)
Streptavidin AMCA	
Anti-mouse IgG+M Cy3	EuroPath Ltd.
Anti-mouse IgG1 FITC / TRIC / biotinylated	(Southern Biotechnology Associates)
Anti-mouse IgG2b FITC / TRIC / biotinylated	
Anti-mouse IgM FITC / TRIC / biotinylated	
Anti-guinea pig Ig Cy2 / Cy3	Dianova Immundiagnosics
Anti-rat FITC / TRIC	(Jackson ImmunoResearch)

## 4.6 BrdU Labelling

### 4.6.1 BrdU Pulse Labelling

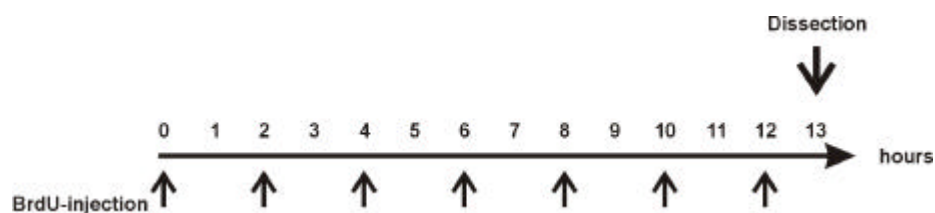
For cell cycle analysis, we labelled cells during DNA-synthesis with 5-bromo-2-deoxyuridin (BrdU; Nowakowski *et al.* 1989). Mice were injected intraperitoneally 1 hour prior to hysterectomy with 5 mg BrdU in PBS per 100g bodyweight. Vibratome sections and dissociated cells were then prepared as described above. For the immunodetection of BrdU, pre-treatment with 2,4N HCl for 30 minutes was required to denature double-stranded DNA. This was followed by two washes with 0.1M sodium-tetraborate-buffer (pH 8,5) for 15 minutes at RT. After three further washes in PBS, the staining with the mAB anti-BrdU (IgG1; 1:10) was performed as described above.

The proportion of cells that have incorporated BrdU (after a single injection) amongst all proliferating cells is the labelling index (LI):

$$LI = \frac{\text{BrdU-positive proliferating cells}}{\text{proliferating cells}}$$

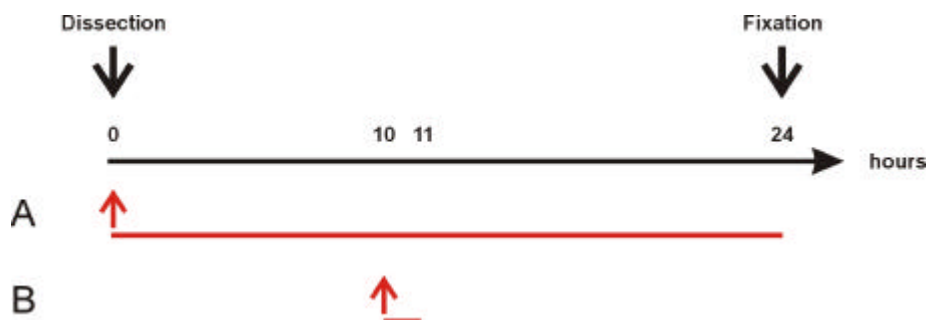
### 4.6.2 Cumulative BrdU Labelling

To determine the number of dividing cells we used the cumulative BrdU-labelling method described by (Nowakowski *et al.* 1989). Pregnant mice (E14) were injected with BrdU over a total period of 12 hours. First injection was done at 7 am followed by 6 injections each 2hour interval (see schematic drawing below). One hour after the last injection, the embryonic brains were isolated and acutely dissociated cells were prepared from the cortex and GE. BrdU-immunostaining was performed as described above.



### 4.6.3 BrdU-labelling in cultures with conditioned medium

To determine the number of dividing cells in 24-hour cultures with conditioned medium, we performed BrdU-labelling experiments following two different paradigms. First, we cultured the cells for 24 hours in the presence of BrdU to label all proliferating cells. Therefore, BrdU was added in a final concentration of 10 $\mu$ M to the medium, directly after cells were plated (A). Second, we performed BrdU-pulse labelling to determine the LI of cells cultured in conditioned medium. Therefore, cells were cultured for 10 hours without BrdU and then BrdU (10 $\mu$ M) was added. 1 hour thereafter, BrdU-medium was washed away and cells were cultured for further 13 hours without BrdU (B).



## 4.7 Tracing experiments

### 4.7.1 Live tracing of precursors by Dil or Beads

To selectively label cells from the pial surface either the lipophilic dye 1,1'-didodecyl-3,3,3',3'-tetramethylindo-carbocyanine perchlorate (Dil) or red fluorescent latex microsphere beads were used (see Katz *et al.* 1984; Voigt 1989; Götz *et al.* 1998). After dissection of the brain and removal of the meninges, 10-20  $\mu$ l of Dil (5mg/ml in ethanol p.a., diluted 1:10 in 300mM sucrose) or 5 $\mu$ l of fluorescent beads (50nM; diluted 1:1 in HEPES-HBSS) were applied on the cortical surface. The brains were transferred in HEPES-HBSS and incubated at RT for 10 minutes. The hemispheres were carefully inspected for contamination with fluorescent tracer at the ventricular surface at both the dissection and the fluorescence microscope. Hemispheres where any dye had entered the ventricle were discarded. Acutely dissociated cells were prepared as described above. Control experiments were performed to examine a potential spread of Dil or beads during the dissociation

procedure. Therefore, DiI-crystals were put in the dissociation solution of unlabelled cells. However, no cells had incorporated the label after dissociation. For double- and triple- immunocytochemistry of DiI-labelled acutely dissociated cells, we used 0.1% polyoxyethylenesorbitanmonolaurate (Tween) for permeabilization, since TritonX-100 lead to a spread of DiI from the labelled cells to most cells on the coverslip.

#### 4.7.2 DiI-labelling from the ventricular surface in fixative and 3D-reconstruction

The lipophilic dye DiI was injected as ethanol/sucrose suspension in the lateral ventricle of embryonic brains or the lumen of the spinal cord (E12-18) *ex vivo* resulting in a complete labelling of cell membranes after 10-20 days in 2% PFA-PBS at RT allowing the diffusion of DiI. Frontal vibratome sections (150µm thick) were cut and analysed by confocal laser scanning microscopy (CLSM). Series of single optical section images ( $\approx 1\mu\text{m}$ ) were assemble for a 3D-reconstruction of the brain slice using Imaris™-program to perform the morphological analysis of DiI-labelled cell as described in 4.12.5.

### 4.8 DNA-labelling

For the detection of condensed chromosomes for the analysis of mitotic cells and the orientation of their spindle-apparatus at the ventricular surface, cryostate-sections were counterstained with DAPI (4,6-diamino-2-phenyl-indol; Naimski *et al.* 1980), propidium-iodide (PI; Crissman *et al.* 1976) or Yo-Pro-1-iodide (Suzuki *et al.* 1997). All three substances are dyes that intercalate into nucleic acid molecules of DNA and RNA. DAPI-staining results in blue, PI in red and Yo-Pro-1-iodide in green fluorescence. Depending on the experimental purpose (double-labelling for CLSM; triple-labelling) the appropriate stain was used. DNA staining (DAPI 1µg/ml in PBS; PI 5µg/ml in PBS containing 50U/ml RNaseA; Yo-Pro-1-iodide 10µM in PBS) was performed after immunohistochemistry in sections for 5-10 minutes at RT followed by three consecutive washing steps in PBS at RT.

## 4.9 In-situ hybridisation

### 4.9.1 Plasmid preparation and *in vitro* transcription

10ng plasmid DNA was added to 25  $\mu$ l chemically competent Top10 cells and incubated for 30 minutes on ice. Cells then were heat shocked at 42°C for 45 seconds. After recovering of the bacteria for 10 minutes on ice 1ml LB-medium was added and cells were incubated on a bacterial shaker for 45 minutes at 37°. Then 50-100 $\mu$ l of bacterial suspension were plated on e.g. ampicillin containing (50 $\mu$ g/ml) LB-agar plates, depending on the resistance encoded by the plasmid, and incubated at 37°C overnight. One colony was picked the next day and grown for about 4 hours in 5ml ampicillin-containing LB-medium. This pre-culture then was added to 50ml LB-ampicillin-medium and was incubated overnight at 37°C on the rotary shaker. Plasmid-DNA was harvested following the Quiagen-Midiprep protocol using a midi Tip100 column. The DNA pellet was dissolved in 200 $\mu$ l ddH<sub>2</sub>O and 20 $\mu$ g of plasmid-DNA, quantified by spectrophotometry at 260nm, were linearized with the appropriate enzyme (40U) in a total volume of 50 $\mu$ l of the appropriate buffer for 2-3 hours at 37°C. The plasmid-DNA then was purified by phenol extraction. First, water was added to a total volume of 200 $\mu$ l, then 200 $\mu$ l phenol-chloroform-isoamylalcohol (50:49:1) was added and strongly vortexed for about 1 minute. After 5 minutes of centrifugation in an Eppendorf-centrifuge at maximum speed (13.1 x 10<sup>3</sup>rpm ~ 16.000 xg), the water phase was recovered and 1/10x volume 3M sodium acetate and 0.7x volume isopropanol were added and incubated for 10 minutes at RT for precipitation. After a centrifugation at maximum speed in an Eppendorf-centrifuge for 15 minutes the pellet was washed shortly with 70% ethanol and resuspended in 18 $\mu$ l TE (pH8, RNase-free). For *in vitro* transcription of the linearized plasmid 1 $\mu$ l (about 1 $\mu$ g) plasmid-DNA was mixed with 2 $\mu$ l NTP-mix containing digoxigenin labelled UTP (DIG-UTP), 4 $\mu$ l 5xtranscription buffer, 1 $\mu$ l RNase inhibitor and 1 $\mu$ l (50U/ $\mu$ l) of the respective RNA-polymerase (T3, T7 or SP6). Pure RNase-free ddH<sub>2</sub>O was added up to a final volume of 20 $\mu$ l and the plasmid-mix was incubated for 2 hours at 37°C. To stop the reaction 2 $\mu$ l 0.2M EDTA was added followed by addition of 2.5 $\mu$ l 4M LiCl and 75 $\mu$ l pure ethanol to precipitate the RNA either at -20°C overnight or at -80°C for two hours. The RNA-probe was centrifuged for 7 minutes at 4°C and the pellet was dissolved in 22.5 $\mu$ l ddH<sub>2</sub>O for 30 minutes at 37°C. RNA-precipitation was repeated by addition of 2.5 $\mu$ l 4M LiCl and 75 $\mu$ l 100% EtOH and incubation for 2 hours at -20°C.

The RNA-probe again was centrifuged for 7 minutes at 4°C. The RNA-probe was resuspended in 20µl ddH<sub>2</sub>O and 200µl hybridisation buffer at a final RNA-concentration of around 100ng/µl.

**Table 4.4 In-situ plasmids (antisense RNA-probes)**

Name	Provider	Reference	Vector	Insert	Digestion	Trkrp
Delta1 (DLL1)	F.Guillemot, NIMR, London, UK	Bettenhausen <i>et al.</i> 1995	pKS-	800bp fragment	EcoR1	T3
Delta3 (DLL3)	F.G.	Dunwoodie <i>et al.</i> 1997	pBSK+	2.1kb Delta3 full length	Not1	T7
Jagged/Serrate1 (Ser1)	F.G.	Lindsell <i>et al.</i> 1996		Excl. IC region, with added FLAG	Xbal	T7
Jagged/Serrate2 (Ser2)	F.G.	Shawber <i>et al.</i> 1996		Full length with point mutation	BamH1	T7
Notch1 (N1)	F.G.	Lindsell <i>et al.</i> 1996			Apa1	Sp6
Notch2 (N2)	F.G.	Lindsell <i>et al.</i> 1996			EcoR1	T3
Notch3 (N3)	F.G.	Lindsell <i>et al.</i> 1996			Not1	T3
Lunatic-fringe (Lfng)	T.F.Vogt Princeton University, NJ, USA	Johnston <i>et al.</i> 1997	PBSKS	600bp insert; Subfragment of coding region; start AA 129	H3	T7
Manic-fringe (Mfng)	T.F.V.	Johnston <i>et al.</i> 1997	PBSII KS+	1.1kb insert	Styl	T3

#### 4.9.2 Non-radioactive in-situ hybridisation

2.25µl RNA-antisense probe were diluted in 150µl hybridisation buffer and denaturated for 5 minutes at 70°C. 120µl hybridisation probe were applied per defrost slide, and either a clean coverslip or a piece of parafilm was put on top to prevent drying of the sections. Slides were incubated overnight at 65°C in a sealed box with Whatman paper, soaked with 1xSSC in 50% formamide, in an hybridisation oven. Slides were washed in pre-warmed (65°C) washing solution, first for 10 minutes at 65°C to allow the coverslips to fall off followed by 2 to 3 consecutive washes for 30 minutes at 65°C. Slides then were washed twice in MABT for 30 minutes at RT

followed by a blocking step in 'blocking-solution' for at least one hour at RT. Anti-digoxigenin Fab fragments coupled to alkaline phosphatase were diluted 1:2500 in blocking-solution. 150µl of this antibody-solution were then applied per slide and sections were covered with parafilm. The antibody staining was performed in a humid chamber overnight at RT. Slides were washed in MABT for 20 minutes at RT 4 to 5 times, and rinsed twice in Alkaline-phosphatase staining buffer for 10 minutes at RT. 150µl NBT/BCIP-containing staining solution was added per slide and covered with parafilm. Slides were incubated 12 to 24 hours at RT. When the staining was strong enough, the reaction was stopped by rinsing the slides in staining buffer and shortly in water. Slides were dried for several hours at RT and mounted in AquaPoly/Mount.

#### **4.10 Westernblotting**

For Reelin-protein (400kD) separation, 10µl of control- or Reelin-conditioned medium were mixed with 5µl of 3xLaemmli buffer, heated at 95°C for 3-5 minutes and loaded onto a SDS-polyacrylamide gel (resolving gel: 6%; stacking gel: 5%, 8 cm x 10 cm x 1.5 mm). Gel was run in SDS-page running buffer with constant 110V for about 1 hour. Proteins were transferred to nitrocellulose by semidry-blotting: Polyvinylidene fluoride (PVDF) membranes were pre-treated with 100%MeOH for 20 seconds, washed for 10 minutes in H<sub>2</sub>O and stored in semidry-blotting buffer. Electrotransfer of proteins to PVDF-membranes took about 2-3 hours at 0.8mA per cm<sup>2</sup>. After protein transfer membranes were washed in TBS for 5 minutes at RT and were blocked for 1 hour in skimmed milk blocking buffer followed by three consecutive washing steps in TBS/T for 5 minutes at RT. Membranes were incubated in primary antibody against Reelin diluted in skimmed milk blocking buffer (E4, mouse mAb IgG1, 1:500) with gentle agitation overnight at 4°C. After washing the membrane in TBS/T three times for 5 minutes, the membrane was incubated in HRP-conjugated secondary anti-mouse antibody (1:2000; diluted in skimmed milk blocking buffer) with gentle agitation for 1 hour at RT. After three further washes in TBS/T for 5 minutes at RT proteins were revealed by luminol reaction with the ECL+plus westernblot detection system for 5 minutes at RT. Membranes were drained of excess of developing solution, wrapped in plastic foil and exposed to x-ray film.

## 4.11 LightCycler real-time RT-PCR

### 4.11.1 RNA extraction

Total RNA was extracted from sorted cells using the RNeasy-kit as described by the manufacturer. RNA isolation was followed by DNaseI digestion to remove DNA residues since RT-PCR is very sensitive to very small amounts of DNA. RNA was quantified by optical density at 260nm and 1 µg of total RNA was used to synthesize cDNA with oligo(dT)<sub>12-18</sub> primers and MoMLV reverse transcriptase in 25 µl reaction mixture at 42°C for 1 hour.

### 4.11.2 LightCycler RT-PCR

RT-PCR was performed with a LightCycler instrument in a total volume of 19 µl containing 1µl of cDNA (40ng), 2.2mM MgCl<sub>2</sub>, 4 µM each primer, LightCycler RT-PCR Reaction Mix SYBR Green I (1x) and LightCycler RT-PCR Enzyme Mix. The protocol consists of two programs: amplification of cDNA and melting curve analysis for product identification. The denaturation and amplification conditions were 95°C for 5 minutes followed by up to 45 cycles of PCR. Each cycle of PCR included immediate denaturation for 15 seconds at 95°C, 8 seconds of primer annealing at 55°C and 25 seconds of extension/synthesis at 72°C. The temperature ramp was 20°C/seconds. At the end of the extension step fluorescence of each sample was measured to allow quantification of the RNA. After amplification a melting curve was obtained by heating at 20°C/seconds to 95°C, cooling at 20°C/seconds to 60°C and slowly heating at 0.1°C/seconds to 98°C with fluorescence data collection at 0.1°C intervals. As negative controls, the reverse transcriptase was omitted at the cDNA synthesis step and the samples then proceeded to the PCR reaction in the same manner as above. These control experiments gave no positive amplification.

**Table 4.5 RT-PCR-Primers**

<b>Primer name</b>	<b>Primer sequence</b>
GAPDH-for	5'-ATTCAACggCACAgTCAAagg-3'
GAPDH-rev	5'-TggATgCAgggATgATgTTC-3'
HPRT-for	5'-gTTggATACAaggCCAgACTTTgT-3'
HPRT-rev	5'-CCACAaggACTAgAACACCTgCTA-3'
ApoER2-for	5'-gCAACCACTCCCAGCATTAT-3'
ApoER2-rev	5'-TACCACTATgggCACgATgA-3'
VLDLR-for	5'-TCCAAgTTgCACATgCTCTC-3'
VLDLR-rev	5'-CCAgCTCTgACCCAgtgAAT-3'

#### 4.11.3 Quantitative analysis of the LightCycler data

Quantitative analysis of the LightCycler data was performed employing LightCycler analysis software. The data analysis is divided into two parts: specificity control of the amplification reaction using the melting curve program of the LightCycler software, followed by use of the quantification program. The SYBR Green I signal of each sample is plotted versus the number of cycles. Using the LightCycler analysis software background fluorescence is removed by setting a noise band. This fluorescence threshold is used to determine cycle numbers that correlate inversely with the log of the initial template concentration. To this end the log-linear portions of the amplification curves are identified and best fit lines calculated. The crossing points (CP) are the intersections between the best-fit lines of the log-linear region and the noise band. These CP correlate inversely with the log of the initial template concentration (LightCycler Operator's Manual, Version 3.3, April 2000, Roche). The CP determined for ApoER2 and VLDLR mRNA were normalized to those of GAPDH and HPRT to compensate for variability in RNA amount and for exclusion of general transcriptional effects. We calculated fold reduction (FR) since our experiments yielded a repressive effect:  $FR = 2^{(CP1-CP2)}$ . Fold induction can be calculated by the same formula by reversing the signs. CP1 indicates the crossing point of the mRNA level of the housekeeper GAPDH or HPRT; CP2 indicates the crossing point of the mRNA level of ApoER2 or VLDLR. The mRNA levels of GAPDH and HPRT in each tissue sample were set to 1.

##### Example:

CP1: GAPDH <sub>neuronal</sub> :	27.11	
CP2: ApoER2 <sub>neuronal</sub> :	32.07	
FR = $2^{(32.07-27.11)}$	0.03	? 33-fold reduction

## 4.12 Data analysis

### 4.12.1 Double-staining in sections

Vibratome sections were analysed at a two-channel confocal laser-scanning microscope (CLSM) using 10x to 63x objectives. Single optical section images (thickness 1-10 $\mu$ m) and maximum intensity images (thickness 10-150 $\mu$ m) were derived.

### 4.12.2 Triple-staining in cell cultures

Acutely dissociated cells were analysed using a fluorescence microscope with 63x oil objective. Quantitative analysis was performed by counting 50 cells of 10 to 15 different optical fields per coverslip that were chosen stochastically throughout the entire surface of the coverslip. In each field, the proportion of single-, double- and triple-labelled cells was determined. To evaluate the proportion of immunoreactive cells at a given stage, 100 phase bright cells of about 10 different optical fields per coverslip were analysed for their immunoreactivity.

20 different combinations of triple-stainings were used to examine and quantify the cell types detected by RC2-, GLAST- and BLBP-immunoreactivity. First we combined the RC2-, GLAST- or BLBP-antisera each in combination with cell type markers such as  $\beta$ -tubulin-III- and/or Ki67- and/or nestin- and/or BrdU-staining. For example, the most frequently used combinations were RC2/ $\beta$ -tub-III/Ki67; RC2/nest/Ki67; RC2/ $\beta$ -tub-III/nest; GLAST/ $\beta$ -tub-III/Ki67; GLAST/nest/Ki67; GLAST/ $\beta$ -tub-III/nest; BLBP/ $\beta$ -tub-III/nest; BLBP/ $\beta$ -tub-III/BrdU; BLBP/nest/TEC3. These stainings revealed that almost all RC2-, GLAST- or BLBP-immunoreactive cells are precursor cells (see results). Combinations of two marker antigens (RC2/GLAST; RC2/BLBP; GLAST/BLBP) with Ki67- or nestin- or BrdU-staining further confirmed this. Since almost all RC2-, GLAST- and BLBP-immunoreactive cells were precursors, we could then use RC2/GLAST/BLBP-triple-labelling to quantify the contribution of the subtypes characterized by their antigenic profile to the progenitor pool (Fig. 5.4). Since our data have a standard error of the mean around 4 (Table 5.1), we excluded populations smaller than 5% for Figure 5.4.

Since these triple-stainings revealed which marker populations co-exist at a given time, we could use the stainings with two markers and Ki67 or nestin described above to evaluate the proportion of precursors immuno-negative for all three marker

antigens, the size of the Ki67-only population in Fig. 5.4. For example, at E14 GLAST and BLBP were subpopulations of the RC2-immunoreactive precursors and therefore the proportion of RC2-negative, Ki67-positive cells was a direct measure of the Ki67-only population at this stage. In E16-18 cortex and E18 GE GLAST was contained in the largest population of precursors, comprising the RC2- and/or BLBP-positive cells. The Ki67-only fraction could therefore be evaluated as the Ki67-positive cells that are GLAST-negative. For the E16 GE, we used the triple-staining of RC2/GLAST/Ki67 to detect the fraction of Ki67-positive cells that were neither GLAST- nor RC2-immunoreactive.

#### 4.12.3 Clonal analysis

For cell fate analysis in FACS- or retrovirus-experiments, clones were analysed for their composition of neurons, astrocytes, oligodendrocytes and precursor cells. Clones are discrete clusters of cells, derived from a single progenitor. The percentage of pure neuronal, pure non-neuronal and mixed clones was calculated per coverslip. Clones from sorted cells were detected by labelling with the antibodies M2 (mouse precursors and glial cells) and M6 (mouse neurons), detecting all mouse cells on the rat feeder layer (Malatesta *et al.* 2000). BAG-infected clones were detected by anti- $\beta$ -gal immunohistochemistry (see as well Table 4.2). M2M6 or anti- $\beta$ -gal respectively were combined with cell type specific markers like anti- $\beta$ -tubulin-III for neurons, anti-GFAP for astrocytes or anti-nestin for precursor cells (see as well Table 4.2). Clones were analysed at 40x magnification. The probability of clonal superimposition was calculated as described in Williams *et al.* (1991), e.g. for coverslips containing a maximum of 65 clones the probability was calculated to be 0.07, for those with 25 clones 0.02. The mean number of clones per coverslip obtained in our experiments was  $32 \pm 2$ .

#### 4.12.4 Analysis of the orientation of cell division

The analysis of the orientation of cell division at the ventricular surface was performed by different DNA-labelling methods (DAPI, PI or Yo-Pro-1-iodide staining). The plane of division respective to the ventricular surface was analysed: angles from 90-60° were interpreted as vertical, 60-30° as oblique and 30-0° as horizontal divisions. Sections were analysed at the fluorescence microscope or by CLSM.

#### 4.12.5 3D-analysis of DiI-labelled ventricular zone cells

For examination of the morphology of ventricular zone precursor cells by ventricular DiI-labelling, injected brains were cut with a vibratome at 150µm thickness and slices were mounted in AquaPoly/Mount mounting medium. Sections were analysed immediately after cutting by CLSM, as after cutting DiI started to leak out from damaged labelled cells, resulting in high background fluorescence already after 1-2 days. Series of 1µm thick single optical section images (SOSI) were taken through the entire slice (stack of up to 200 SOSI). SOSI-stacks were reconstructed to 3D-images using Imaris™-Program. The analysis of the labelled cells then was performed using CorelPhotopoint, which allowed rotation of the 3D-image step by step with an angle of about 5°. Only cells, where the soma and the entire process were discernable were taken into account for the analysis. Visualization of mitotic figures in DiI-labelled sections was performed by counterstaining with Yo-Pro-1-Iodide free floating.

#### 4.12.6 Statistics

For all data sets, the arithmetic average  $\bar{x} = \frac{1}{n} \sum_{i=1}^n x_i$  was calculated and the

standard deviation  $s = \sqrt{\frac{\sum_{i=1}^n (x_i - \bar{x})^2}{n - 1}}$  and the standard error of the mean  $SEM = \frac{s}{\sqrt{n}}$

were computed. Error bars depict the SEM. The Student's t-test was used to examine whether data sets differed significantly. Data were considered as significant with  $p < 0.05$  and as highly significant with  $p < 0.01$ . Calculations of the arithmetic average, the standard deviation, the standard error of the mean were performed with Microsoft Excel. The significance of the obtained data was tested using the program Statistics W1.59.

## 4.13 Material

### 4.13.1 Microscopy

Fluorescent microscope	
AxioPhot microscope	Zeiss
HBO 100W fluorescent lamp	Zeiss
AxioCam HRc camera	Zeiss
AxioVision 3.1.1.1 program	Zeiss
Objective Plan Neofluar 5x/0,15 (Phase 1)	Zeiss
Objective Plan Neofluar 10x/0,30 (Phase 1)	Zeiss
Objective Plan Neofluar 20x/0,50 (Phase 2)	Zeiss
Objective Plan Neofluar 40x/0,75 (Phase 2)	Zeiss
Objektive Plan-Apochromat 40x/1,30 Oil	Zeiss
Objektive Plan-Apochromat 63x/1,40 Oil (Phase 3)	Zeiss
Fluorescent stereomicroscope	
SZX 12 microscope	Olympus
U-RFL-T fluorescent lamp	Olympus
U-CMAD3 incl. U-TV1 X camera	Olympus
AnalySIS 3.1 program	Soft Imaging Systems
Confocal microscope	
Leitz DM RBE microscope	Leica
Leica TCS NT confocal	Leica
HBO 50W fluorescent lamp	Leica
TCS NT Vers.1.6.587 program	Leica
Objective HC PL APO 10x/0.40 IMM	Leica
Objective HC PL APO 20x/0.70 IMM CORR	Leica
Objective PL APO 40x/1.25 oil Ph3	Leica
Objective PL APO 63x/1.32 oil Ph3	Leica
Time lapse microscope	
AxioVert 10	Zeiss
MicroMax Camera and Controller	Princeton Instruments
Objective LD-Achroplan 20x/0,40 korr (Phase 2)	Zeiss
Objective LD-A Plan 40x/0,50 (Phase 2)	Zeiss
MetaVue imaging program	Visitron Systems

## 4.13.2 Complex media, buffers and solutions

Name	Protocol
ACSF (artificial cerebro-spinal fluid)	124mM NaCl 3mM KCl 1.25mM KH <sub>2</sub> PO <sub>4</sub> 2mM MgSO <sub>4</sub> ·7H <sub>2</sub> O 26mM NaHCO <sub>3</sub> 2.5mM CaCl <sub>2</sub> 10mM d-glucose in ddH <sub>2</sub> O
ACSF-digestion medium	ACSF 1.3mg/ml Trypsin 0.67mg/ml hyaluronidase 0.2 mg/ml kynurenic acid
Alkaline-phosphatase staining buffer (AP-buffer)	100mM NaCl 50mM MgCl <sub>2</sub> 100mM Tris pH9.5 0.1% tween-20 1mM levamisole in ddH <sub>2</sub> O
AP - NBT/BCIP	AP 350µg/ml NBT 175µg/ml BCIP
Beads stock-solution	50nM beads in 1x PBS
Blocking-solution	MABT 2% blocking reagent 20% heat inactivated sheep serum
BrdU-Solution for cell culture	1mM BrdU in ddH <sub>2</sub> O
BrdU-Solution for <i>i.p.</i> -Injection	5mg/ml (w/v) BrdU in 1x PBS
Dil stock solution	5mg/ml DiI-crystals in ethanol absolute
Dil working dilutions	1:10 – 1:500 Dil stock solution in 300mM sucrose
Di-sodium-tetraborate-buffer (0.1M) pH 8.5	0.1 M Na <sub>2</sub> B <sub>4</sub> O <sub>7</sub> · H <sub>2</sub> O in ddH <sub>2</sub> O
Ethanol-glacial acetic acid	10% (v/v) glacial acetic acid in ethanol absolute
FCS-PS-Medium	10% (v/v) FCS (heat inactivated 30 min. at 56°C) 1% (v/v) Penicillin-Streptomycin in DMEM
HCl (2.4 N)	2.4 N HCl (37 % (w/v)) in ddH <sub>2</sub> O

HEPES-HBSS-Medium	10 mM HEPES in HBSS
Hybridisation buffer	1x salt solution 50% formamide 10% dextran sulfate 1mg/ml wheat germ tRNA 1X Denhardt's solution ddH <sub>2</sub> O
Laemmli buffer (3x)	20% glycerol 3% SDS 10mM EDTA 0.05% bromphenol blue 1% β-mercaptoethanol
LB (Luria-Bertani) medium PH 7.0	20g/l LB broth base in ddH <sub>2</sub> O
LB-agar	LB-medium 15g/l agar
LiCl (4M)	4M LiCl ddH <sub>2</sub> O
Lysis buffer pH 8.5	100mM TrisHCl 5mM EDTA 0.2% SDS 200mM NaCl 100µg/ml proteinase K
MABT (5x) pH 7.5	500mM maleic acid 750mM NaCl 0.1% tween-20 ddH <sub>2</sub> O
NaN <sub>3</sub> -PBS (0.05%)	0.05% (w/v) NaN <sub>3</sub> in 1x PBS
Neurosphere complete medium (embryonic)	DMEM/Nut.Mix.F12 1% (v/v) Penicillin-Streptomycin 3.5mM glucose (additional!) 20ng/ml bFGF 20ng/ml EGF 1x B27-supplement
Neurosphere complete-medium (adult)	DMEM/Nut.Mix.F12 2mM L-glutamine 0.6% (w/v) glucose 9.6 ng/ml putrescine 6.3 ng/ml progesterone 5.2 ng/ml sodium selenite 0.025 mg/ml insulin 0.1mg/ml transferrin 2 µg/ml heparin 20ng/ml FGF2 20ng/ml EGF
Neurosphere ovomucoid-medium	DMEM/Nut.Mix.F12 0.7mg/ml ovomucoid

NP40 (0.1%)	0.1% NP40 (v/v) in 1x PBS
PBS (Phosphate buffered salt solution, 1x) pH 7.4	137 mM NaCl 2.7 mM KCl 80.9 mM Na <sub>2</sub> HPO <sub>4</sub> 1.5 mM KH <sub>2</sub> PO <sub>4</sub> in ddH <sub>2</sub> O
PFA (2%)	2% (w/v) paraformaldehyde in 1x PBS
PFA (4%)	4% (w/v) paraformaldehyde in 1x PBS
Poly-D-lysine-hydrobromide solution	1% (v/v) PDL <sub>solved</sub> (1mg/ml PDL in ddH <sub>2</sub> O o/n solved) in 0.1M sodium-tetraborate buffer
Saline (isoton.)	0.9% (w/v) NaCl in ddH <sub>2</sub> O
Salt solution (10x)	2M NaCl 90mM Tris HCl, pH7.5 10mM Tris base 70mM NaH <sub>2</sub> PO <sub>4</sub> 50mM Na <sub>2</sub> H PO <sub>4</sub> 50mM EDTA ddH <sub>2</sub> O
SATO-medium	DMEM 1g/l Glucose 2mM Glutamine 10µg/ml Insulin (bovine) 100µg/ml Transferrin (human) 0.0286% BSA-pathocyte 0.2µM Progesterone 0.1mM Putrescine 0.45µM Thyroxine 0.224µM Selenite 0.5µM Tri-iodo-thyronine
SDS-page running buffer	25mM TrisBase pH 8.3 192 mM Glycin 0.1% SDS in ddH <sub>2</sub> O
SDS-polyacrylamide gel Resolving gel	30% acrylamide mix (acrylamide-bisacrylamide 30:0.8) 1.5M Tris (pH 8.8) 10% SDS 10% ammoniumpersulfate TEMED ddH <sub>2</sub> O
SDS-polyacrylamide gel Stacking gel	30% acrylamide mix (acrylamide-bisacrylamide 30:0.8) 1.0M Tris (pH 6.8) 10% SDS 10% ammoniumpersulfate TEMED in ddH <sub>2</sub> O

Semidry blotting buffer	48mM Tris 39mM Glycin 1.3mM SDS 20% MeOH in ddH <sub>2</sub> O
Skimmed milk blocking buffer	1x TBS 0.1% Tween-20 5% (w/v) skimmed dry milk
SSC (20x)	3M NaCl 0.3M sodium citrate in ddH <sub>2</sub> O
Sucrose-PBS-solution (30%)	30% (w/v) sucrose in 1x PBS
Sucrose-solution (300mM)	300mM sucrose in ddH <sub>2</sub> O
TBE (10x)	450mM Tris base 440mM boric acid 10mM EDTA in ddH <sub>2</sub> O
TBS (Tris-buffered saline, 10x) pH 7.6	200mM Tris base 1.37M NaCl in ddH <sub>2</sub> O
TBS/T	1x TBS 0.1% Tween-20
TE pH 8.0	10mM TrisHCl 1mM EDTA in ddH <sub>2</sub> O
TE-buffer pH 7.5	10mM TrisHCl 0.1mM EDTA in ddH <sub>2</sub> O
Timelapse-medium	DMEM/Nut.Mix.F12 1% (v/v) Penicillin-Streptomycin 3.5mM glucose (additional!) 20ng/ml bFGF 20ng/ml EGF 1x B27-supplement
Triton X-100 (0.1% / 0.5%)	0.1% / 0.5% (v/v) Triton X-100 in 1x PBS
Tween-20 (0.1% / 0.5%)	0.1% / 0.5% (v/v) Tween-20 in 1x PBS
Washing solution	1xSSC 50% formamide 0.1% tween-20

## 4.13.3 Product list

<b>Name</b>	<b>Supplier</b>
Acrylamide mix Protogel	National diagnostics
Agarose (electrophorase)	Biozym
Agarose high EEO	Biomol
Ammoniumpersulfate (APS)	Sigma
Ampicillin	Sigma
Anti-DIG-FAB-fragments alkaline phosphatase	Roche
Aqua Poly/Mount mounting medium	Polysciences
B27 Supplement (50x)	Gibco
Bacto-Agar	DIFCO Laboratories
BCIP (5-bromo-4-chloro-3-indolyl-phosphate, 4-toluidine salt)	Roche
beta-mercaptoethanol	Merck
BFGF	Sigma
Blocking reagent	Roche
Boric acid	Merck
BrdU (5-Bromo-2-Deoxyuridin)	Sigma
Bromphenol blue	Merck
BSA	Sigma
CaCl <sub>2</sub>	Sigma
CO <sub>2</sub> -Gas	Air Liquide
DAPI (Hoechst 33258)	Pierce
Denhardt's solution	Sigma
Dextran sulfate	Sigma
Diethylether for anesthesia	Hoechst
DIG-RNA labelling mix (10x ; DIG-UTP)	Roche
Dil (1,1'-didodecyl-3,3,3',3'-tetramethylindo-carbocyanine perchlorate)	Molecular Probes
Di-Sodiumhydrogenphosphate Na <sub>2</sub> HPO <sub>4</sub>	Merck
DMEM/Nut.Mix.F12 1:1 v/v	Gibco
DNTP (for PCR)	Pharmacia Biotech
Dulbecco's modified Eagle Medium (DMEM) (with Glutamax-1 (L-Alanyl-L-Glutamin) without Natriumpyruvate with Glucose with Pyridoxin)	Gibco
ECL+plaus westernblot detection system	Amersham Biosciences
EDTA (Titrplex)	Merck
EGF	Sigma
Ethanol absolute (EtOH)	Riedel-deHaën
Fetal Calf Serum (FCS)	Sigma
FGF2	Preprotech

Formamide	Merck
Geneticin (G418-sulfate)	Gibco
Gentamycin	Gibco
Glacial acetic acid (99,8 % w/v)	Merck
Glucose (d-glucose)	Merck
Glycerol (87%)	Merck
Glycin	Sigma
Hank's buffered salt solution (HBSS)	Gibco
Heat inactivated sheep serum	Sigma
Heparin sodium salt, grade II	Sigma
HEPES-Buffersolution 1 M, pH 7,2 - 7,5	Gibco
HotStarTaq-Ploymerase	Quiagen
HRP-conjugated secondary anti-mouse antibody	Amersham LifeScience
Hyaluronidase 2000 unit/mg	Sigma
Hydrochloric acid (37 %) HCl	Merck
Immersion oil 518N	Zeiss
Insulin	Sigma
Isopropanol	Merck
Kaliumchloride KCl	Merck
Kaliumdihydrogenphosphate $\text{KH}_2\text{PO}_4$	Merck
Kynurenic acid	Sigma
LB broth base	Gibco
Levamisole	Sigma
l-glutamine (200mM)	Gibco
LiCl	Merck
Maleic acid	Fluka
Methanol absolut (MeOH)	Merck
$\text{MgCl}_2$	Merck
$\text{MgSO}_4 \cdot 7\text{H}_2\text{O}$	Merck
MidiPrep-Kit	Quiagen
MidiTip 100 column	Quiagen
Molecular weight marker (1kb-ladder)	Gibco
Molecular weight marker (rainbow marker)	Amersham PharmaciaBiotech
MoMLV reverse transcriptase	Roche
NaCl	Merck
$\text{NaH}_2\text{PO}_4$	Merck
$\text{NaHCO}_3$	Merck
$\text{NaN}_3$ (pure)	Merck
Natriumtetraborate (Borax) $\text{Na}_2\text{B}_4\text{O}_7 \cdot \text{H}_2\text{O}$	Sigma
NBT (Nitroblue tetrazolium chloride)	Roche

Normal goat serum (NGS)	Boehringer Ingelheim (Vector Laboratories)
NP40 – Igepal	Sigma
Oligo(dT)12-18 primers	Roche
Ovomucoid	Sigma
Paraformaldehyde (PFA)	Merck
PCR-buffer (10x)	Quiagen
Penicillin/Streptomycin-Solution 10 000 E Penicillin, 10 0000 µg/ml Streptomycin, as PenicillinG (Sodiumsalt) & Streptomycinsulfate	Gibco
Phenol-chloroform-isoamylalcohol (50:49:1)	Gibco
Poly-D-Lysine Hydrobromide (PDL)	Sigma
Polyoxyethylenesorbitanmonolaurate (Tween-20)	Biorad
Progesterone	Sigma
Propidium-iodide (PI)	Sigma
Proteinase K	Roche
Putrescine	Sigma
PVDF-membrane HybondECL	Amersham LifeScience
Q-Solution (5x)	Quiagen
Red fluorescent RetroBeads™ (Beads)	Lumafuor
Restriction enzymes	New England Biolabs
RNA polymerase 50U/µl (T3, T7, SP6)	Stratagene
RNase A	Quiagen
RNase inhibitor	Boehringer Mannheim
RNeasy Kit	Quiagen
RT-PCR Enzyme Mix	Roche
RT-PCR Reaction Mix SYBR green	Roche
SDS/Natriumlaurylsulfat	Roth
Selenite	Sigma
Skimmed dry milk	Glücksklee
Sodium citrate	Merck
Sodium selenite	Merck
Sodiumacetate	Merck
Sucrose	Merck
Taq-DNA-Polymerase	Quiagen
TEMED	Pharmacia Biotech
Thyraxine	Sigma
Top10 cells	Invitrogen living Science
Transcription buffer (5x)	Stratagene
Transferrin	Sigma

Tri-iodo-thyronine	Sigma
TrisBase	Merck
TrisHCl	Merck
Triton X-100	Roth
Trypsin Type XII, 9000 BASF units/mg	Sigma
Trypsin-EDTA (1x) 0,05 % (w/v) Trypsin in HBSS without Ca <sup>2+</sup> , Mg <sup>2+</sup> with 0,02 % (w/v) EDTA (4Na)	Gibco
Wheat germ tRNA	Sigma
Yo-Pro-1	MoBiTec

#### 4.13.4 Consumables

Name	Supplier
Cell culture dishes, sterile (100-, 200 mm)	Falcon
Cell culture flasks (75-, 175 cm <sup>2</sup> )	Falcon
Cell culture tubes, sterile (15-, 50 ml)	Falcon
Colour slide film Elite Chrome 100	Kodak
Colour slide film Fujichrome 1600 Professional	Fujifilm
Coverslips 24 x 24 mm	Marienfeld
Coverslips 24 x 50 mm	Marienfeld
Coverslips Ø 13 mm, autoclaved	BDH
Eppendorf tubes (0.5-, 1.5-, 2.0 ml)	Eppendorf
Glass slides 76 x 26 mm, frosted end	Menzel Gläser
Glass slides Superfrost <sup>®</sup> -Plus 76 x 26mm	Menzel Gläser
Multi-well cell culture-plates, sterile (6-, 24-, 48-wells)	Nunc
Parafilm	American National can
Pasteur pipettes, autoclaved	Volac
PCR-tubes (0.2ml)	Roth
Permeable filtermembrane inserts Millicell-CM (0,4µm pore, 30mm diameter)	Millipore
Pipettes, sterile (5-, 10-, 25 ml)	Falcon
Razor blades, extra thin, Rotbart	Gillette
Superglue	UHU
Syringe filters 0.45µm	Renner
Syringe needles (Neolus, 0,4mm)	Terumo
Syringe - fine dosage (1ml)	Braun
Syringes (10-50ml)	Becton Dickinson
Whatman chromatography paper	Whatman
X-ray films	Kodak

## 4.13.5 Instruments

Name	Supplier
Agarose gel chambers	MPI-workshop
Bakterial incubator	Heraeus
Bakterial shaker Innova 4000	New Brunswick Scientific
Bench centrifuge 5415 C	Eppendorf
Cell culture incubator	Heraeus
Cooling centrifuge Sepatech Omnifuge 2.0 RS	Heraeus
Cryostate CM 3050	Leica
FACSort	Beckton Dickinson
FACSVantage	Beckton Dickinson
Forceps Dumont #5 'Biologie' (0,05 x 0,01) mm	Fine Science Tools
Heating block	Liebisch
Hybridisation oven	Memmert
Hybridisation oven HB-1000 Hybridizer (for DNA lysis)	UVP Laboratory Products
Lightcycler	Roche
Neubauer-counting chamber improved bright-line (depth 0,100 mm/0,0025 mm <sup>2</sup> )	Superior
Orbital shaker KS 500,	Janke & Kunkel
Phase contrast microscope Diavert	Leitz
Pneumatic pico pump PV820 ()	WPI
Power supply	Biorad
Preparation lights KL1500 electronic	Leica
Semibry blotting chamber	MPI-workshop
Sorvall RC-5B refrigerated superspeed centrifuge	DuPont Instruments
Spectrophotometer, Ultrospec 3000	Pharmacia Biotech
Stereomicroscope, Wild M3Z	Heerbrugg
Stereomicroscope, Wild M8,	Leica
Steril hood "Edge Gard Hood"	The Baker Company
Steril hood Class II Typ A/B3	Nuaire Biological Safety Instruments
Tissue chopper	Mickle Laboratory Engineering
Vibratome Vibraslice 752M	Campden Instruments
Waterbath	GFL
Waterbath for in-situ	GFL
Western-blotting chamber	Biorad

## 5. RESULTS

### 5.1 Immunohistochemical analysis in sections of the telencephalon

To detect a possible heterogeneity in the radial glial cell population, which might serve the dual role of providing a static guiding scaffold for migrating neurons and being a dividing precursor cell, we first analysed the developmental pattern of the putative radial glial markers RC2, anti-GLAST and anti-BLBP in sections of the telencephalon from embryonic day (E) 12 to postnatal day (P) 6 mice. The antibodies RC2 (mouse monoclonal), anti-BLBP (rabbit polyclonal) and anti-GLAST (guinea pig polyclonal) were combined in double-stainings for two-channel confocal analysis (see methods). As described previously (Misson *et al.* 1988a; Feng *et al.* 1994; Kurtz *et al.* 1994; Shibata *et al.* 1997), all three antibodies labelled radial cells with somata in the ventricular zone and radial processes reaching the pial surface (Fig. 5.1A-C). Strongly RC2-immunoreactive radial cells were observed from the earliest stages analysed (E12), whereas GLAST and BLBP appeared at this time in a ventral to dorsal sequence. At E12, for example, radial glial cells in the ganglionic eminence (GE) were stronger immunoreactive for BLBP and GLAST than their counterparts in the cortex.

The co-localization analysis of RC2, GLAST and BLBP revealed that most cells contained all three antigens and only some lacked BLBP- or GLAST-immunoreactivity: while all BLBP-positive cell somata in the ventricular zone (VZ) were also RC2- and GLAST-immunoreactive, not all RC2- or GLAST-positive somata contained as well BLBP (data not shown). Likewise, BLBP-positive radial processes in the cortical plate were double-labelled with RC2- or GLAST-antiserum in all cases analysed (Fig. 5.1D), but some RC2- or GLAST-immunoreactive radial processes were BLBP-negative (Fig. 5.1D). This co-localization analysis therefore suggests heterogeneity amongst radial glial cells such that GLAST and BLBP are contained in subpopulations of RC2-positive radial glial cells. It is important to note that all three antibodies also labelled tangentially oriented cells with a non-radial morphology (Fig. 5.1D, arrowheads). These cells were detected already at E14 with a ventral to dorsal gradient (Fig. 5.1E) and increased strongly in number during further development (Fig. 5.1F). Double-labelling with AN2-antiserum indicated that these cells might include oligodendrocyte precursors (data not shown, Niehaus *et al.* 1999).

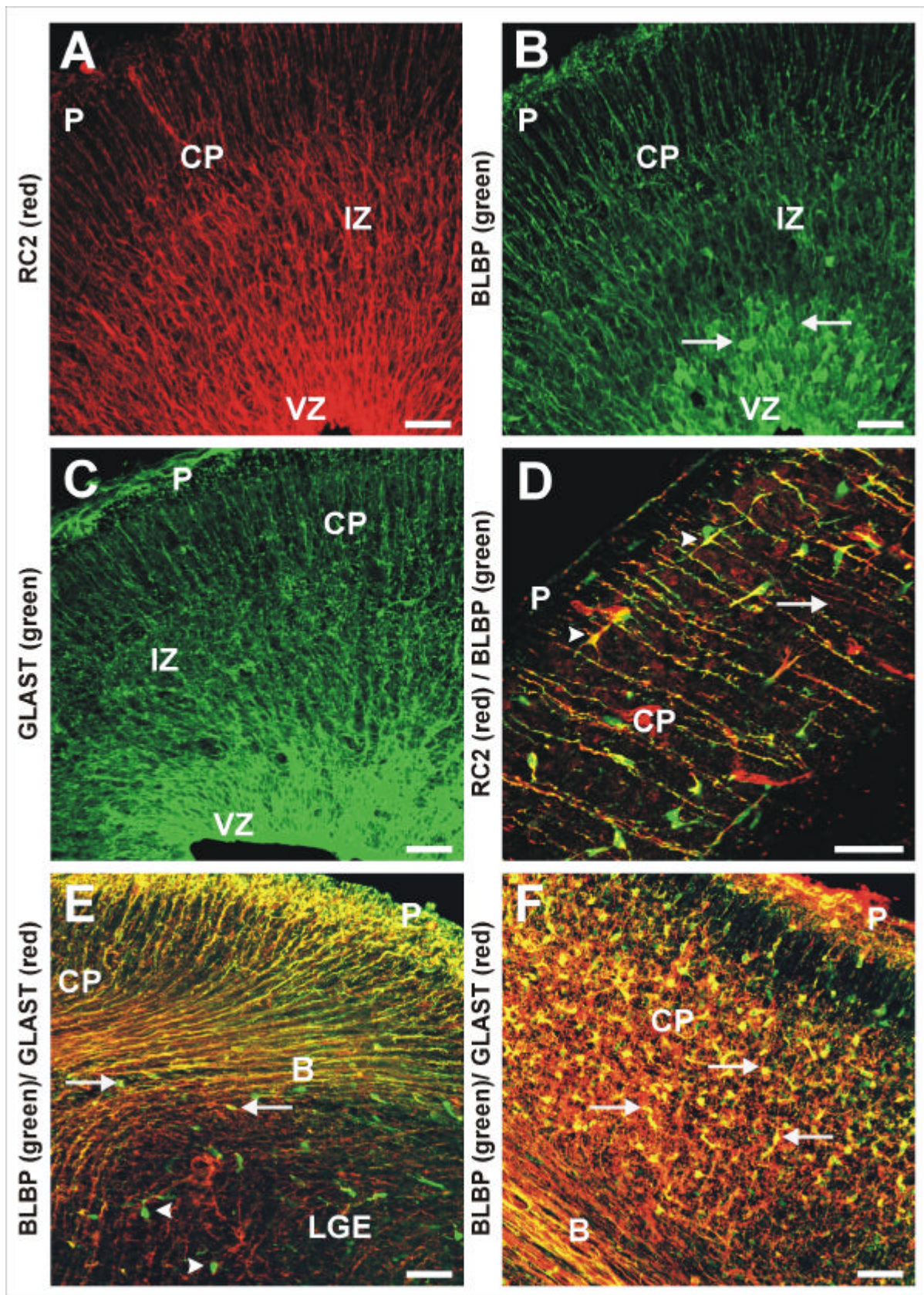


Figure 5.1 Staining of cortex sections with radial glial markers.

### Figure 5.1 Staining of cortex sections with radial glial markers.

Fluorescent micrographs of frontal (A, B, D, E, F) and horizontal sections (C) of embryonic day E16 (A, B, D), E15 (C), E14 (E) and postnatal day P2 (F). Sections were stained with the antibodies indicated in the figure. Note that all three antigens label radial glial cells (arrow in D), but also other, morphologically distinct cell types (arrowhead in D, arrows in E, F). Note the increase in the non-radial GLAST/BLBP+ cells during development in the cortex (F). RC2 gives a filament-like staining (A, D), GLAST is localized in the cell membranes and BLBP is contained in the cytoplasm and hence best shows cell somata in the ventricular zone (arrows in B). D depicts an example of RC2 and BLBP co-localization in radial processes. Processes double-labelled with RC2 and BLBP appear yellow in D, processes labelled only by RC2-antiserum are red (arrow). Note that RC2, anti-GLAST and anti-BLBP label radial glial cells and most, but not all, processes appear double-labelled. All panels are confocal pictures, A-C and E-F are maximum intensity images (superimposition of 10-15 optical sections), whereas D is a superimpositions of 2-3 single optical sections. VZ: ventricular zone, IZ: intermediate zone, CP: cortical plate, LGE: lateral ganglionic eminence, P: pial surface, B: boundary. Scale bar: 50µm. (A,B,D-F adapted from Hartfuss 1998)

## 5.2 Immunocytochemical analysis of acutely dissociated cells

In order to discriminate between a cellular heterogeneity and an in-homogeneity in antigen distribution along the radial processes, we used acutely dissociated cell preparations (Luskin *et al.* 1997; Götz *et al.* 1998) as illustrated in Fig. 5.2 and 5.3 and described in the methods.

### 5.2.1 Characterization of acutely dissociated cells

To assess the validity of this preparation we examined the developmental profile of precursor cells and postmitotic neurons (Table 5.1). The proportion of neurons (immunoreactive for  $\beta$ -tubulin-III) increased while the proportion of precursor cells (immunoreactive for Ki67 or nestin) decreased during development as expected (Table 5.1). Neither nestin- nor Ki67-staining was detected in  $\beta$ -tubulin-III-positive cells, indicating that these antisera specifically label non-overlapping populations that would be expected to be postmitotic neurons ( $\beta$ -tubulin-III+) and precursor cells (Ki67+, nestin+). Indeed, the proportions of Ki67+ and nestin+ cells are almost identical (Table 5.1) and double staining showed that these antigens are almost completely co-localized from E12 to E16. To examine whether Ki67- and nestin- antisera label actively dividing precursor cells we also performed cumulative BrdU-labelling experiments as described by Nowakowski *et al.* (1989). BrdU was injected in two-hour intervals for the duration of 12 hours (see methods) thereby covering the cell cycle length of cortical precursors at E14 (Nowakowski *et al.* 1989). Almost all (cortex: 99%, n=108; GE: 100%, n=124) Ki67-positive cells were BrdU-immunoreactive in these experiments (Fig. 5.2).

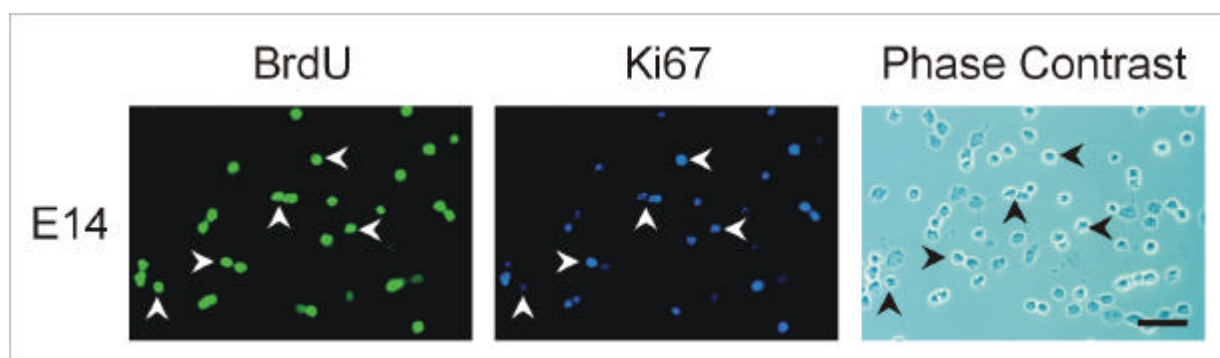


**Figure 5.2 Cumulative BrdU-labelling**

Acutely dissociated cells from E14 cerebral cortex after cumulative BrdU-labelling. Note that almost all Ki67-immunoreactive cells also contain BrdU (arrowheads), indicating that Ki67 is a high fidelity marker of actively dividing precursors. Scale bar 50 $\mu$ m.

This demonstrates that Ki67 is a high fidelity marker of dividing precursor cells in the developing telencephalon and that no quiescent subpopulation of precursor cells (Ki67-immunopositive, BrdU-negative in the cumulative labelling) is detectable during the stages analysed. Moreover, the numbers of neurons and precursor cells obtained in our analysis are in good agreement with previous quantitative data on neurons and precursor cells obtained by fluorescent-activated cell sorting (Maric *et al.* 1997).

**Table 5.1 Percentage of cell types during the development of the telencephalon**

	E12	E14	E16	E18
<b>Cortex</b>				
<b>Ki67</b>	77 ? 3 (n=2)	56 ? 3 (n=31)	30 ? 2 (n=13)	16 ? 2 (n=10)
<b>Nestin</b>	79 ? 2 (n=9)	57 ? 3 (n=12)	30 ? 3 (n=8)	16 ? 2 (n=11)
<b>Tubulin</b>	23 ? 3 (n=9)	53 ? 4 (n=3)	59 ? 3 (n=6)	52 ? 6 (n=4)
<b>RC2</b>	82 ? 2 (n=21)	52 ? 2 (n=49)	28 ? 1 (n=40)	11 ? 1 (n=26)
<b>GLAST</b>	44 ? 2 (n=16)	46 ? 2 (n=47)	33 ? 1 (n=33)	21 ? 2 (n=24)
<b>BLBP</b>	30 ? 3 (n=13)	31 ? 2 (n=55)	27 ? 1 (n=36)	25 ? 2 (n=28)
<b>GE</b>				
<b>Ki67</b>	62 ? 8 (n=2)	60 ? 3 (n=25)	46 ? 2 (n=11)	34 ? 3 (n=10)
<b>Nestin</b>	67 ? 3 (n=9)	54 ? 3 (n=12)	42 ? 3 (n=9)	24 ? 3 (n=8)
<b>Tubulin</b>	40 ? 3 (n=6)	51 ? 4 (n=4)	62 ? 2 (n=5)	43 ? 8 (n=4)
<b>RC2</b>	69 ? 3 (n=17)	48 ? 2 (n=46)	35 ? 2 (n=28)	19 ? 1 (n=26)
<b>GLAST</b>	41 ? 2 (n=12)	33 ? 1 (n=35)	31 ? 2 (n=28)	19 ? 1 (n=24)
<b>BLBP</b>	24 ? 3 (n=7)	24 ? 1 (n=37)	25 ? 2 (n=32)	23 ? 2 (n=30)

*Note.* The percentage of immunoreactive acutely dissociated cells from the cortex and ganglionic eminence is indicated for different developmental stages (E12–18). Ki67 and nestin labels precursor cells, tubulin ( $\beta$ III) postmitotic neurons, and RC2, GLAST (astrocyte-specific glutamate transporter), and BLBP (brain lipid-binding protein) are contained in radial and non-radial precursor cells (see text). The number of coverslips analysed is indicated by (n), derived from different batches: E12: 4; E14: 12; E16: 7; E18: 3.  $\pm$ , standard error of the mean (SEM).

### 5.2.2 Co-localization of RC2, GLAST and BLBP in acutely dissociated cells

To further assess the distribution of the radial glial antigens RC2, GLAST and BLBP and to elucidate a putative heterogeneity of the radial glial population we performed triple-labelling in acutely dissociated cell preparations of the dorsal and ventral telencephalon from E12 till E18. The quantitative developmental analysis of RC2-, GLAST- and BLBP-immunoreactive cells showed a decrease in the RC2-immunoreactive cells during development that closely matched the percentage of proliferating cells (Table 5.1). In contrast, GLAST- and BLBP-antisera labelled a smaller proportion of cells than RC2 at early developmental stages, but increased during development. The developmental profile of these markers was well comparable between cortex and GE. The co-localization analysis demonstrated a clear heterogeneity of acutely dissociated telencephalic cells in their RC2-, GLAST- and BLBP-immunoreactivity (Fig. 5.3), suggesting that not only a variation of the intracellular antigen distribution is the reason for the heterogeneity observed in sections.

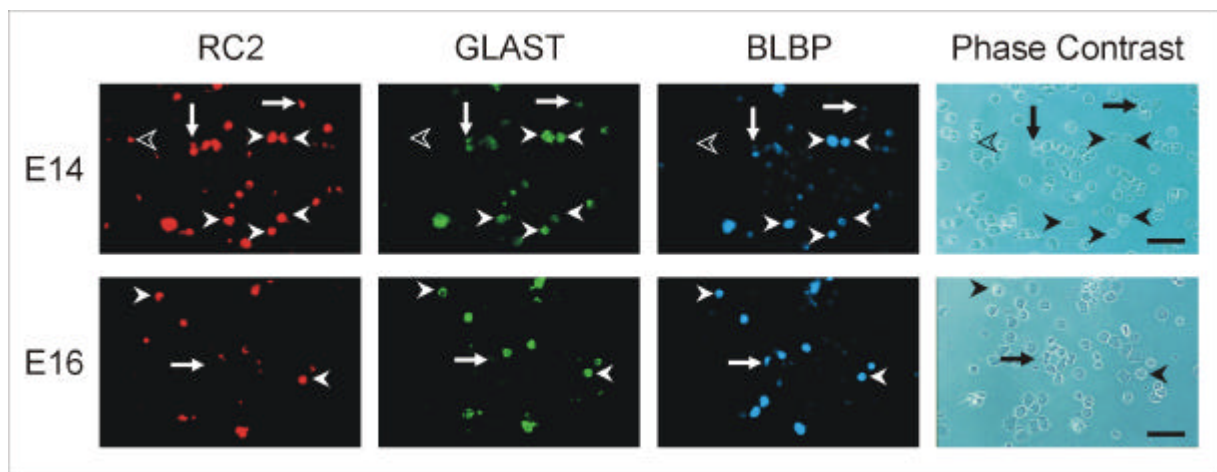


**Figure 5.3 Co-localization of RC2, GLAST and BLBP in acutely dissociated cortical cells.**

Acutely dissociated cortical cells from embryonic day E14 and E16 cortex (as indicated) were triple-stained with the antisera RC2, GLAST and BLBP (as indicated). Filled arrowheads depict triple-, arrows double- and empty arrowheads single-labelled cells, respectively. E14 cortical cells are heterogeneous and contain RC2+ (empty arrowhead), RC2/GLAST+ (arrows) and RC2/GLAST/BLBP+ cells (filled arrowheads). This heterogeneity decreases during development when more cells are triple-labelled (E16) and GLAST/BLBP+ cells (arrows in B, E16) can be detected. (For quantification, see Table 5.2.) Thus, radial glial cells are heterogeneous in their RC2-, GLAST- and BLBP-content, as also detected in sections (Fig. 5.1). Scale bar: 50µm. (adapted from Hartfuss 1998).

In total, five distinct populations (out of 7 possible, not considering the cells negative for all three markers) were detected of which up to four co-existed simultaneously (Table 5.2). The same subsets were observed in the cortex and GE with some quantitative and developmental differences (Table 5.2).

**Table 5.2 Co-localization analysis of the radial glial markers RC2, GLAST, and BLBP in the Cortex and the ganglionic eminence (GE)**

	<b>E12</b>	<b>E14</b>	<b>E16</b>	<b>E18</b>
<b>Cortex</b>				
<b>RC2-only</b>	25%	8%	0%	0%
<b>RC2/GLAST</b>	26%	22%	5%	0%
<b>RC2/GLAST/BLBP</b>	25%	27%	22%	14%
<b>RC2/BLBP</b>	9%	0%	0%	0%
<b>GLAST/BLBP</b>	0%	0%	5%	7%
<b>GE</b>				
<b>RC2-only</b>	20%	10%	6%	0%
<b>RC2/GLAST</b>	19%	10%	5%	5%
<b>RC2/GLAST/BLBP</b>	21%	22%	21%	13%
<b>RC2/BLBP</b>	5%	0%	0%	0%
<b>GLAST/BLBP</b>	0%	0%	4%	6%

*Note.* The percentage of single-, double-, and triple-immunoreactive cells of all phase-bright cells is depicted for acutely dissociated cells from cortex and ganglionic eminence (GE) at the developmental stages indicated. (*n*) depicted in Table 5.1

In addition, in other regions of the CNS, such as the hippocampus (HC), the olfactory bulb (OB), the dorsal and ventral midbrain (MB) and the spinal cord (SC), the co-localization of the radial glial markers revealed the same subsets with quantitative differences as in the developing telencephalon (Table 5.3). Interestingly, the observed quantitative differences between the analysed brain regions might reflect differences in the developmental maturation since development follows a ventral to dorsal and caudal to rostral gradient in the CNS.

**Table 5.3 Co-localization analysis of the radial glial markers RC2 and BLBP**

	<b>Ctx</b>	<b>LGE</b>	<b>MGE</b>	<b>HC</b>	<b>OB</b>	<b>v-MB</b>	<b>d-MB</b>	<b>SC</b>
<b>RC2-only</b>	25%	30%	32%	33%	18%	10%	10%	13%
<b>RC2/BLBP</b>	30%	30%	30%	32%	45%	13%	6%	17%
<b>BLBP</b>	0%	0%	6%	5%	5%	6%	5%	19%

*Note.* The percentage of single- and double-immunoreactive cells of all phase-bright cells is depicted for acutely dissociated cells from E14 cortex (Ctx), medial ganglionic eminence (MGE), lateral ganglionic eminence (LGE), hippocampus (HC), ventral midbrain (v-MB), dorsal midbrain (d-MB) and spinal cord (SC). (*n*) for each area a total of 3 coverslips was analysed.

### 5.2.3 Analysis of the precursor pool

Furthermore, we wanted to examine the overall contribution of radial glial cells to the progenitor pool by means of their cytochemical characteristics. We therefore assessed the portion of the RC2-, GLAST- and BLBP-immunoreactive cells within the precursor population by double- and triple-labelling with Ki67- and/or nestin-antisera (see methods for further details). Almost all RC2-, GLAST- or BLBP-immunoreactive cells co-localized with the precursor cell markers Ki67 and nestin and did not contain  $\beta$ -tubulin-III. Thus, only precursor cells express RC2-, GLAST and BLBP during neurogenesis (E12 - E17 in the cortex). This allowed us to use triple-immunostaining with RC2-, GLAST- and BLBP-antisera to determine the subtypes of precursor cells containing these markers. While at E12 almost all Ki67- and/or nestin-positive cells were immunoreactive for RC2, and subsets for GLAST and BLBP, at E14 a notable proportion of precursors was not immunoreactive for RC2. Since GLAST- and BLBP-immunoreactive cells are contained within the RC2-positive cell-pool at this stage (Table 5.2 and methods), it can be concluded that some cortical progenitors (12%) were immuno-negative for all three radial glial markers (Ki67-only, Fig. 5.4). However, this population was not detected at other developmental stages in the cortex (for staining details see methods). In contrast, GE precursor cells contained a prominent population of RC2-negative cells comprising about a quarter to a third of all progenitor cells (Fig. 5.4). Using the total number of precursor cells (Ki67-positive cells, Table 5.1), the percentage of Ki67-only precursor cells and the percentages of the different RC2-, and/or GLAST- and/or BLBP-immunoreactive populations from the RC2/GLAST/BLBP-triple-stainings (Table 5.2), we calculated the composition of the precursor pool as depicted in Fig. 5.4.

The composition of the progenitor pool changed during development with some populations detected only during neurogenesis and others only during gliogenesis (Fig. 5.4). This correlation was particularly clear in the developing cortex where the last neurons are generated around E17 (Bayer and Altman 1991). The precursor heterogeneity in the cortex was larger during neurogenesis when four subpopulations were detected in contrast to the phase of gliogenesis when only two populations comprised the dividing progenitor pool. The precursor subtypes at the onset of neurogenesis (E12) were the RC2+, RC2/BLBP+, RC2/GLAST+ and RC2/GLAST/BLBP+ cells. Three of these populations were restricted to the phase of neurogenesis (E12-E16, Fig. 5.4) and were no longer detected at E18, the phase of

gliogenesis in the cerebral cortex. In contrast, the RC2/GLAST/BLBP+ cells persisted throughout neuro- and gliogenesis and increased from 30% at E12 to 70% at E18 (Fig. 5.4). The GLAST/BLBP+ cells appeared in correlation to the phase of gliogenesis and became prominent amongst E18 cortical progenitors.

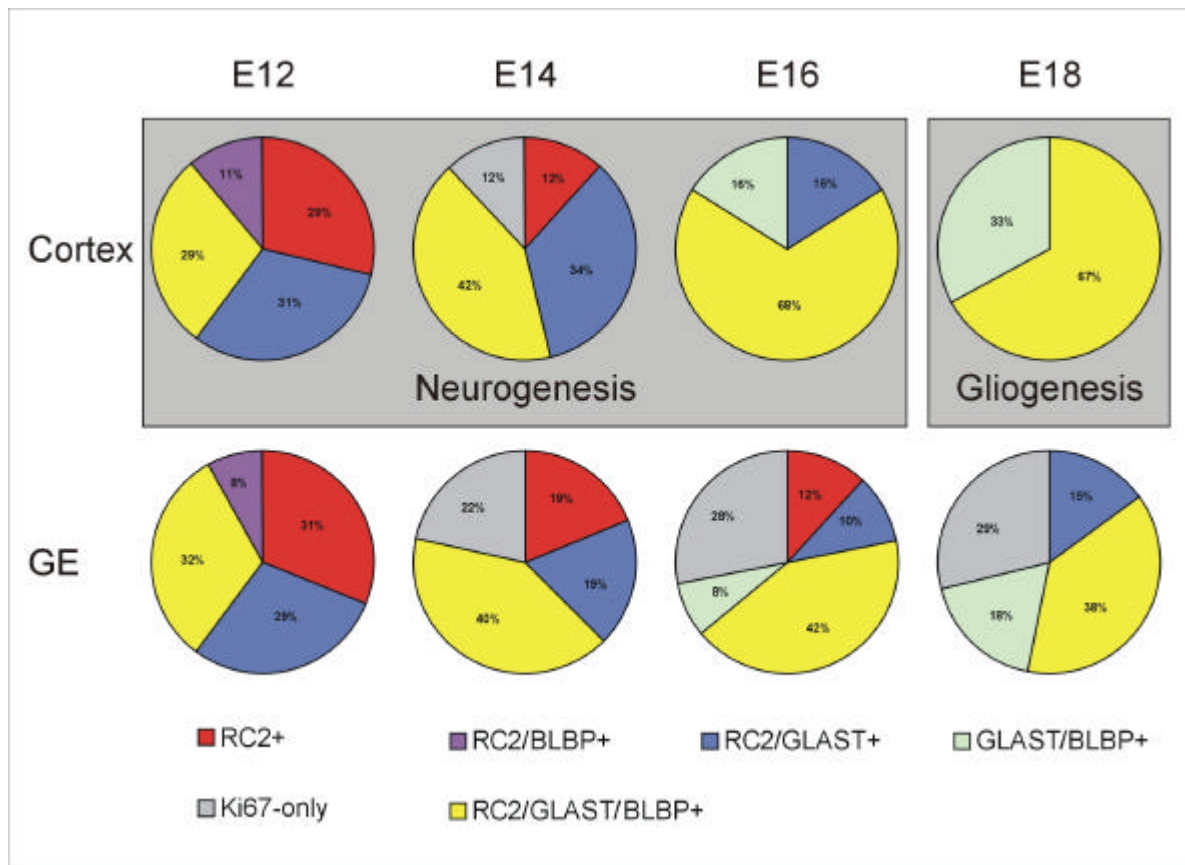


**Figure 5.4 Composition of telencephalic precursor cells during embryonic development**

Co-localization analysis using RC2, GLAST and BLBP was performed for cells from the cortex or the ganglionic eminence (GE). Distinct precursor populations can be detected, some of which are restricted to specific developmental stages. In the cortex, RC2+, RC2/BLBP+ and RC2/GLAST+ cells are restricted to the phase of neurogenesis (E12-17), whereas the appearance of GLAST/BLBP+ cells coincides with the onset of gliogenesis. The composition of precursor cells of the cortex and GE is very similar at early stages, but diverges during further development (see also results).

The composition of precursor cells in the GE and cortex was almost identical at E12, but increasingly diverged as development proceeded (Fig. 5.4). The main difference between GE and cortex was the persistence of the RC2/GLAST-positive and the RC2/GLAST/BLBP-negative precursor cells in the GE. By E18, these subsets had disappeared in the cortex whereas they still constituted 44% (Ki67-only 29%, RC2/GLAST+ 15%) of the progenitor pool at this stage in the GE (Fig. 5.4). This is intriguing in regard to the prolonged neurogenesis in parts of the GE (Luskin 1993; Lois and Alvarez-Buylla 1994; Luskin *et al.* 1997; Doetsch *et al.* 1999). These data therefore show a correlation of RC2-positive, but BLBP-negative precursor cells

to the phase of neurogenesis in the embryonic telencephalon, and excitingly, that the population of cells immunoreactive for the radial glial markers covers almost the entire precursor pool of the cerebral cortex. This suggests either that indeed radial glial cells are the major precursor cell type during neurogenesis or that the putative radial glial markers are not specific.

### 5.3 Antigenic profile of identified precursor populations

#### 5.3.1 Precursors with specific progeny

To examine a potential correlation between these markers and the fate of the progeny we next analysed functionally identified precursor subsets in regard to their antigenic profile. As described above, BLBP increases during development inversely correlated to the phase of neurogenesis. To examine whether the increase in BLBP-immunoreactivity is a general developmental feature, we analysed a region in the postnatal brain, the rostral migratory stream (RMS) that still contains neuronal precursors into adulthood (Luskin 1993; Menezes *et al.* 1995). In contrast, only glial cells divide at these stages in the surrounding telencephalon. Interestingly, BLBP-immunoreactive cells were mostly located outside or at the border of the RMS in sections of the postnatal telencephalon (Fig. 5.5A,B). In contrast, RC2-staining was detected mostly inside the RMS and co-localized with Ki67-positive, supposedly neuronal precursor cells (Fig. 5.5C). To determine whether the BLBP-positive cells present at the border of the RMS were dividing we carefully examined whether these cells co-localized with BrdU (1 hour pulse-labelling). Very few double-positive cells could be detected, i.e. the BLBP-positive cells along the border of the RMS seem to divide rarely or not at all. These data show that the acquisition of BLBP and the loss of RC2 is not a general developmental feature, since one distinct region in the postnatal forebrain, the RMS, is mostly devoid of BLBP- and maintains RC2-antigenicity. Moreover, the dividing cells present in the RMS mostly contain the RC2-antigen, and only rarely BLBP. The BLBP-immunoreactive cells of the RMS might therefore represent the as 'glial tubes' or 'glial slings' described glial cells in the RMS that are sheathing and guiding the neuroblasts during their tangential migration (Doetsch and Alvarez-Buylla 1996; Lois *et al.* 1996; Peretto *et al.* 1997). Thus, it appears as if the neurogenic precursors of the RMS remain BLBP-negative also in the postnatal brain.

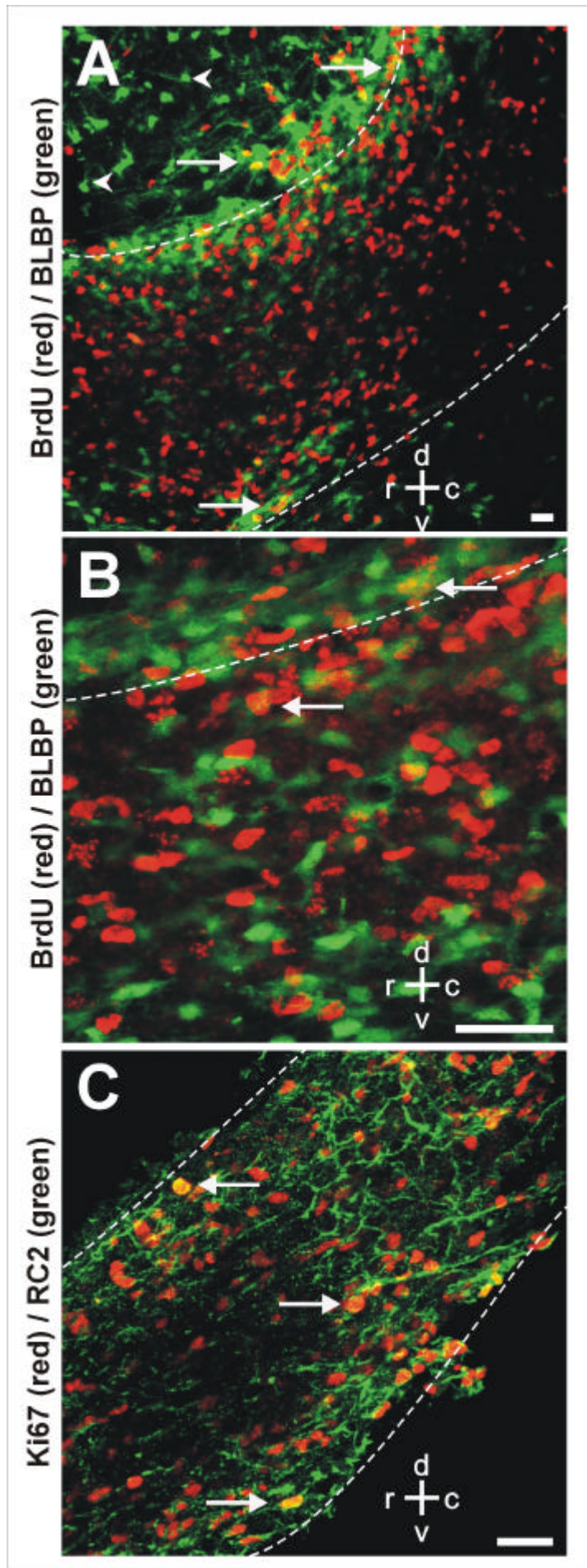


### Figure 5.5. Antigenic profile of precursor cells in the rostral migratory stream

Panel A-C depict fluorescent micrographs of sagittal vibratome sections of the olfactory bulb stained with antisera as indicated in the figure. A and B are maximum intensity images, whereas C is a single optical section image taken at postnatal day 5 (A, B) and 6 (C). Dashed lines delineate the rostral migratory stream (RMS). Note that most BLBP-immunoreactive cells (arrows and arrowheads) are located outside the RMS (A), while BrdU-pulse-labelled precursor cells reside mostly inside the RMS. Panel B depicts a high power view of the border of the RMS where BLBP- and BrdU-staining overlaps. Only some BLBP-positive cells are double-labelled with BrdU along the border of the RMS (arrows in A and B), whereas most BrdU-positive cells are not BLBP-immunoreactive. Complementary to the BLBP-staining, RC2-immunoreactivity is mostly confined to the RMS (C) and many RC2/Ki67-double-positive cells (arrows) can be observed. Thus, most precursors of the RMS are RC2-positive, but BLBP-negative. Sections are oriented as indicated in the figure. d: dorsal, v: ventral, c: caudal, r: rostral. Scale bar: 50µm

In a second approach, we examined the marker-profile of cells derived from embryonic or adult cortical neurospheres (see methods) as a model of an enriched population of multipotent cells (see e.g. Reynolds *et al.* 1992; Gritti *et al.* 1996). When cells of neurospheres after several passages were dissociated and fixed few hours after plating, 95% of the cells were immunoreactive for RC2, GLAST and BLBP (Fig. 5.6; observations by N.Heins and M.Götz).

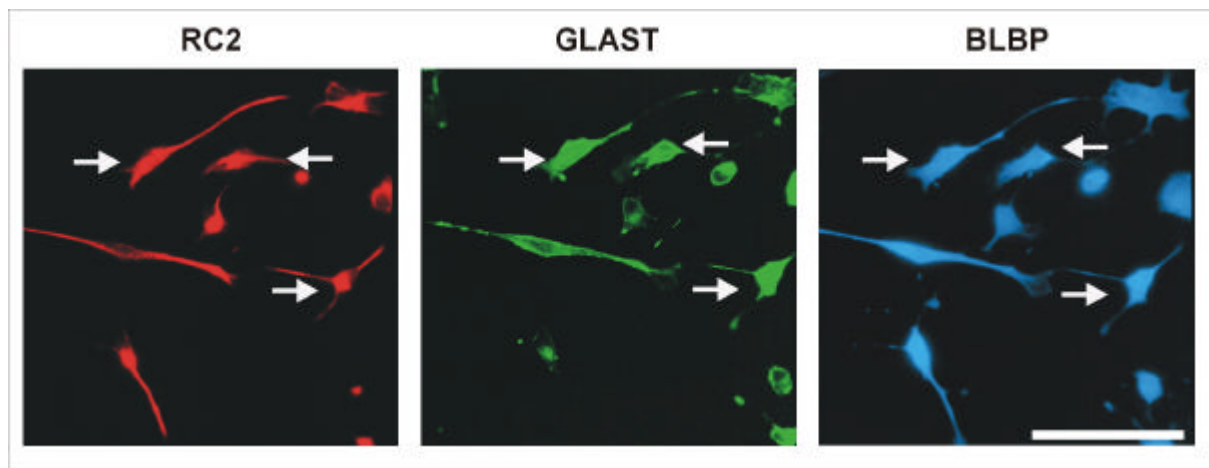


**Figure 5.6 Antigenic profile of neurosphere cells**

Acutely dissociated neurosphere cells from the adult telencephalon were triple-stained with the antisera as indicated. Note that almost all cells are RC2/GLAST/BLBP+ (arrows). Thus, the antigenic profile of neurosphere cells differs from the staining pattern of precursors in the RMS. Scale bar: 50µm

Since multipotent cells in the adult SVZ comprise astrocytes or astrocyte-like cells (Doetsch *et al.* 1999), we also analysed the staining profile of astrocytes purified from postnatal cortex after several passages *in vitro* (see methods). Almost all GFAP-positive astrocytes were also immunoreactive for GLAST and BLBP, but only few were RC2-positive (data not shown; observations by M.Öcalan and M.Götz). This staining profile is consistent with our results obtained in sections demonstrating multipolar GLAST/BLBP+ cells throughout the postnatal cortex (Fig. 5.1F), suggesting that these cells are astrocyte precursors or differentiating astrocytes.

Taken together, these data correlate the antigenic profile of precursor cells to a specific fate of the progeny. Furthermore, these experiments show that the so-called radial glial markers RC2, BLBP and GLAST do not only detect radial glial cells, but label as well cells with a distinct morphology. We therefore can conclude that these markers are not radial glia specific.

### 5.3.2 Precursors identified by transcription factors

Precursor cells in the  $\mathcal{G}\mathcal{E}$  are characterized by a sequence of transcription factor expression (Torii *et al.* 1999). First, cells are Mash1-negative, then become Mash1-positive at the transition between VZ and SVZ (Fig. 5.7), and later lose Mash1 while they turn on Prox1 between the SVZ and the mantle zone where the differentiating neurons reside (Torii *et al.* 1999).

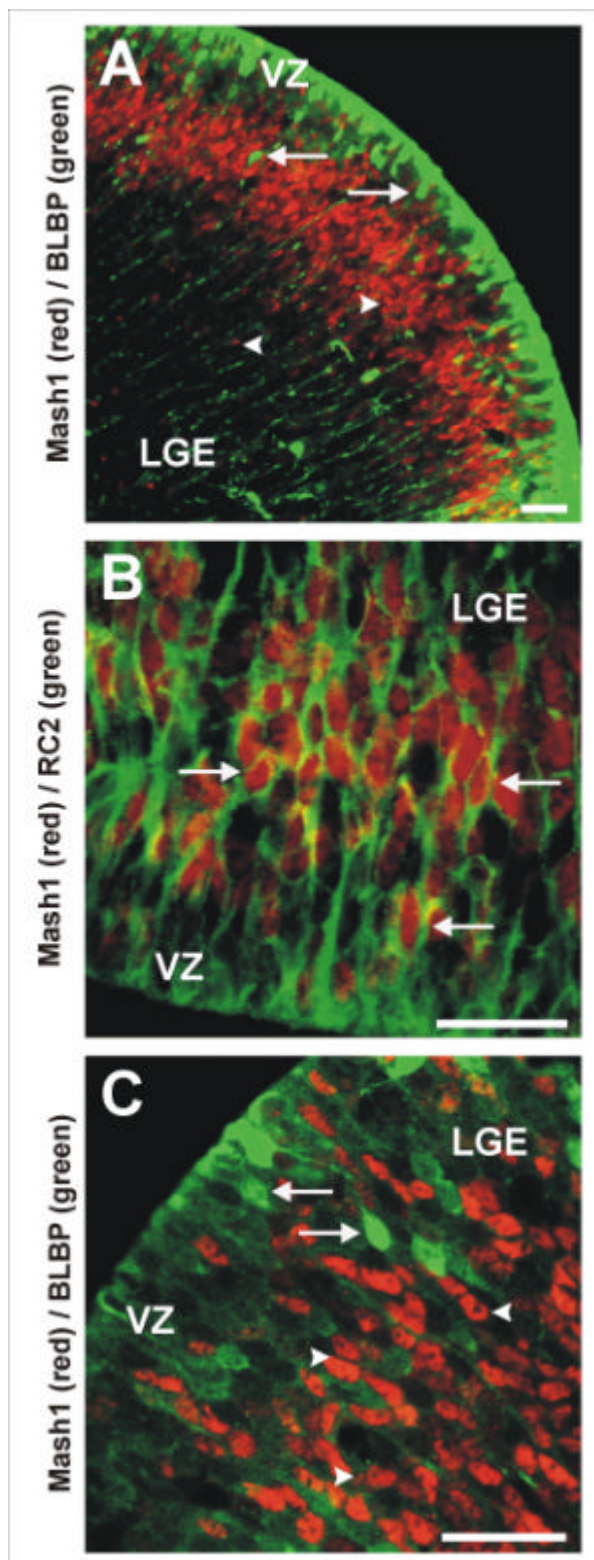


**Figure 5.7 Expression of the bHLH transcription factor Mash1**

Fluorescent micrographs of frontal (A-C) sections of E14 lateral ganglionic eminence (LGE) stained with the antisera indicated in the figure. A depicts a low power view showing that Mash1-immunoreactive cells mostly reside above the BLBP-positive cell somata in the ventricular zone (VZ). High power views in B and C show that Mash1-positive cells co-localize with RC2 (B, examples indicated by arrows), but not with BLBP (C). In A and C arrows depict BLBP-positive and arrowheads Mash1-positive cell somata. Scale bar: 50 $\mu$ m.

In Mash1/BLBP-double staining, we noted that Mash1-positive cells form a horizontal band just above the BLBP-immunoreactive cell somata (Fig. 5.7). Double-staining of Mash1- and RC2-antiserum showed, however, many double-positive cells (Fig. 5.7B), while even in the zone of overlap between BLBP and Mash1 no double-positive cells could be detected (Fig. 5.7C). Thus, Mash1 seems to be localized in the RC2-positive, BLBP-negative subpopulation of precursor cells. These results were confirmed at the quantitative level in acutely dissociated cells of the GE at E14 (Fig. 5.8). Whereas all Mash1-positive cells (10% of the entire progenitor pool) were double-labelled with RC2-antiserum (100%) only 26%±3 contained GLAST or BLBP (less than 4% of all precursor cells). Thus, the precursor subtypes detected by the co-localization of RC2, GLAST and BLBP also differ in their transcription factor expression.

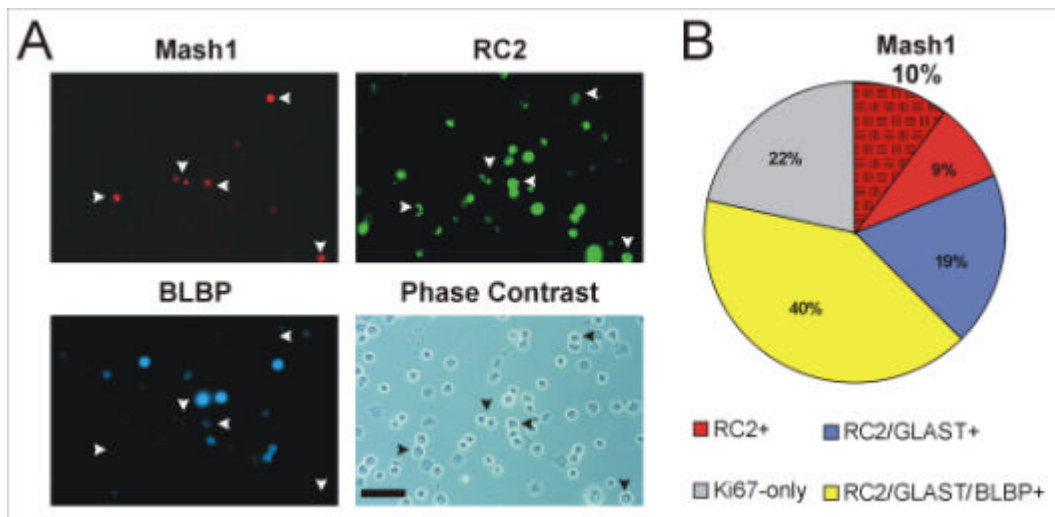


**Figure 5.8 Expression of the bHLH transcription factor Mash1 in acutely dissociated cells**

Panel A shows fluorescent micrographs of acutely dissociated cells from the ganglionic eminence at E14 triple-stained with Mash1, RC2 and BLBP. As in sections, Mash1 co-localizes with RC2 (arrowheads), but not with BLBP. Panel B shows the quantitative composition of the precursor pool at E14 in the GE. Only 10% of precursors are immunopositive for the bHLH-transcription factor Mash1, which are all RC2-only positive precursors. Scale bar: 50µm. n=351 analysed cells.

### 5.3.3 Subventricular zone (SVZ) precursor cells

Notably one population of precursor cells was immuno-negative for RC2, BLBP and GLAST. To examine whether they might represent the precursors of the second proliferative layer, the subventricular zone (SVZ) we performed immunostaining in vibratome sections. Stainings for RC2 and GLAST were combined with a marker for cells in mitosis, anti-PH3, the phosphorylated form of histone H3. The major characteristic of precursor cells of the SVZ is that these cells do not

undergo interkinetic nuclear migration and divide at the ventricular surface but reside throughout all phases of the cell cycle in the SVZ. The SVZ of the GE has been shown to be more prominent compared to the SVZ of the cortex (Smart 1976; Bayer and Altman 1991). Interestingly, RC2/BLBP/GLAST-negative precursors, the Ki67-only population (see Fig. 5.4) are more frequent in the GE than in the cortex, and thus might correspond to the precursor cells of the SVZ. For this reason we analysed whether PH3-positive cells that are not located in the VZ are immunopositive for RC2 and GLAST. Interestingly, as well in the cortex as in the GE, PH3-positive cells, situated in the SVZ were RC2- and GLAST-immunonegative (Fig. 5.9). Furthermore we can conclude, that the PH3-positive cells in the SVZ are as well negative for BLBP-immunoreactivity, since all BLBP-positive cells at E14 in the cerebral cortex and the GE are as well RC2- and GLAST-immunopositive (see Fig. 5.4). However, PH3-positive cells in the VZ were RC2- and GLAST-positive (Fig. 5.9), thus showing, that these antigens are not differentially regulated during the cell cycle (see as well Results 5.4). These data therefore suggest that indeed Ki67-only immunoreactive cells represent the precursor cells of the SVZ.

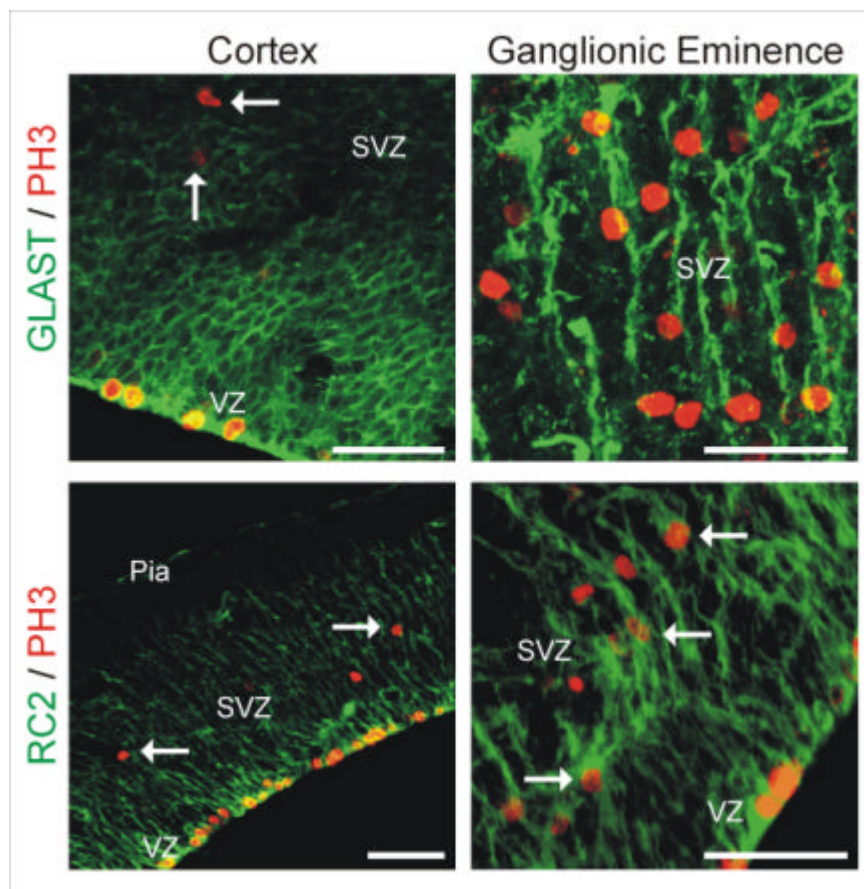


**Figure 5.9** Subventricular zone (SVZ) precursor cells do not express radial glial markers

**Figure 5.9 Subventricular zone (SVZ) precursor cells do not express radial glial markers**

Single optical sections images (~10µm) of frontal sections of E14 mouse cortex and GE (as indicated on the pictures) stained with the radial glial markers GLAST or RC2 and anti-PH3 (phosphorylated histone H3; as indicated). While GLAST and RC2 are contained in mitotic precursors at the ventricular surface, SVZ-precursors undergoing mitosis at non-surface positions in the cortex and GE are neither GLAST- nor RC2-immunoreactive. Scale bar 50µm.

**5.4 Cell cycle parameters of precursor cell subpopulations**

We further analysed the function of the novel precursor subtypes by BrdU-pulse-labelling as a first assay for their cell cycle characteristics. BrdU was injected into timed-pregnant mice one hour prior to cell dissociation (see methods). The labelling index (LI) was determined as the percentage of BrdU-labelled cells amongst all proliferating cells. The LI of Ki67-only cells was determined from the RC2/Ki67/BrdU combination for E14. This is possible since at this stage GLAST- and BLBP-immunoreactive cells are included in the RC2-positive population, i.e. all RC2-negative, Ki67-positive cells are also negative for GLAST and BLBP (Table 5.1 and Fig. 5.4). At later stages, however, when e.g. GLAST/BLBP-positive cells exist, we could not determine the LI of the Ki67-only population anymore (n.d. in Table 5.4).

Since our analysis described above had shown that almost all RC2- and/or GLAST- and/or BLBP-positive cells are also Ki67-positive precursors, we could use triple-labelling combining two of the marker antigens (RC2/GLAST, RC2/BLBP and GLAST/BLBP) with BrdU-antiserum. These data provide the LI of 9 possible cell types: (1) RC2+/GLAST-; (2) RC2-/GLAST+; (3) RC2+/GLAST+; (4) RC2+/BLBP-; (5) RC2-/BLBP+; (6) RC2+/BLBP+; (7) GLAST+/BLBP-; (8) GLAST-/BLBP+; (9) GLAST+/BLBP+. Since maximal 4 combinations of RC2-, GLAST- and BLBP-immunoreactive cells co-exist at any time analysed, these data allowed us to determine the LI for each subpopulation directly (Table 5.2 and 5.4; Fig. 5.4). For example, the LI of the RC2-only population can be deduced directly from the #1 staining combination, since RC2-positive cells that are not GLAST-positive are the RC2-only population from E14-E18. (This is not the case at E12, when also the RC2/BLBP+ cells exist. Therefore, we could not assess the LIs for E12.) Likewise, the LI of the RC2+/GLAST+ population was measured directly in the staining combination #7, since no other GLAST-positive and BLBP-negative population exists at the stages analysed. The LI of the RC2+/GLAST+/BLBP+ cells was measured in the staining combination #6, since the RC2- and BLBP-immunoreactive cells are also

GLAST-positive at the stages E14-18. The LI of the GLAST+/BLBP+ population was measured in the #2 and #5 staining combinations, since there is no other GLAST-, respectively BLBP-positive, and RC2-negative population.

**Table 5.4 Labelling index of precursor subtypes labelled by RC2, GLAST and BLBP**

	E14	E16	E18
<b>Cortex</b>			
RC2-only	0.28	/	/
RC2/GLAST	0.39	0.39	/
GLAST/BLBP	/	0.14	0.04
RC2/GLAST/BLBP	0.36	0.33	0.21
Ki67-only	0.00	/	/
<b>GE</b>			
RC2-only	0.49	0.60	/
RC2/GLAST	0.46	0.55	0.32
GLAST/BLBP	/	0.31	0.23
RC2/GLAST/BLBP	0.36	0.26	0.18
Ki67-only	0.27	n.d.	n.d.

*Note.* The labeling index (LI) is the proportion of immunoreactive precursor cells labeled by a single BrdU pulse for 1 h. Note that the precursor subtypes characterized by differential co-localization of RC2, GLAST, and BLBP exhibit a different LI. - Indicates that these populations do not exist at the respective developmental stage; n.d., the LI of these populations could not be assessed by different combinations of triple-stainings using our markers. n(E14)=43; n(E16)=8; n(E18)=5; (*n*) is the number of analysed coverslips.

We found that our LI values closely corresponded to previous *in vivo* results (Reznikov and van der Kooy 1995; Takahashi *et al.* 1995b; Bhide 1996; Cai *et al.* 1997a), e.g. showing a decrease of the LI between E14 and E18 (Takahashi *et al.* 1995a). Interestingly, some precursor populations characterized by distinct antigenic profiles differed in their LI (Table 5.4). For example, the cortical precursors labelled only by RC2 had a smaller LI than the RC2/GLAST+ or RC2/GLAST/BLBP+ cells. The GLAST/BLBP+ cells also showed a clearly lower LI compared to other precursor cells present at the respective developmental stage. Notably, some populations of GE cells exhibited a higher LI than their counterparts in the cortex. For example, the LI of RC2+ or GLAST/BLBP+ cells in the GE was almost double the value obtained for this population in the cortex (Table 5.4). In contrast, the LI of the RC2/GLAST/BLBP+ cells was similar in the cortex and GE and gradually decreased during development in both regions (cortex: 0.36(E14)-0.21(E18); GE: 0.36(E14)-0.18(E18)).

## 5.5 Morphology of precursor cells

### 5.5.1 Morphologically identified precursors

These data show a major contribution of precursors expressing glial markers to the progenitor pool. This is intriguing taking into account that during neurogenesis nearly all precursors are neuronal precursors, which were suspected to have only short processes. Thus, we wanted to examine whether radial glial cells indeed comprise the majority of precursors during CNS development. We therefore analysed the antigenic profile of radial glial cells identified by their morphological characteristic, the long radial process. Application of Dil or red-fluorescent latex beads (Katz *et al.* 1984) onto the pial surface of the telencephalic hemispheres was used to trace radial glial cells as described previously (Voigt 1989; Götz *et al.* 1998). After fluorescent labelling, cells from E14 cortex were dissociated in order to visualize the entire cell soma and to assess the co-localization of the RC2-antigen, GLAST and BLBP (Fig. 5.10).

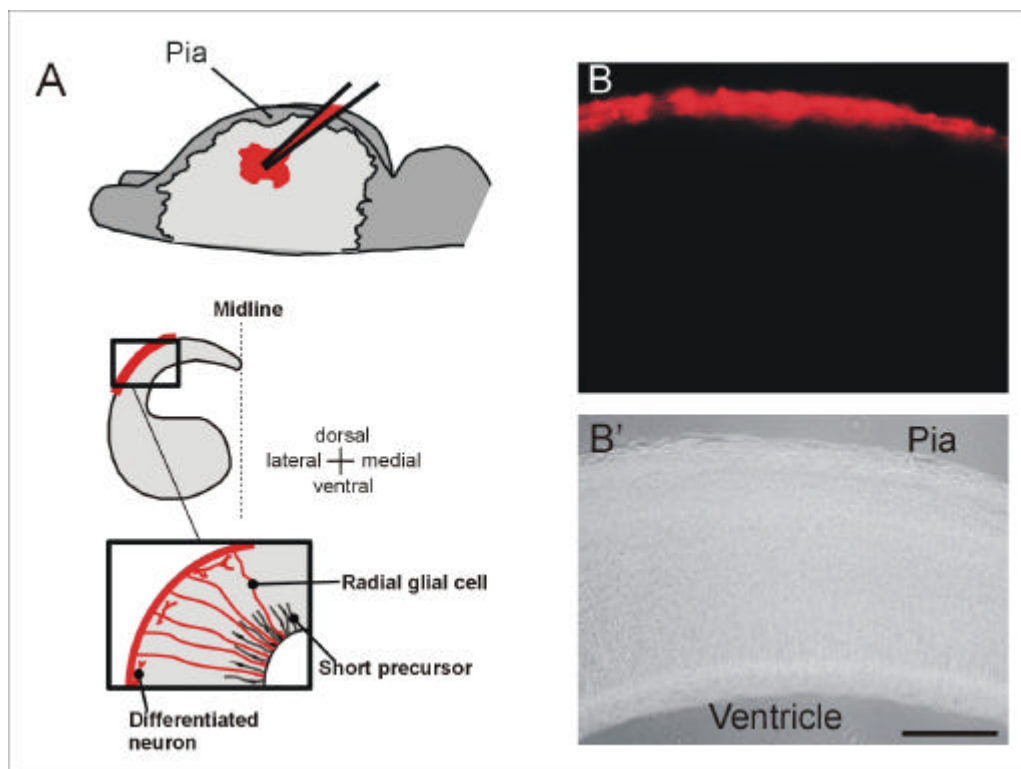


**Figure 5.10 Fluorescent tracing of cells from the pial surface.**

A) The application of the red fluorescent tracers Dil (Voigt 1989; Götz *et al.* 1998) or microsphere beads (Katz *et al.* 1984; Voigt 1989) on the surface of a cerebral hemisphere after removal of the meninges. A) schematic drawing of a section through the cortex indicates the red fluorescent dye on the brain surface (lower left drawing in A) and the back-traced radial glial cells, neurons and unlabeled precursor cells with a short process. (B,B') Corresponding micrographs showing beads fluorescence (B) and phase contrast (B') of a 100 $\mu$ m frontal section of E14 telencephalon 20 minutes after application of the dye on the surface of the cortex. Scale bar 100 $\mu$ m.

The majority of cells labelled from the pial surface were neurons ( $\beta$ -tubulin-III-positive; 82%,  $n=450$ ) and only a small proportion were precursor cells (Ki67-positive; 18%,  $n=250$ ). Control experiments with tracer application onto the ventricular surface revealed a predominance of precursor cells, thereby demonstrating the restriction of the tracer to the site of application. Most precursor cells labelled from the pial surface ( $92\% \pm 4$ ,  $n=150$ ) were RC2-positive, but only 58% also contained BLBP and GLAST while 18% were double-labelled with RC2- and GLAST-antiserum (Fig. 5.11A). This is consistent with the staining in sections, where we observed some radial processes negative for BLBP or GLAST (Fig. 5.1D). Interestingly, no significant differences could be observed between the composition of the precursor pool labelled from the pial surface and the composition of acutely dissociated precursor cells (Fig. 5.11B,B'). This suggests that first, all precursor subpopulations contain radial glial cells and second, as radial glial cells and all precursor cells show the same quantitative subtype-composition, that they might represent the majority of precursor cells. Thus, precursor cells contacting the pial surface present the same heterogeneity in their antigenic profile as the entire population of precursor cells in the cerebral cortex.

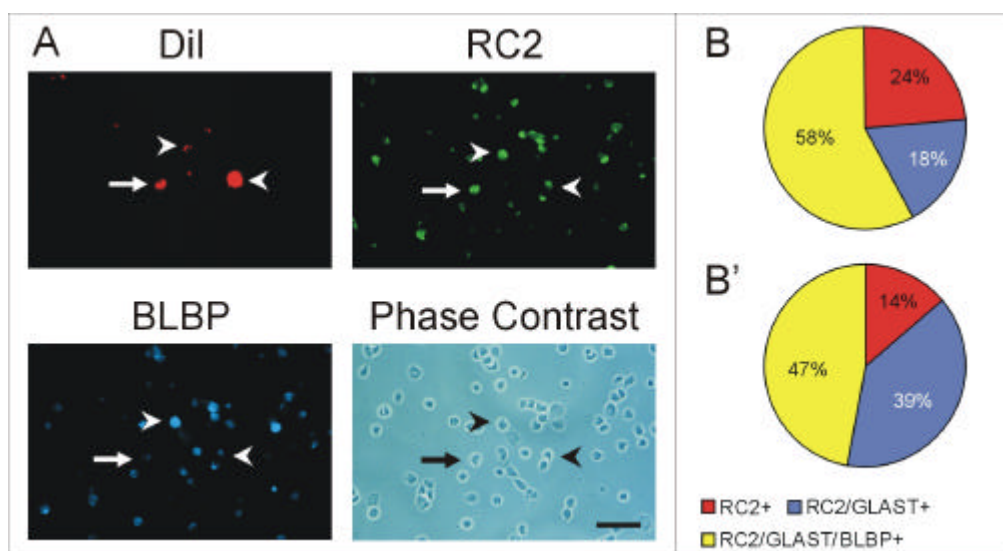


**Figure 5.11 Composition of precursor cells traced from the pial surface**

Panel A depicts E14 cortical cells labelled by Dil from the pial surface (Voigt 1989; Götz *et al.* 1998). Dil-labelled precursor cells are RC2 positive (arrow and arrowhead), but only some are also BLBP immunoreactive (arrowheads). Thus, radial glial cells are heterogeneous in their BLBP content, as also detected in sections (Fig. 5.1). Scale bar: 50  $\mu$ m. In B the pie diagram shows the antigenic profile of E14 cortical precursors traced by their long radial processes from the pial surface (compare to Fig. 5.4). The pie diagram in B' shows the overall precursor composition normalized to all RC2-positive cells. Interestingly, the composition of back-labelled radial glial cells contains the same subpopulations as the overall precursor composition, showing, that all precursor subpopulations contain long radial glial cells.

### 5.5.2 3D-reconstruction of ventricular zone (VZ) precursor morphology

The analysis of the antigenic profile of precursors traced by Dil from the pial surface showed that indeed all precursor subpopulations identified by the so-called radial glial markers contain cells with long radial processes. However, it was still not clear to which extent radial glial cells contribute to the precursor pool. If all the cells labelled by the so-called radial glial markers would indeed have a long radial process, radial glial cells would constitute the majority rather than the minority of precursors during neurogenesis. We therefore analysed the morphology of precursor cells at a quantitative level by tracing cells from the ventricular surface by the lipophilic dye Dil and inspecting the morphology of the labelled cells. All cells located in the VZ are attached by an apical process to the ventricular surface throughout all phases of the cell cycle where only the nucleus moves up and down (Sauer 1935). Because of this, only cells in direct contact with the lateral ventricle, either situated directly at the ventricular surface without any visible apical process, or connected by a short apical process to the surface of the ventricle, could be labelled. Confocal microscopy in 150 $\mu$ m thick vibratome sections and 3D-reconstructions were used to reliably separate superimposed cells as exemplified in Fig. 5.12 and to exclude cells whose processes were cut and ran out of the section (Fig. 5.12; Movie 5.1).

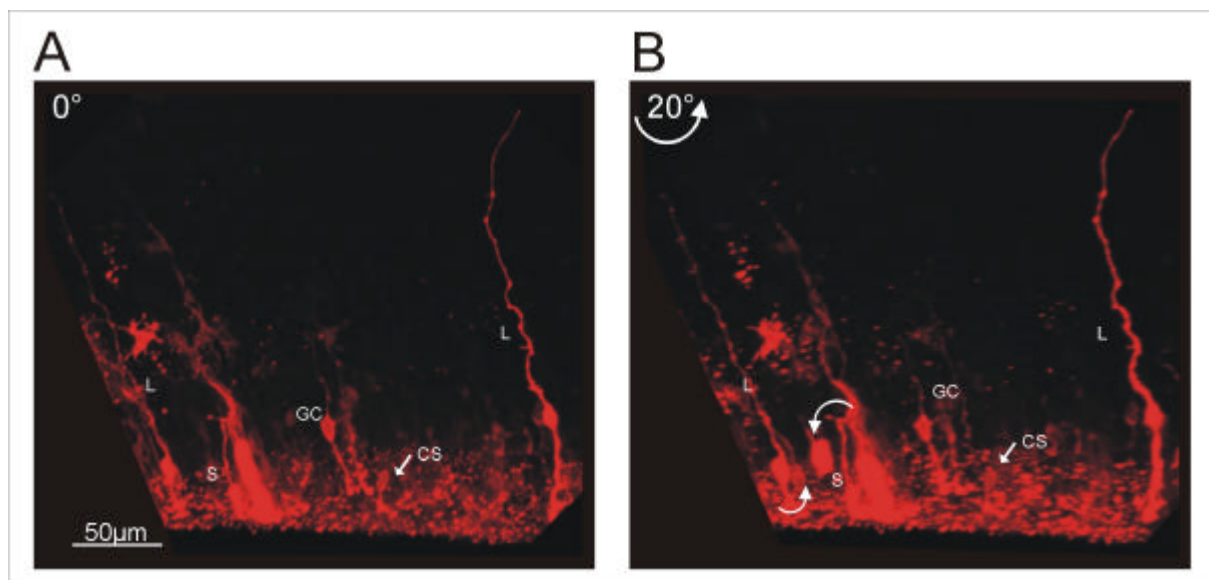


**Figure 5.12 3D-reconstruction of precursor morphology in the cortical ventricular zone**

Single frames of a 3D-reconstruction of a 150 $\mu$ m thick mouse cortical section showing precursors traced from the ventricular surface by Dil (see methods) at E14. The frame B represents a rotation of 20° (y-axis) with regard to frame A. Note the two cells indicated by the curved arrows previously hidden behind cells with long radial processes.

Four classes of precursors during neurogenesis (E12-16 in mouse cortex; Polleux *et al.* 1997) were discernible by the shape and length of their radial processes (Fig. 5.13). The first class comprises cells with a long basal process reaching up to the pial surface, spanning the entire thickness of the cortex. These cells we classified as 'long' cells. The second class of cells comprises cells similar to 'long' cells but with a shorter basal process ending underneath the cortical plate ('short' cells). The third cell type had a clear growth-cone at the tip of its basal process that appeared as if it was still extending towards the pial surface ('growth-cone' cells). Finally, we detected also cells with only a very short (<10 $\mu$ m) or no basal process ('club shaped' cells).

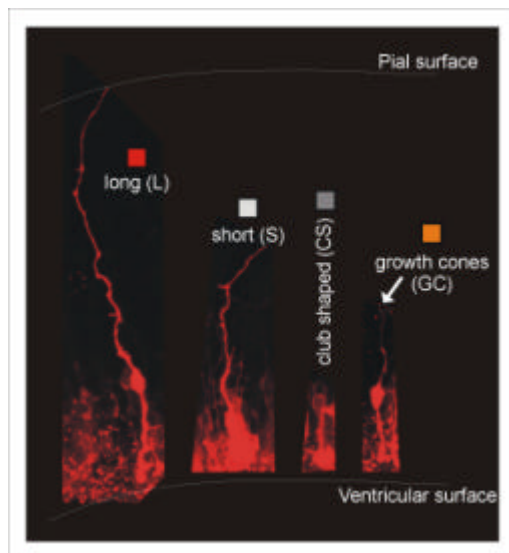


**Figure 5.13 Morphologically identified ventricular zone (VZ) precursor subtypes**

For the quantification depicted in Figure 5.14 the morphology of precursors was classified as L: long precursor with the radial process reaching the pial surface (red in Fig. 5.14)

S: short precursor with the process ending below the cortical plate (white in Fig. 5.14)

CS: club shaped precursors without a basally oriented process (grey in Fig. 5.14)

GC: precursors with a radial process terminating with a growth cone-like structure (orange in Fig. 5.14)

When quantifying the proportion of these morphologically distinct types of ventricular zone cells in the cortex during development, it became apparent that the majority of cells labelled from the ventricular surface possess long radial processes extending into the cortical plate (80% (E14) - 52% (E18); Fig. 5.14). The predominance of cells with long radial processes was also observed in other regions of the developing CNS, such as the ganglionic eminence and the spinal cord (Fig. 5.14), which is consistent with the predominance of radial glial cells amongst all VZ precursors. Note that in all regions very few labelled cells (1-13%) have a short radial process ending below the cortical plate, the morphology previously assigned to 'neuronal' precursors (Fig. 5.14). Taken together with the data obtained by labelling acutely dissociated cells with the antisera RC2, anti-GLAST and anti-BLBP, the analysis of the morphological tracing of precursors of the VZ further suggests a predominance of radial glia during neurogenesis in the cerebral cortex (Fig. 5.14).

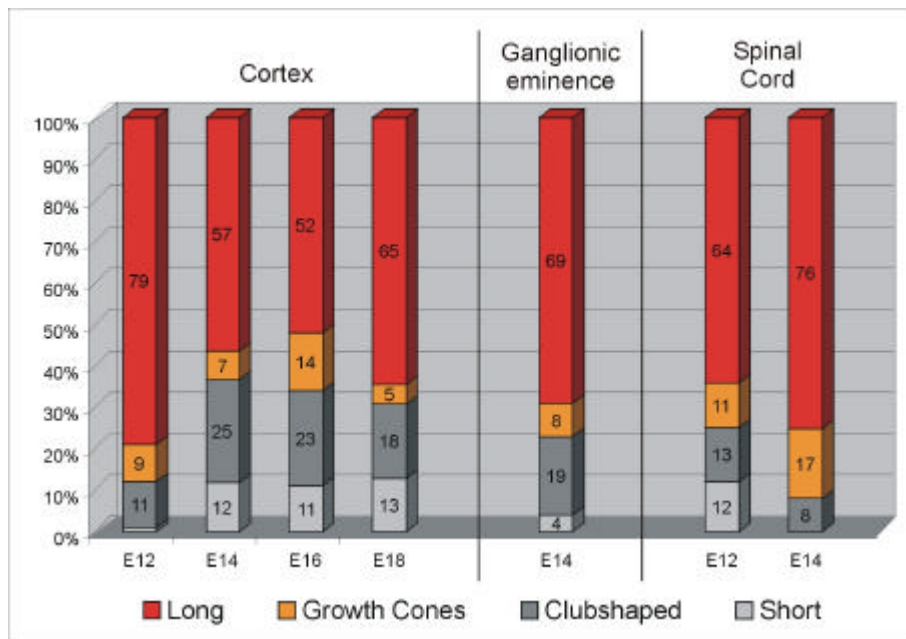


**Figure 5.14**  
Quantitative analysis of morphologically identified precursor subtypes during CNS development

Note that during all stages and in all CNS regions analysed the majority of VZ-precursor cells has long radial processes.

n(E12)=90; n(E14)=97;  
n(E16)=116; n(E18)=40;  
n(GE)=191; SC: n(E12)=100; n(E14)=30.

(n) number of analyzed cells.

## 5.6 Process retraction or maintenance during radial glial cell division

### 5.6.1 Process length and soma-position during interkinetic nuclear migration

The data mentioned above showed that radial glial cells constitute the majority of precursors cells of the VZ. Moreover, the quantitative analysis of the progenitor pool in the developing cerebral cortex detected no quiescent cells. This prompts the question of how radial glial cells coordinate neuronal migration along their radial processes and proliferation while cell division has been supposed to be accompanied by process retraction in M-phase? Two possible scenarios are conceivable: either cells are not synchronized in their cell cycle and hence only some would retract their processes at a time whereas the migrating neurons would just switch to the closest remaining radial fiber, or radial glial cells divide without retracting their processes. Interestingly, in contrast to retracting processes, however, we could detect many radial processes with growth cones at their tips when we labelled precursor cells from the ventricular surface (E14 ~10%, see Fig. 5.14), suggesting that newly generated cells extend a radial process.

Ventricular zone precursor cells undergo interkinetic nuclear migration, a process where the cell soma translocates from the ventricular surface into deeper parts of the ventricular zone and back to the surface, during cell division (Fig. 5.15A). As M-phase always takes place directly at the ventricle, we were wondering whether the soma of e.g. 'long cells' is far more distant from the ventricle than that of e.g. 'club shaped cells', indicating, that the morphologically identified precursor subsets are in

distinct phases of cell division. We therefore measured the distance between the cell soma and the ventricular surface in 3D-reconstructions of cells, labelled with Dil from the ventricle in the cerebral cortex at E14. The mean soma-ventricle distance for all subpopulations was between 34 - 44 $\mu$ m and no significant differences could be observed (Fig. 5.15B). These data suggest that the morphologically distinct precursor subpopulations are not correlated to different cell cycle phases and therefore suggesting that radial glial cells might not retract their processes during cell division.

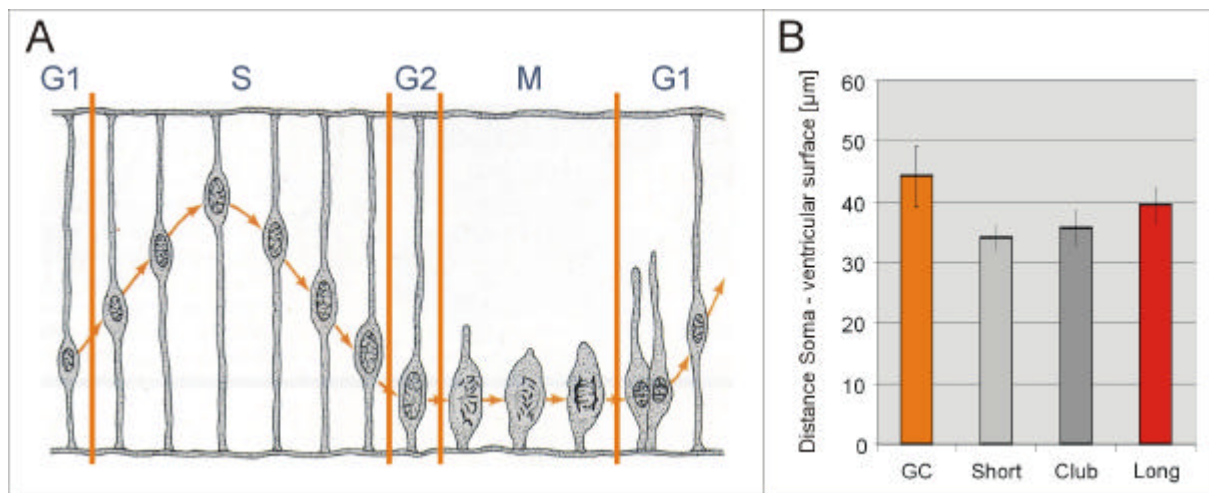


**Figure 5.15 Interkinetic nuclear migration and soma-position of morphologically identified precursors**

Panel A depicts a schematical illustration of the soma-translocation of precursor cells in correlation to distinct cell-cycle phases in the developing neural tube (adapted from Gilbert 1994). In B the diagram shows the mean distance between the ventricular surface and the soma of the morphologically identified precursor populations in the mouse cerebral cortex at E14 (see as well Fig. 5.13-14). Note that there is no significant difference in the soma-position between the subtypes, showing that they are not correlated to the distinct cell-cycle phases.  $n(\text{GC})=4$ ;  $n(\text{Short})=11$ ;  $n(\text{Club})=17$ ;  $n(\text{Long})=18$ . ( $n$ ) number of analysed cells. Error bars depict the SEM.

### 5.6.2 Time-lapse video microscopy of dividing radial glial cells *in vitro*

To clarify whether radial glial cells retract or maintain their processes during mitosis we aimed to directly examine the proliferation of radial glial cells *in situ* by time-lapse video microscopy in slice preparations. Before we could start with the analysis of radial glial cell proliferation we had to establish the right parameters for long-term imaging like media, temperature,  $\text{CO}_2$ -percentage, time-lapse exposure time and time intervals for cell-survival during the phase of imaging. In a first attempt, we used cell-lines in order to do the experimental set-up since the effective cultivation of slice-preparations requires many parameters.

Using HEK-293 cells plated on PDL-coated plastic-dishes, we were able to image dividing cells by light microscopy up to 48 hours after plating (Movie 5.2). Cells

were kept at 37°C and 8%CO<sub>2</sub> in FCS-PS-Medium in a self-made humid incubation-chamber under semi-sterile conditions on an inverted microscope. Pictures were taken every 10 minutes with an exposure time of 1-1.5s. Since we actually wanted to visualize fluorescently traced radial glial cells in slice preparations and phototoxicity due to the fluorescent light might alter or even inhibit cell proliferation, we additionally used GFP-expressing HEK-293 cells for the experimental set-up (see Methods 4.4). However, under the conditions described above, we were able to image proliferating GFP-expressing cells (Movie 5.3). In a next step, we used mouse derived NIH 3T3 cells and infected them with a mouse leukaemia GFP-retrovirus (Flügel *et al.* 1999; see Methods 4.4) to test any influences of viral infection on the proliferation behaviour of the cells. Cells were infected and incubated in a cell-culture incubator (37°C, 5%CO<sub>2</sub>) for at least 8 hours until GFP-expression was visible. Subsequently cells were placed in the time-lapse set-up incubation chamber. Despite viral infection, cells proliferated without further modifications of the conditions.

As a next step to establish the required conditions for primary slice cultures, we prepared primary cortical dissociated cell cultures from E14 mouse embryos, plated them on PDL-coated plastic-dishes, and performed time-lapse video microscopy under the described conditions. Surprisingly, the primary cortical cells were dying already after only 1 hour. Since we imaged the cells by normal light microscopy with very low light-intensities, this effect could hardly be due to phototoxicity. We therefore tested several different conditions, concerning temperature, CO<sub>2</sub>-concentration and media. We finally succeeded in maintaining the cells in a healthy and proliferative state by applying the growth factors EGF and bFGF and additional glucose to a serum-free medium containing as well B27-supplement, which supports cell growth and viability (time-lapse (TL) medium; see methods). Primary cortical cells cultured in TL-medium at 37°C and 8%CO<sub>2</sub> survived and proliferated, so we could image them over a longer period by time-lapse video microscopy. Furthermore, we infected primary cells with the GFP-retrovirus and were as well able to image dividing cells. To minimize phototoxicity we doubled the time-intervals to 20 minutes and reduced the exposure-time to only 600ms.

Finally, we prepared 300µm frontal slices of E14 mouse telencephalon. Slices were laid on permeable filter-membrane inserts that were placed in plastic-dishes containing TL-medium. After preparation, slices were infected with the GFP-retrovirus. Unfortunately, only the cell soma was labelled since the GFP-content in

the infected cells was too low to visualize the processes of the cells. Therefore, we switched to an eGFP-adenovirus (Chapouton *et al.* 1999), which expressed higher amounts of eGFP that also the long radial processes of infected radial glial cells were visible. Using an adenovirus, had the disadvantage that also non-proliferating cells like neurons were infected. We therefore pressure injected the eGFP-adenovirus focally in the cortical VZ of the slices, where mostly precursors are located, to minimize the number of infected neurons. However, even if the amount of the pressure-injected virus was very low (0.1-0.5 $\mu$ l), the virus flowed into the culture medium and around the slices and thus as well other cells than precursor cells of the VZ were infected. Infected slices were cultured for at least 8 hours at 37°C and 5%CO<sub>2</sub> in a cell-culture incubator to allow expression of eGFP in the infected cells (Fig. 5.16). At the time when eGFP was visible in radial glial cells, slices were placed in the time-lapse set-up at 37°C and 8%CO<sub>2</sub> in TL-medium. Initially we removed the slices from the filter-inserts and placed them in a glass-chamber with a flow-through of the medium to guarantee the supply of the sections with fresh medium. Nevertheless, with a flow-through of the medium slices were mostly slightly moving, such that cells went out of focus after only 1 hour. Furthermore, bacterial contamination increased in this culture-system, so we had to change to a steady-state culture. We therefore directly placed the slices attached to the filter-membrane inserts in plastic dishes containing TL-medium in the time-lapse set-up. However, only rarely we could observe dividing cells, most probably all astrocytes but we failed in imaging radial glial cells during cell division (Movie 5.4). To rule out phototoxic effects we tried to further improve the TL-medium by adding the antioxidants vitamin C, vitamin E (?-tocopherol) and Na-Selenite, protecting the cells against free radicals. Additionally, we further increased the acquisition time intervals to 30 minutes, and used exposure-times of only 300-500ms to decrease phototoxicity to a minimum. Nevertheless, we could not improve the proliferation of the infected cells. It might be conceivable that the high amount of eGFP interfered with the cellular division machinery or that it was even cytotoxic for the cells. For these reasons, we were not successful in live imaging dividing radial glial cells by time-lapse video microscopy.

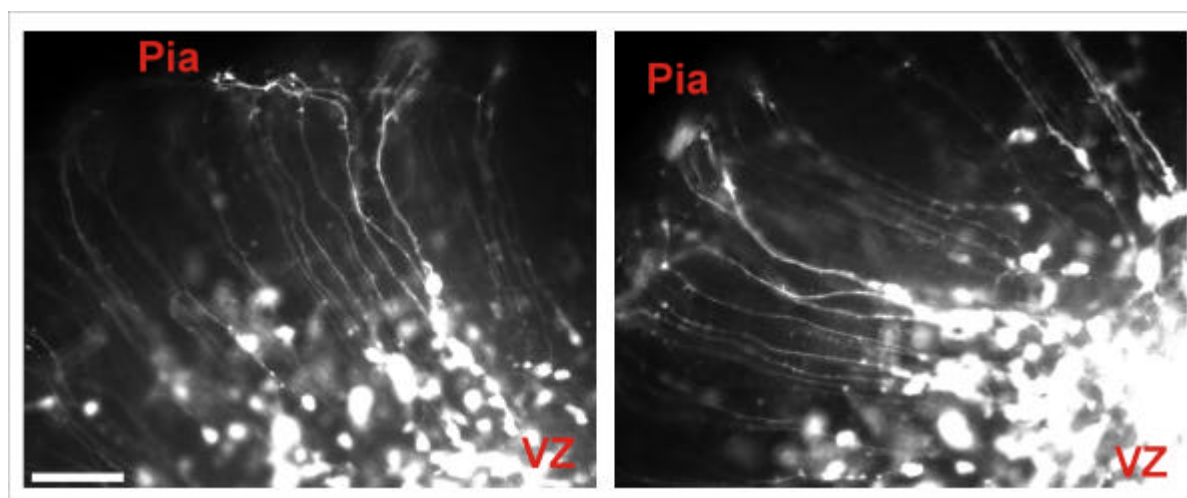


**Figure 5.16 Timelapse analysis of radial glial cells infected with an eGFP-adenovirus**

Micrographs show examples of E14 mouse forebrain slice-preparations. Radial glial cells were infected with an eGFP-adenovirus to visualize the entire cell, including processes and somata. Scale bar 50 $\mu$ m.

### 5.6.3 Visualization of radial glial cells during M-Phase

Since we were not able to examine the mode of proliferation of radial glial cells with time-lapse video microscopy, we used alternative approaches to assess the issue of process maintenance or retraction in M-phase. The first attempt was to visualize mitotic figures and their morphology in 3D-reconstructions. We therefore counterstained DiI-labelled vibratome sections with Yo-Pro-1, a cell membrane impermeant green-fluorescent cyanine nucleic acid stain. Mitotic figures could be determined at the microscope. The 3D-reconstructions of the DiI/Yo-Pro-1-double labelled sections revealed, that indeed long cells were found to be in M-phase (Fig. 5.17).

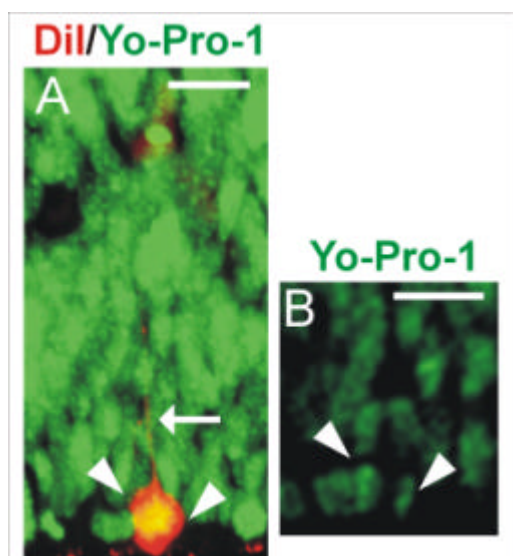


**Figure 5.17 Visualization of mitotic radial glia by DiI-tracing and Yo-Pro-I-iodide staining**

Vibratome sections of E14 DiI-labelled (red) brains were counterstained with Yo-Pro-I-iodide (green) to visualize condensed chromosomes and were processed for 3D-reconstruction.

A The fluorescent micrograph shows the merged 3D-reconstruction ( $\sim$ 50 $\mu$ m) of a DiI-labelled ventricular zone cell with a long radial process (arrow) and condensed chromosomes in M-phase (arrowheads).

B depicts a single optical frame (1-2 $\mu$ m) of the 3D-reconstruction shown in A. Only Yo-Pro-1 staining is shown to better demonstrate the condensed M-phase chromosomes of the DiI-labelled radial glial cell. Scale bar 20 $\mu$ m.

Using a parallel approach to analyse the morphology of mitotic cells we stained with the antibody 4A4, which specifically recognizes the cdc2-kinase phosphorylated form of vimentin and therefore labels cells in the G2/M phase of the cell cycle (Kamei *et al.* 1998). The analysis of 4A4-staining during neurogenesis in vibratome sections revealed many immunoreactive cells in M-phase with radial processes reaching out to the pial surface (Fig. 5.18).

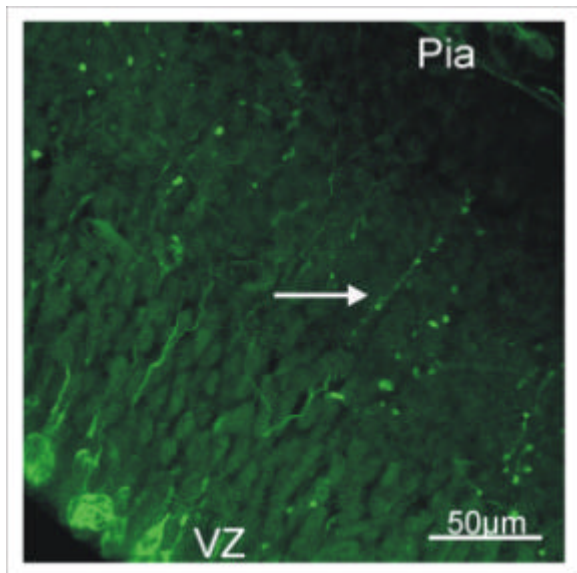


**Figure 5.18 Visualization of mitotic radial glia with the 4A4-antiserum**

Micrograph of a frontal vibratome section of the cerebral cortex at E14 stained with the 4A4-antiserum directed against the cdc2-kinase phosphorylated form of vimentin (Kamei *et al.* 1998). Note that 4A4-positive cells in M-Phase extend long radial processes, some of which reach the pial surface (indicated by an arrow).

These approaches still did not clarify if only some radial glial cells do not retract their processes or whether it is a general feature, that radial glial cells maintain their processes during division. To quantify how many radial glial cells might retract or maintain their processes during M-phase we again used the back-tracing paradigm with Dil from the pial surface. We reasoned that the radial glial cells that retract their processes during M-phase could not be back-labelled from the pial surface during this period (Fig. 5.19). BrdU was injected into pregnant mice to label cells in S-phase and cells were analysed at different time intervals after this pulse. From previous cell cycle analysis, it is predicted that most BrdU-labelled cells should have reached M-phase by 3-5 hours after the BrdU-pulse (Nowakowski *et al.* 1989). We therefore asked whether a considerable number of radial glial cells have retracted their processes at this time, which should be reflected in a decreased number of BrdU-labelled cells traceable from the pial surface 3-5 hours after the BrdU-injection (Fig. 5.19). To allow accurate quantification of Dil-labelled and BrdU-positive cells, we used the acutely dissociated cell preparation. The quantification of BrdU-labelled cells, that were also back-labelled from the pial surface 1, 3 and 5 hours after the

BrdU-pulse revealed no decrease over time (Fig. 5.19B), suggesting that most cells in G2/M-phase still have a process in the vicinity of the surface of the cortex. These results therefore further support the notion that many, if not most, radial glial cells do not retract their process during cell division. These observations on the maintenance of the radial process during cytokinesis might have implications on the mode of cell division as depicted in Fig. 5.19A

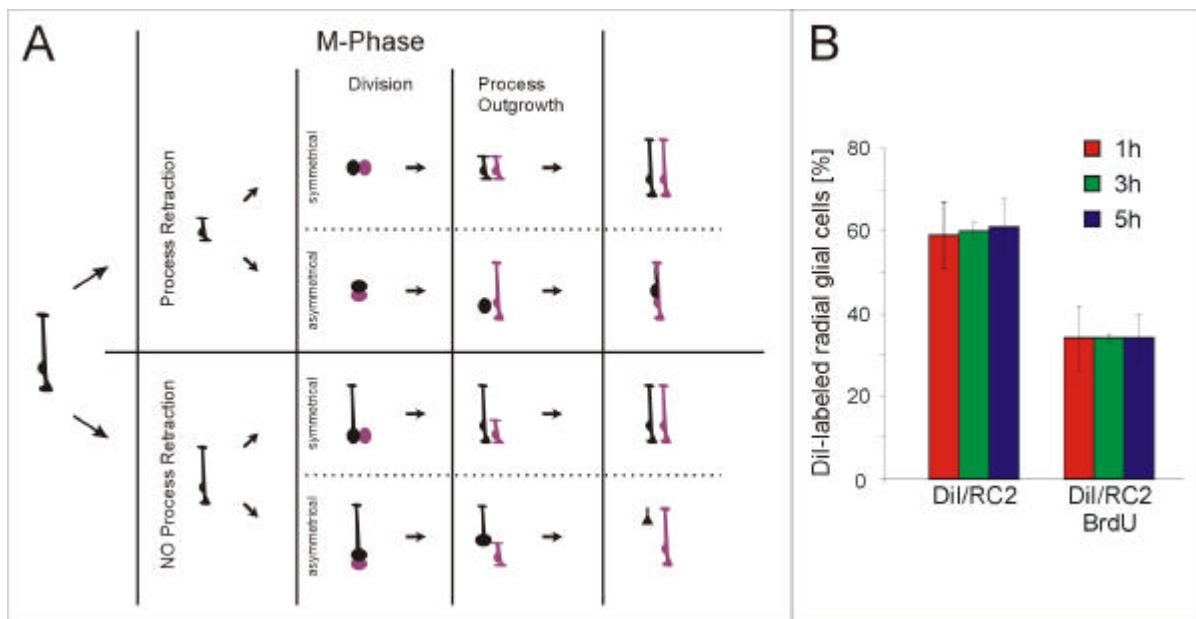


### Figure 5.19 Process retraction or maintenance during cell division

Panel A shows a schematical drawing of cell divisions oriented horizontal or vertical to the ventricular surface with retraction or maintenance of the radial process in M-phase. So far, cell divisions oriented parallel to the ventricular surface are called asymmetrical and are thought to generate a neuron and a precursor cell, while symmetrical divisions should be oriented vertical and produce two precursor cells (Chenn and McConnell 1995). Panel B shows the quantitative analysis of process retraction of E14 cortical radial cells examined by back-tracing from the pial surface 1, 3, or 5 h after labelling with BrdU (see text for details). DiI-labelled precursors were detected by double-staining with the monoclonal antibody RC2 and the proportion of BrdU-immunoreactive cells is depicted at the different stages after S-phase labelling. Note that even 5 hours after S-phase labelling the proportion of RC2-positive cells traced from the pial surface does not change, suggesting that few, if any cells have retracted their radial process at this stage in M-phase.  $n(1h)=3$ ;  $n(3h)=13$ ;  $n(5h)=8$ ; ( $n$ ) is the number of analysed coverslips.

## 5.7 The *reeler* mouse

The data mentioned before show, that radial glial cells are an crucial cell type throughout the entire developing central nervous system. Therefore, it is important to understand how radial glial identity is acquired and as well regulated during development. One intrinsic factor regulating radial glial characteristics is the transcription factor Pax6, which has been shown to affect proliferation, cell-fate, morphology, biochemical characteristics and region-specific differences of radial glial cells (Götz *et al.* 1998; Heins *et al.* 2002). In this analysis, we were concentrating on finding extrinsic regulators of radial glial characteristics. Regulators of first their morphology, since this is one of the most crucial characteristics of radial glia and second of their BLBP-content in view of the fact that BLBP has been implicated in neuron-glia signalling (Feng *et al.* 1994; Anton *et al.* 1997) and might play a role in cell-fate determination as hypothesized above.

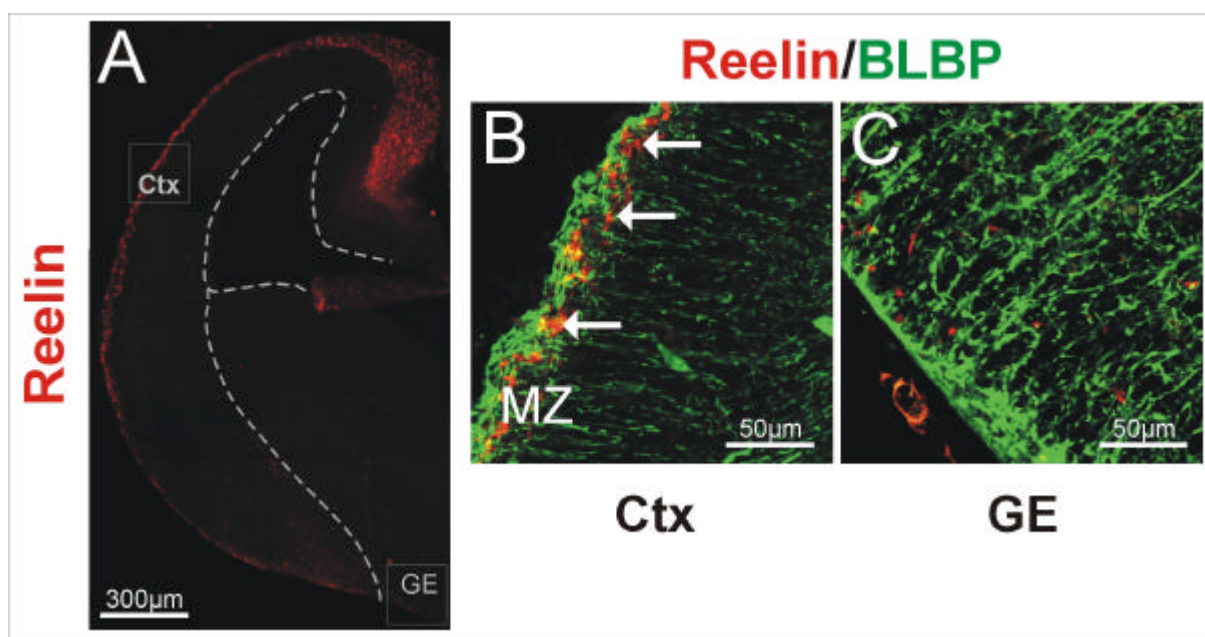


**Figure 5.20 Reelin and BLBP immunoreactivity in the embryonic telencephalon**

Frontal vibratome sections of E14 WT telencephalon stained for Reelin (A-C, red) and BLBP (B-C, green). Panel A is a low power picture showing high levels of Reelin in the cortical marginal zone (MZ; A, B) but lower levels in the ganglionic eminence (GE; A, C). Dashed line in A delineates the boundary between cortex and GE and the border of the lateral ventricle. Note the clear contact of Reelin-immunoreactive neurons and BLBP-positive radial glial endfeet in the MZ of the cerebral cortex (arrows in B) but not the GE.

To assess this topic we analysed radial glial cells in the *reeler* mouse for their immunoreactivity to radial glial markers, for their morphology and their precursor characteristics. The *reeler* mouse is lacking functional Reelin protein due to a point mutation in the reelin-gene and shows severe cortical defects (see introduction for further details). Reelin is a large extracellular matrix glycoprotein expressed and secreted from neurons in the marginal zone (MZ; Fig. 5.20A). The basal processes of radial glial cells span the entire thickness of the cortex and anchor in the basement membrane underneath the pia mater just above the MZ. The specialized end-feet of radial glial cells are therefore in direct contact with Reelin (Fig. 5.20B). Interestingly, the loss of Reelin has profound effects on neuronal migration in the cerebral cortex and cerebellum, but not the basal ganglia (for review see : Caviness, Jr. and Rakic 1978; Lambert de Rouvroit and Goffinet 1998; Curran and D'Arcangelo 1998), where there are only few Reelin-positive cells located. However, Reelin-immunoreactive cells in the GE are not located in direct contact with the radial glial endfeet (Fig. 5.20C). The close proximity of cortical radial glia and Reelin and the regional difference of Reelin-position between the dorsal and the ventral telencephalon prompted us to examine the potential influences of Reelin on radial glial cells.

#### 5.7.1 Precursor cell subtypes in the *reeler* telencephalon

First, we examined whether the precursor heterogeneity described before might be altered in the absence of Reelin-signalling. The antigens of RC2, GLAST and BLBP were examined in the cortex of the *reeler* mouse during the peak of neurogenesis (E14-16) in vibratome sections. Whereas the immunoreactivity of the RC2-antigen was similar between WT and *reeler* radial glial cells in the cortex BLBP-immunoreactivity appeared greatly reduced at E16 (Fig. 5.21). Interestingly, this decrease in BLBP-immunoreactivity in the *reeler* telencephalon was restricted to the cortex and was not observed in the GE, where only few Reelin-immunoreactive cells are located (Fig. 5.22, see as well Fig. 5.20C).

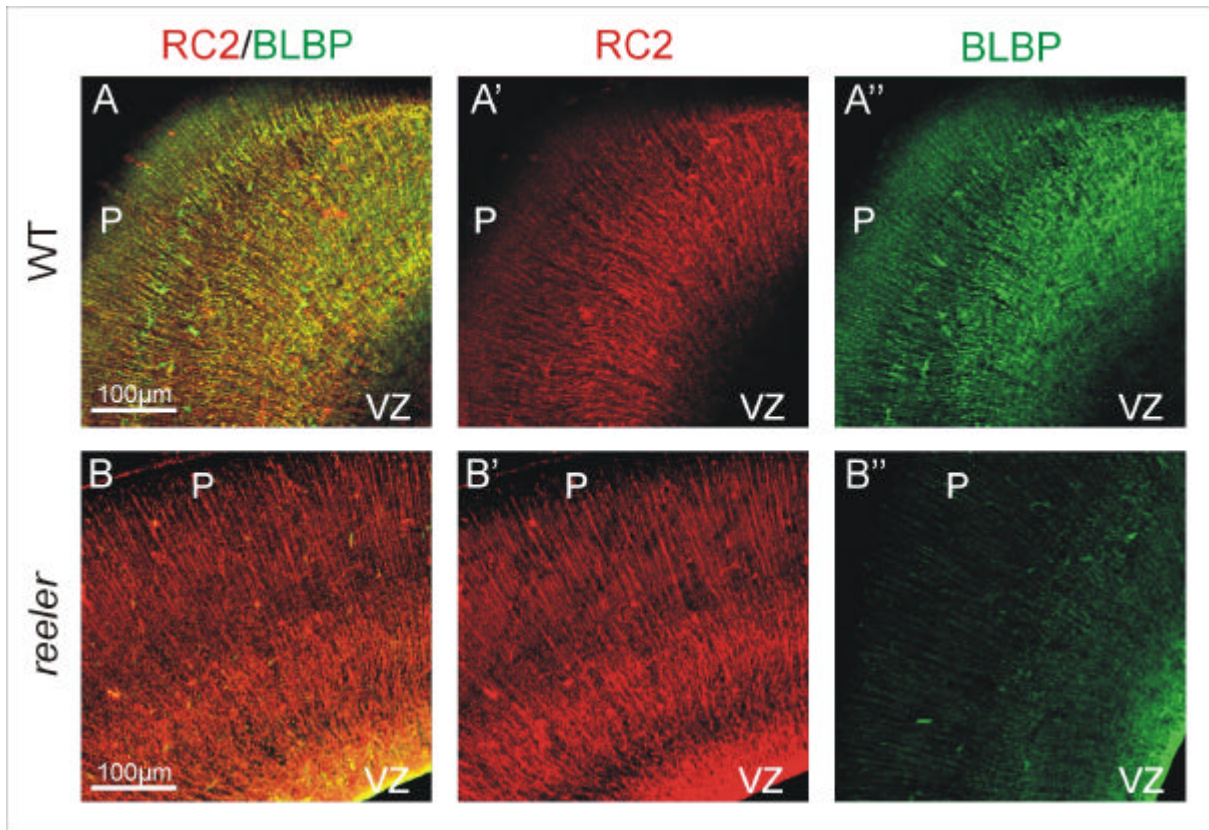


**Figure 5.21 Radial glial markers in sections of WT and *reeler* cerebral cortex**

Frontal vibratome sections of E16 WT (A) and *reeler* (B) cortex stained for RC2 and BLBP as indicated on the micrographs. A and B show maximum intensity pictures (~50 $\mu$ m); in A', A'' and B', B'' only single optical sections (~5 $\mu$ m) are shown. While RC2-staining appears normal in WT and *reeler* cortex, BLBP-immunoreactivity is highly reduced in the *reeler* cortex.

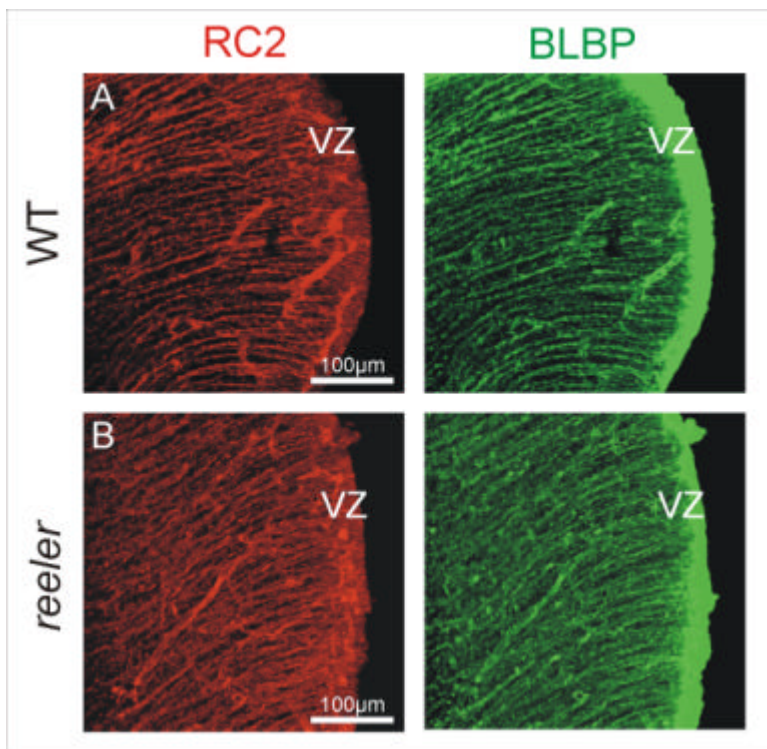


**Figure 5.22 Radial glial markers in sections of WT and *reeler* GE**

Frontal vibratome sections of E16 WT (A) and *reeler* (B) ganglionic eminence (GE) stained for RC2 and BLBP as indicated on the micrographs. Pictures shown are maximum intensity images (~50 $\mu$ m). Note, that levels of both RC2- and BLBP-immunoreactivity are comparable between WT and *reeler* GE.

In sections, it is difficult to discriminate whether BLBP is reduced only in the radial processes, but still persists in the soma (Fig. 5.21 A'' and B''), or whether the subpopulation of radial glia containing BLBP is truly reduced in the *reeler* cortex. To address this, we used acutely dissociated cell preparations where co-localization at the single cell level could be clearly assessed. The quantitative analysis of RC2-, GLAST- and BLBP-immunoreactive precursor cells (double-stained with anti-Ki67, for details see methods) revealed that in the early developing cortex, around the onset of neurogenesis (E12), the number of BLBP-immunoreactive cells was still comparable between WT and *reeler* cortex (WT: 29% of Ki67-positive cells were BLBP-positive; *reeler* 20%; Fig. 5.23).

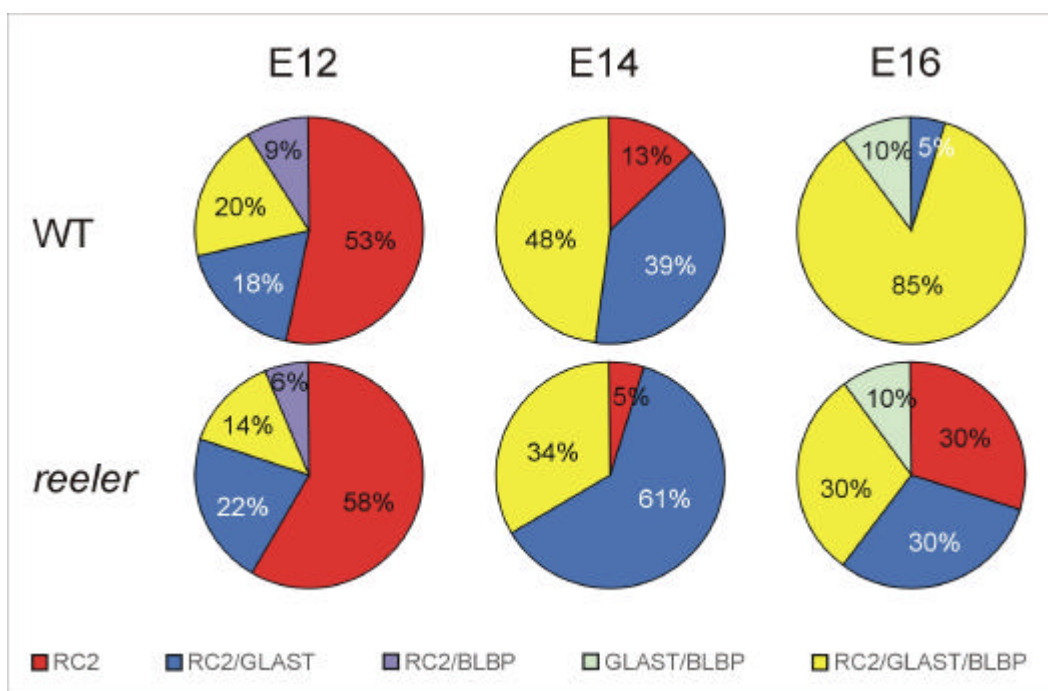


**Figure 5.23 Precursor subtypes in WT and *reeler* telencephalon**

The diagram depicts the quantitative co-localization analysis of precursor cells using RC2, anti-BLBP and anti-GLAST antisera in acutely dissociated cells of WT and *reeler* cortex at E12, E14 and E16. Note that alterations of the precursor subtype composition in the *reeler* cortex became more severe during development: At E12 no significant alteration of subtypes could be observed. At E14 the number of BLBP-immunoreactive cells is significantly decreased ( $p < 0.01$ ), whereas the number of GLAST-positive cells remained unchanged. Consistent with an increasing radial glia phenotype in the *reeler* during development at E16 the number of BLBP-immunopositive cells further decreased ( $p < 0.01$ ) and as well the number of GLAST-immunoreactive cells decreased in comparison to the WT ( $p < 0.05$ ). Note that the population of BLBP/GLAST-double-positive cells, putative astrocyte-precursors, remained unchanged. WT: n(E12)=311; n(E14)=1821; n(E16)=302; *reeler*: n(E12)=307; n(E14)=1853; n(E16)=295; (n) is the number of analysed cells.

However, at E14, the time when BLBP-immunoreactivity was first seen reduced in sections, also the number of BLBP-immunoreactive cortical cells was reduced in acutely dissociated cells (Fig. 5.23; WT: 48%, *reeler*: 34%;  $p < 0.01$ ). Further

consistent with the *in vivo* results obtained in sections, this defect in BLBP-positive cells in the *reeler* cortex became stronger during development (Fig. 5.23; E16: WT: 95%, *reeler*: 40%;  $p < 0.01$ ). Notably, the *reeler*-mutant BLBP-positive cells remained at a constant level from on E12, whereas in the WT neocortex BLBP-immunoreactivity constantly increases until almost all precursors contain BLBP (E16). This radial glia differentiation seems to depend on the presence of Reelin. At later stages (E16) also the number of GLAST-immunoreactive cells was slightly reduced (WT: 100%, *reeler*: 70%;  $p < 0.05$ ; Fig. 5.23). Thus, the maturation of radial glial cells in the cerebral cortex seems to depend on the presence of Reelin.

### 5.7.2 Radial glial morphology is impaired in the *reeler* cortex, but not in the GE

BLBP has been suggested to play a role in neuronal attachment thereby mediating bipolar morphology allowing neuronal migration (Feng *et al.* 1994; Anton *et al.* 1997). Previous work examining radial glial cells in the *reeler* cortex has reported impaired branching of pial endfeet (Pinto-Lord *et al.* 1982; Gadisseux and Evrard 1985; Hunter-Schaedle 1997) and morphological aberrations in the hippocampus (Förster *et al.* 2002), but nothing is known so far whether the process extension of radial glial cells is affected in the absence of Reelin. We therefore examined the length of radial processes by reconstructing the complete morphology of precursors of the VZ by tracing cells from the ventricular surface with Dil and classified the labelled cells according to the length of their basal processes as 'long', 'short', 'growth-cone' or 'club shaped' cells as described before (see as well Results 5.5.2).

Notably, the proportion of VZ cells with a long radial process was significantly decreased in the *reeler* cortex (WT: 57%; RIn: 43%;  $p < 0.01$ ; Fig. 5.24) and the population of 'club shaped' cells, characterized by a complete absence of a basal radial process, constituted the largest subpopulation of VZ cells in the *reeler* cortex (WT: 25%; RIn: 45%; Fig. 5.24). Even the population with 'short' basal processes ending underneath the cortical plate was reduced in the *reeler* cortex to less than half of their proportion in WT cortex (Fig. 5.24), suggesting severe problems in radial fiber extension in the absence of Reelin. Interestingly, radial glial cells of the GE were not altered in their morphology in the absence of Reelin (Fig. 5.24), consistent with their normal BLBP-content (see Fig. 5.22) and the absence of a migrational phenotype in the *reeler* mutant in this region (for review see: Caviness, Jr. and Rakic 1978; Lambert de Rouvroit and Goffinet 1998; Curran and D'Arcangelo 1998).

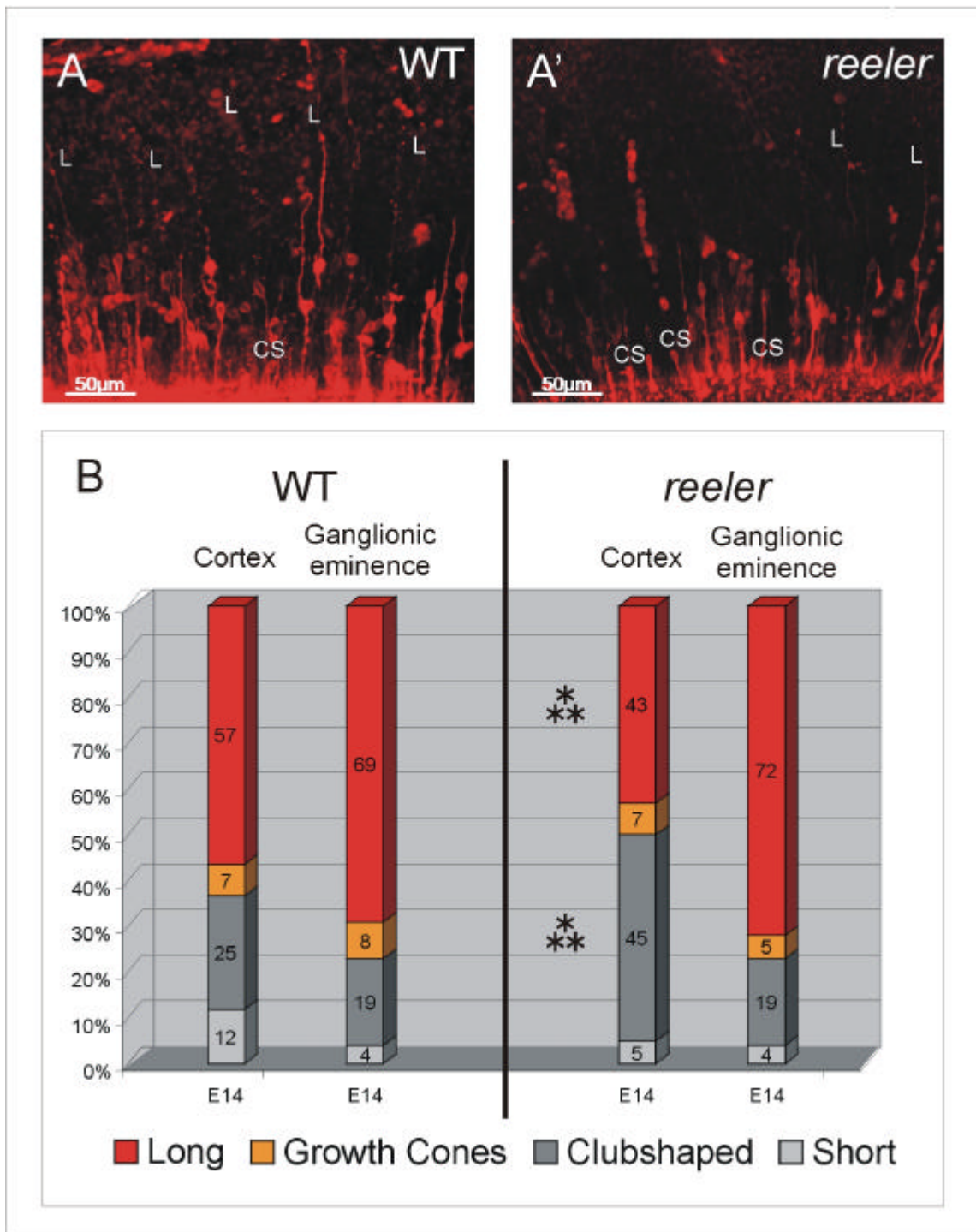


**Figure 5.24 3D-analysis of morphologically identified VZ precursor subtypes in the WT and *reeler* telencephalon**

3D-reconstruction of precursor morphology in the ventricular zone were performed as described before (Results 5.5.2). Panel A shows fluorescent pictures of 3D-reconstructions of DiI-labelled E14 cortices of WT (A) and *reeler* (A') littermates. In B the quantification of VZ precursor subtypes of WT and *reeler* telencephalon is depicted. Note that in the WT situation the majority of VZ precursor cells have a long 'radial glia like' morphology, both in the cortex and the ganglionic eminence. Comparing WT (left side) and *reeler*-mutant (right side) cortex the number of long VZ precursors is significantly reduced and the number of club-shaped cells is increased in the *reeler* cortex accordingly ( $p < 0.01$ ). Short cells and cells with a growth-cone are not affected by the loss of Reelin in the mutant. Note that there is no alteration of the morphologically identified subtypes of precursors in the ganglionic eminence between the WT and the *reeler*. L: long cell; CS club shaped cell. WT:  $n(\text{Ctx})=153$ ;  $n(\text{GE})=76$ ; *reeler*:  $n(\text{Ctx})=294$ ;  $n(\text{GE})=61$ ; ( $n$ ) gives the number of analysed cells.

Indeed, the proportion of BLBP-positive precursor cells closely resembles the proportion of VZ cells extending a long radial process, consistent with the suggestion that Reelin might regulate process extension in cortical radial glia by affecting BLBP (E14 WT: 48% BLBP+ cells, 57% long cells; E14 *reeler*: 34% BLBP+ cells, 43% long cells). Unfortunately, it is not possible to combine BLBP-immunolabelling with Dil tracing in sections to directly examine this idea, since Dil leaks from the cell membranes after cutting. However, we performed gain-of-function experiments *in vitro* to directly examine whether Reelin signalling might regulate the BLBP-content and the morphology of radial glial cells.

### 5.7.3 In-situ hybridisation analysis of the Notch pathway in the *reeler*

Recently it has been shown that over-expression of Notch1-ICD could induce a radial glial like phenotype and could up-regulate BLBP *in vivo* (Gaiano *et al.* 2000; Gaiano and Fishell 2002), thus representing the opposite phenotype of what we found in *reeler* radial glia. Since however the signalling mechanisms by which Notch1-activation may regulate radial glial morphology and BLBP-content remain unclear, we were wondering whether Reelin- and Notch-signalling might interact. Moreover it has been shown that in the *reeler* brain galactosyltransferase activity is greatly reduced (Shur 1982) and the fringe gene family, modulators of Notch, act as galactosyltransferases (Bruckner *et al.* 2000; Moloney *et al.* 2000). Hence, we wanted to examine whether the Notch pathway might be altered in the *reeler* mutant mice. We first analysed the mRNA expression of members of the fringe gene family, manic and lunatic Fringe (Mfng, Lfng), by in-situ hybridisation in WT and *reeler* E14 cortex. The analysis revealed that none of the two fringes is misexpressed in the *reeler* cortex during neurogenesis (Fig. 5.25). We further analysed the expression of Notch (N1-3) and its ligands Delta (DLL1,3), and Jagged the mammalian homologue of *Drosophila* Serrate (Ser1,2) in the *reeler* forebrain but no alterations in the expression pattern of the components of the Notch-pathway could be observed (Fig. 5.25), suggesting that several mechanisms exist by which radial morphology and BLBP-immunoreactivity is induced in the cerebral cortex during development.

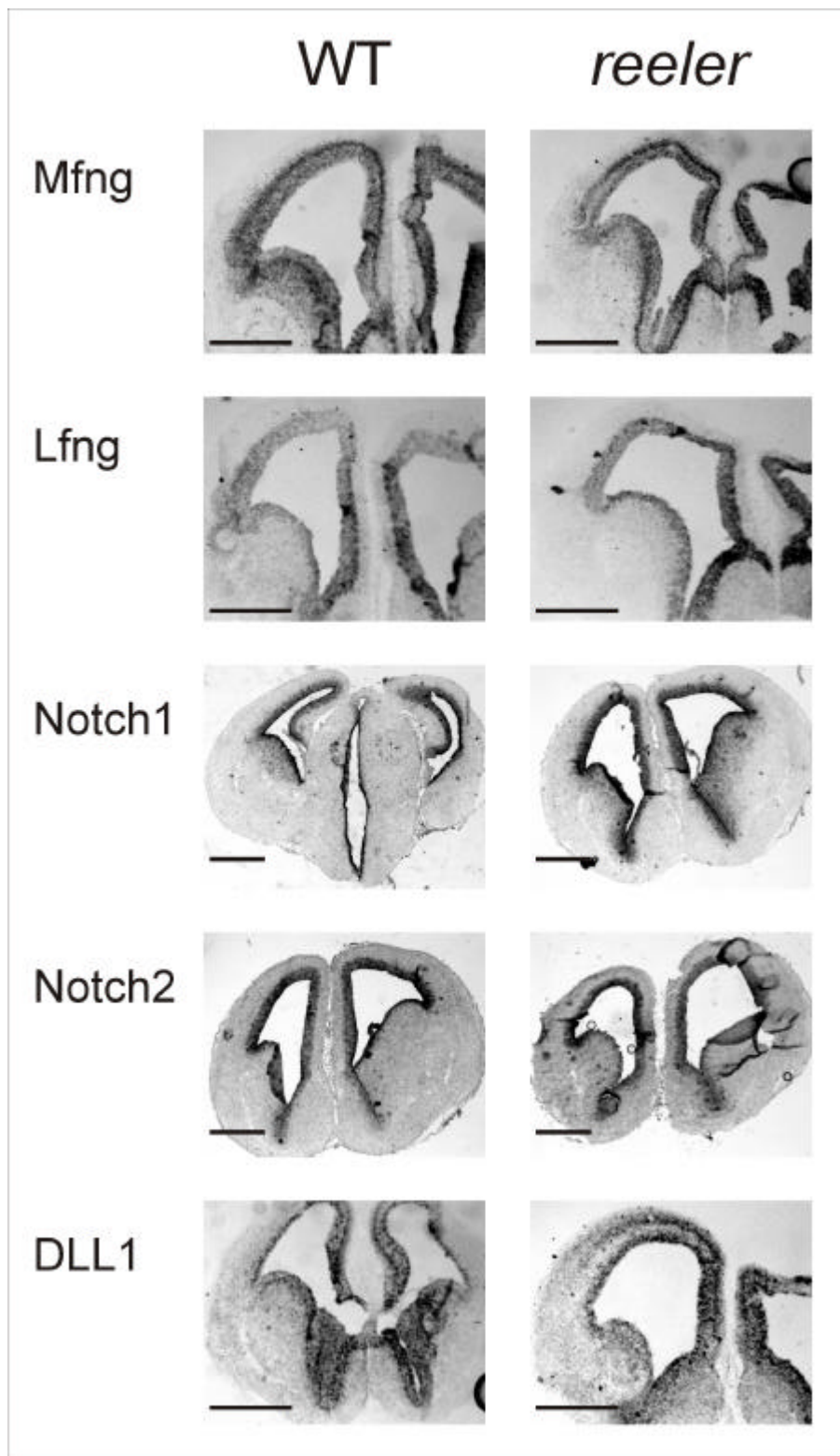


**Figure 5.25**  
**Expression-pattern**  
**of components of the**  
**Notch-pathway in the**  
**WT and *reeler***  
**forebrain**

Micrographs show the in-situ hybridisation analysis of components of the Notch-pathway (as indicated) at E14 in WT and *reeler* forebrain. Note, that the expression-pattern of none of the examined molecules is changed between WT and *reeler*. Scale bar 400µm

#### 5.7.4 Proliferation in the *reeler* telencephalon

Beside the suggestion that BLBP is involved in neuronal attachment and radial glia morphology, we hypothesized its potential role in proliferation or cell fate decision as described before. We therefore examined these aspects in the *reeler* mutant cortex that contains a reduced level of BLBP. First, we analysed the proliferation characteristics of precursor cells in the *reeler* cerebral cortex by quantifying the number of mitotic cells in the cortical ventricular (VZ) and subventricular zone (SVZ) by PH3-immunohistochemistry (Hendzel *et al.* 1997) in E14 WT and *reeler* littermates. The analysis revealed that the number of mitotic cells per section and region was well comparable between WT and *reeler* cerebral cortex (WT-cortex: VZ:  $54 \pm 2$  PH3+ cells/section,  $n=804$ ; SVZ:  $31 \pm 2$  PH3+ cells/section,  $n=463$ ; *reeler* cortex: VZ:  $49 \pm 2$  PH3+ cells/section,  $n=985$ ; SVZ:  $23 \pm 2$  PH3+ cells/section,  $n=456$ ; ( $n$ ) gives the number of analysed cells).

In addition, we analysed the plane of cell division in the *reeler* cortex. Previously it has been hypothesized, that cells dividing horizontally to the ventricular surface generate two daughter cells, which behave differently: whereas the upper cell radially migrates away and differentiates into a neuron, the lower one remains in the ventricular zone as precursor cell. This mode of cell division is considered as an asymmetrical division (Chenn and McConnell 1995). In contrast, divisions vertically to the ventricular surface are considered as symmetrical divisions, as two daughter cells are generated, that remain in the ventricular zone proliferating. Both daughter cells are supposed to behave identically (Chenn and McConnell 1995).

We therefore analysed the orientation of cell division by labelling the DNA with propidium-iodide (PI; Fig. 5.26A and B). Cell divisions were considered as vertical when the mitotic spindle was oriented in an angle of  $90^\circ$ - $60^\circ$  and horizontal with an angle of  $30^\circ$ - $0^\circ$  to the ventricular surface. The remainder ( $60^\circ$ - $30^\circ$ ) were classified as oblique. In regard to the orientation of cell division, no differences could be observed between WT and *reeler* mutant littermates (Fig. 5.26C). Thus, neither Reelin nor BLBP seem to exert a detectable effect on cell proliferation.

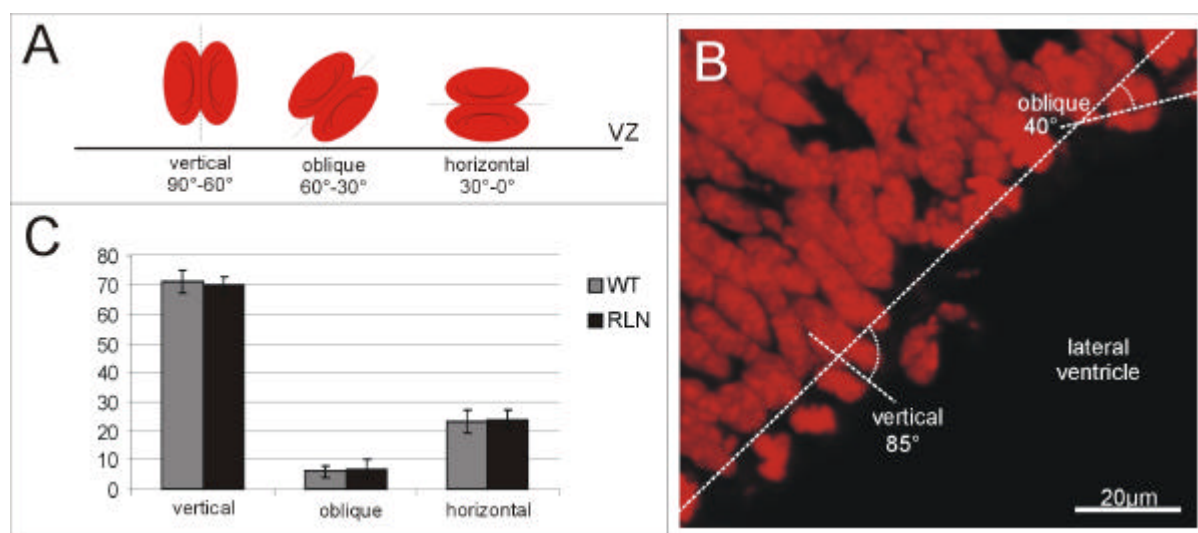


**Figure 5.26 Mode of cell division**

Panel A schematically depicts the angle of cell division relative to the ventricular surface. Panel B shows a fluorescent micrograph of a PI-labelled E14 WT cortical section. Ventricular zone cells in M-phase (vertical and oblique division) are depicted. Panel C shows the quantification of the plane of division in WT (gray) and *reeler* (black) E14 cortex.  $n(\text{WT})=111$ ;  $n(\text{reeler})=97$ ; ( $n$ ) gives the number of analysed cells: Error bars depict the SEM.

### 5.7.5 Neuronal differentiation and cell fate analysis in the *reeler* cortex

To examine the possibility that BLBP is involved in neuronal specification we first quantified the number of neurons in the embryonic cortex of normal and *reeler* mice. Therefore, we labelled WT and *reeler* vibratome sections from E16 telencephalon for  $\beta$ -tubulin-III but we could not detect any difference in the immunoreactivity of the neuronal marker between WT and *reeler* mice (Fig. 5.27A).

Since, however, the precursors with long radial processes were reduced by only 14% in the *reeler* cerebral cortex (see as well Fig. 5.24) one might expect only a small reduction in the number of neurons generated. To detect even small alterations of the neuron-number in the *reeler* cerebral cortex which were not visible by immunohistochemistry, we additionally crossed *reeler* mice with Tau::GFP-mice that show GFP-expression in all neurons (Tucker *et al.* 2001) and analysed the number of neurons in the embryonic cortex by FACS (Fig. 5.27B). However, the number of neurons is identical in the WT and *reeler* cerebral cortex at E14.

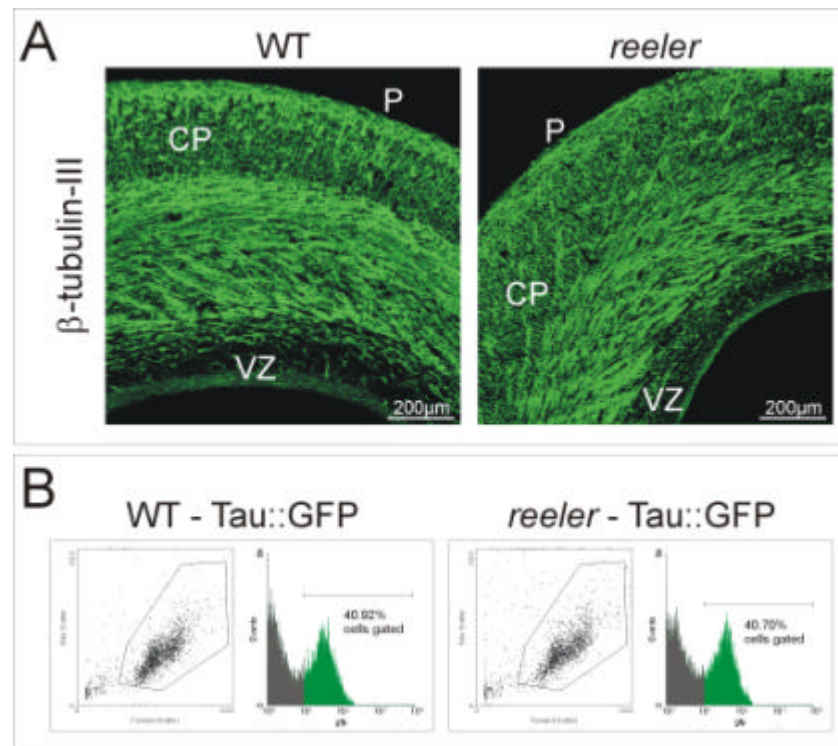


**Figure 5.27 The number of neurons remains unchanged in the *reeler* cortex**

A shows confocal maximum intensity pictures of E16 frontal sections of WT and *reeler* cerebral cortex stained with anti- $\beta$ -tubulin-III. Note that there is no visible difference in  $\beta$ -tubulin-III-immunoreactivity between WT and *reeler* cortex, while alterations in the organization of the cortical plate are already visible in the *reeler*. B shows examples of sort profiles of a WT-Tau::GFP and a *reeler*-Tau::GFP cortex at E14. Left histograms show the dot plot of cells in forward scatter (FSC; x-axis) and side scatter (SSC; y-axis). The polygonal area is indicating the gated, i.e. analysed, healthy cells. The histograms on the right side show the number of events (x-axis) and the GFP intensity (y-axis) of the cells analysed. Profiles show quantitatively, that in both the WT and the *reeler* cortex the number of green-fluorescent cells (GFP intensity  $> 1 \times 10^1$ ) is identical ( $\sim 41\%$  of all gated cells), suggesting, that the number of neurons at E14 is not altered between WT and *reeler* cortex.

A second set of experiments should elucidate more deeply cell fate alterations or proliferation defects. We crossed *reeler* and hGFAP-GFP(94-4) mice, a mouse-line where GFP is expressed under the hGFAP-promoter in all GLAST-immunoreactive radial glial cells (Zhuo *et al.* 1997; Malatesta *et al.* 2000). Consistent with the similar proportion of GLAST-immunoreactive cells in WT and *reeler*-mutant cortical cells at E14, no difference between the FACS-profile of WT-hGFAP-GFP(94-4) and *reeler*-hGFAP-GFP(94-4) cortical GFP-positive cells could be found (Fig. 5.28A). GFP-positive cortical cells were sorted by FACS, plated on a rat feeder-layer and cultured for 5 to 7 DM to perform clonal cell fate analysis of WT and *reeler* cortical precursors (see methods; Malatesta *et al.* 2000). Cells were stained with the mouse specific antibodies M2 and M6 (Lagenaur and Schachner 1981; Lund *et al.* 1985) to detect the sorted cells and their progeny (Malatesta *et al.* 2000). Triple-immunolabelling with cell-type specific antisera (anti- $\beta$ -tubulin-III for neurons, anti-GFAP for astrocytes, anti-nestin for precursor cells) was then used to identify the composition of the

M2M6-immuno-positive clones (cell clusters) derived from a single sorted precursor cell. Clones were classified as either pure neuronal clones (containing exclusively  $\beta$ -tubulin-III-positive cells), pure non-neuronal clones (containing no  $\beta$ -tubulin-III-positive cells) or mixed clones (containing both  $\beta$ -tubulin-III-positive and -negative cells). The analysis revealed that 60% to 70% of both WT and *reeler*-derived cortical clones were composed only of neurons; whereas 20% to 30% of the clones were pure non-neuronal and only a minority of about 10% were mixed clones. No significant differences in the clonal composition of WT and *reeler* cortical cells could be observed (Fig. 5.28B).

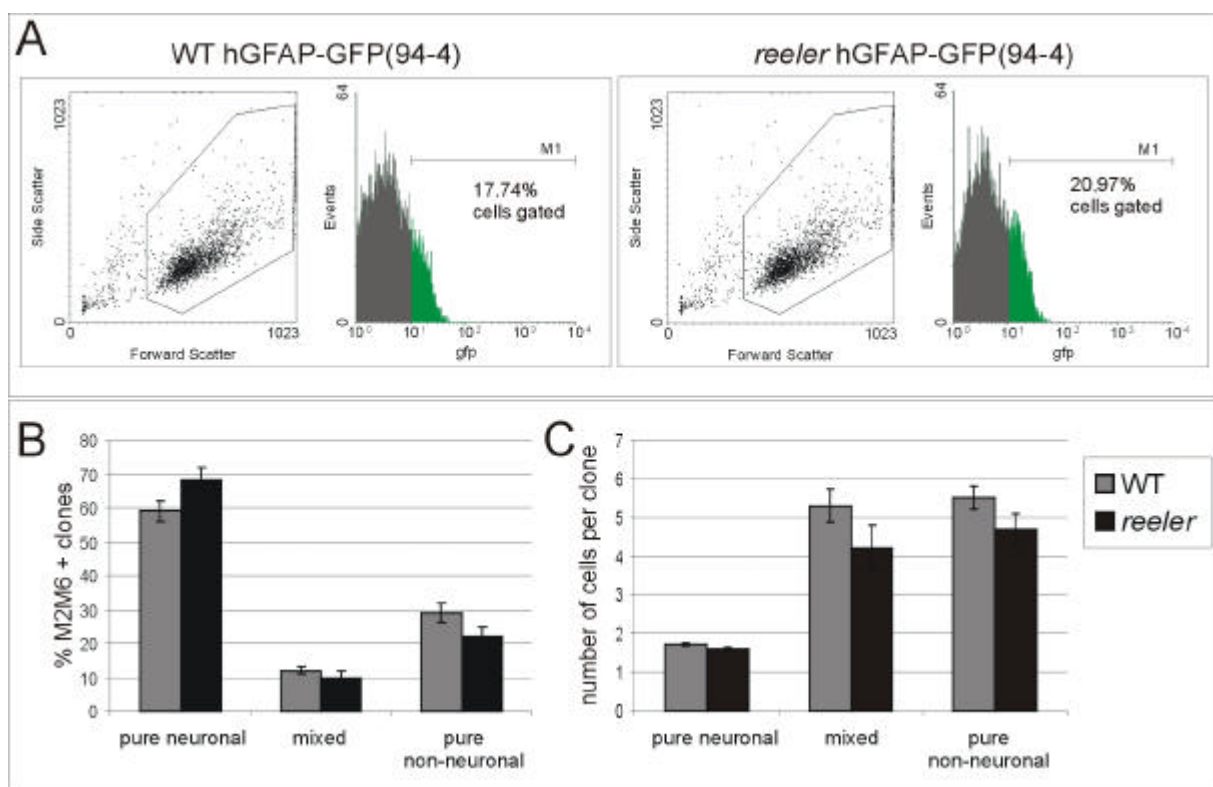


**Figure 5.28 Cell fate is not altered in the *reeler* cerebral cortex**

Panel A shows examples of sort profiles of a WT hGFAP-GFP(94-4) and a *reeler* hGFAP-GFP(94-4) cortex at E14. Left histograms show the dot plot of cells in forward scatter (FSC; x-axis) and side scatter (SSC; y-axis). The polygonal area is indicating the gated, i.e. analysed, healthy cells. The histograms on the right side show the number of events (x-axis) and the GFP-intensity (y-axis) of the cells analysed. Note that there are no quantitative differences in the number of GFP-positive precursors in WT and *reeler* cortex. Panel B and C depict the clonal analysis of FACS-sorted cells after 5-7 DIV on rat feeder layer. Cell clusters mostly comprised several cells and were interpreted as clones derived from single plated precursor cells. Clusters were classified as pure neuronal when all cells of a cluster were  $\beta$ -tubulin-III-immunoreactive, as pure non-neuronal when no cell of a clone was  $\beta$ -tubulin-III-immunoreactive and as mixed neuronal and non-neuronal when clones contained  $\beta$ -tubulin-III-positive and -negative cells. In B the clonal composition of WT- (gray) and *reeler*-sorted cells (black) is depicted. Note, that there is no alteration in cell fate in the *reeler* cortex. Panel C depicts the mean number of cells per clone, separately for pure neuronal, mixed and pure non-neuronal clones. As well the clonal size is the same in WT and *reeler* cortex, suggesting, that neither cell differentiation nor proliferation is impaired in the *reeler* cortex. n(WT)=718; n(*reeler*)=719; (n) gives the number of analysed clones. Error bars depict the SEM.

The analysis of the size of the clones in WT and *reeler* cortex showed as well that neither the mean clonal size nor the clonal size distribution (see as well Heins *et al.* 2001) were affected in *reeler* cortical precursor cells (Fig. 5.28C), which supports the data that precursor proliferation is normal in the *reeler* telencephalon.

In these experiments, however, sorted cells were plated on a feeder-layer derived from WT wistar rats. Since we can not exclude, that the endogenous amount of Reelin in rat cortical cells was sufficient to rescue any differentiation or proliferation defects of *reeler* cortical cells, we recapitulated the clonal cell fate analysis by infecting pure WT or *reeler* cortical cell cultures (E14) with a replication incompetent BAG-retrovirus (Price *et al.* 1987) carrying the reporter gene lacZ encoding  $\beta$ -galactosidase (see Methods 4.3.5). Analysing the  $\beta$ -galactosidase positive clones after 5 to 7 DIV for their clonal composition and size confirmed that neither fate nor proliferation of cortical precursor cells were altered in the *reeler* telencephalon (data not shown). These experiments show, that in the *reeler* telencephalon cell proliferation and cell fate is normal and BLBP seems not to be implicated in these important precursor functions.

### 5.7.6 Reelin signalling affects radial glial identity *in vitro*

#### 5.7.6.1 Reelin-signalling affects BLBP-content *in vitro*

To examine whether the observed reduction of BLBP in the *reeler* cortex is a direct consequence of the loss of the Reelin-protein, WT and *reeler* mutant cells from E14 cortex were cultured in Reelin-conditioned medium, containing high amounts of Reelin-protein or in control medium. After 24 hours *in vitro*, cells were fixed and stained for RC2 and BLBP. The number of RC2- and BLBP-immunoreactive precursors was analysed (Fig. 5.29). The content of Reelin protein in medium collected from 293-cells stably transfected with a control or Reelin-expression plasmid was confirmed by western blot analysis (see Methods 4.3.6; D'Arcangelo *et al.* 1995; Förster *et al.* 2002).

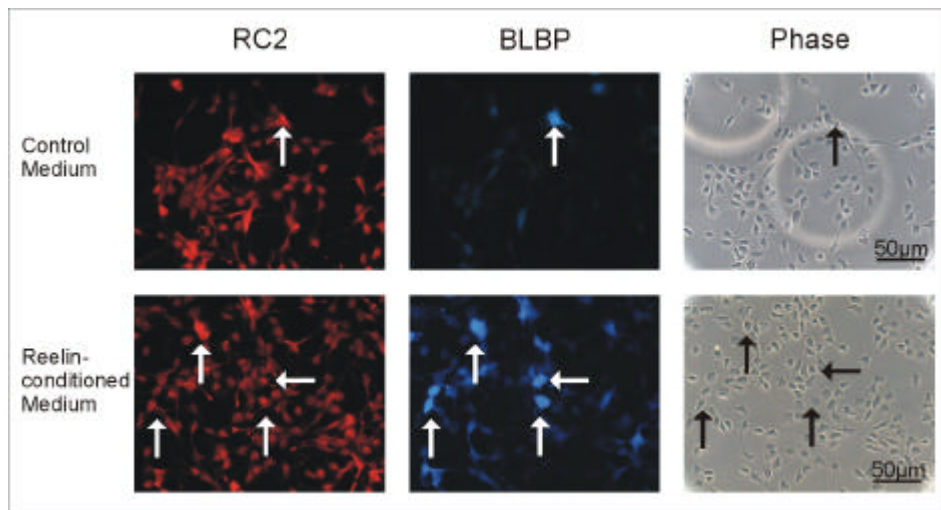


**Figure 5.29 Reelin-signalling affects BLBP-immunoreactivity *in vitro***

Fluorescent micrographs of E14 cortical dissociated WT-cells cultured in control or Reelin-conditioned medium (as indicated) for 24 hours and stained for RC2 and BLBP (as indicated). Note the increase of BLBP-immunoreactivity in the cells cultured in the presence of Reelin-protein.

For control, we also fixed cells shortly after plating (2 hours) when indeed no differences were detected in the number of RC2- and BLBP-immunopositive cells cultured in control- or Reelin-conditioned medium (Fig. 5.30A). Thus, after 2 hours *in vitro* Reelin had no effect on BLBP-immunoreactivity in cortical precursor cells. However, when cells were fixed after 24 hours *in vitro*, the number of BLBP-immunoreactive cells cultured in Reelin-containing medium was significantly increased. In the presence of Reelin 55-60% of RC2+ cells were also BLBP-immunopositive ( $p < 0.01$  compared to control-medium; Fig. 5.29 and 5.30A) and no significant difference between cells from WT or *reeler* cortex could be detected any longer (Fig. 5.30B). We also confirmed this effect in chemically defined medium conditioned from control or Reelin-secreting cells to rule out any unspecific effects of the medium (RC2/BLBP-immunoreactivity: control medium:  $39\% \pm 1$ ,  $n=123$  cells; Reelin-cond.medium:  $61\% \pm 1$ ,  $n=142$  cells;  $p < 0.01$ ).

These results demonstrate that first *reeler* mutant cells that have never been in contact with Reelin protein are still able to respond to Reelin-signalling and second that the addition of Reelin *in vitro* leads to a complete rescue of the decrease in BLBP-positive cells from *reeler* mutant cerebral cortex *in vitro*. Furthermore, these results demonstrate that the amount of Reelin released by marginal zone cells in cultures from WT cortex is limiting and higher Reelin-content in the medium further increases the number of BLBP-immunoreactive cells. Interestingly, however, cells from the GE and spinal cord, do not react to Reelin *in vitro*, further supporting the specificity of the observed effects (Fig. 5.30C).

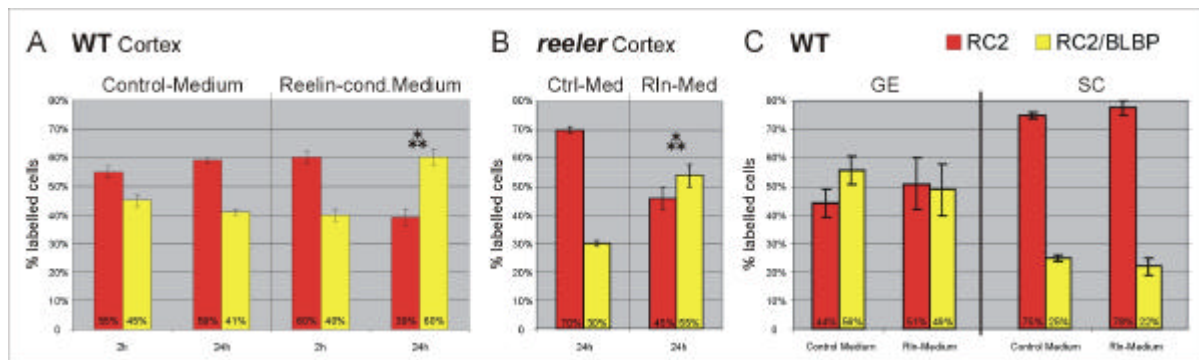


**Figure 5.30 Reelin-signalling affects BLBP-immunoreactivity *in vitro* (Quantification)**

Diagrams show the quantitative analysis of RC2- and BLBP-immunoreactivity of E14 dissociated cells cultured for 2 or 24 hours in control or Reelin-conditioned medium, respectively. Either WT (A) or *reeler* (B) cortical cells were cultured. In cells cultured in the presence of Reelin for 24 hours BLBP-immunoreactivity was significantly increased ( $p < 0.01$ ). For the *reeler*-cells note first, that in the *reeler* cortex BLBP-immunoreactivity was significantly decreased in the control-condition compared to the WT (see as well Fig. 5.23) and second, that *reeler* cortical cells still have the competence to react to Reelin-signalling and up-regulate BLBP when cultured in Reelin-conditioned medium for 24 hours. Note, that a comparable amount of WT and *reeler* cortical cells are BLBP-immunoreactive after 24 hours in the presence of Reelin. In C the quantitative analysis shows that E14 cells of neither the ganglionic eminence (left panel) nor the spinal cord (right panel) have the competence to up-regulate BLBP in the presence of Reelin. WT: n(CTRL, 2h)=1652, n(CTRL, 24h)=2247, n(RIn-med, 2h)=1523, n(RIn-med, 24h)=2271; *reeler*: n(CTRL, 24h)=1263, n(RIn-med, 24h)=1274; n(GE)=973; n(SC)=886: (n) gives the number of analysed cells. Error bars depict the SEM.

The increase of BLBP-positive cells could be due to an up-regulation of BLBP protein in formerly negative cells, or by selectively increased proliferation of the BLBP-immunopositive subpopulation of precursors. To discriminate between these possibilities, cells were cultured in the presence of BrdU in Reelin-conditioned or control-medium. BrdU was added to the culture medium either for 24 hours or for only 1 hour (see Methods 4.6.3 for details). In order to label all cells that proliferated during the 24h-incubation, and thus to detect precursors, that might have stopped proliferation due to the conditioned medium, BrdU was present throughout the entire incubation time (Methods 4.6.3 paradigm A). In a second approach, we performed a 1 hour BrdU-pulse labelling (Methods 4.6.3 paradigm B) to detect differences in the cell cycle length. The analysis of the LI (see methods; Nowakowski *et al.* 1989) of RC2-single- and RC2/BLBP-double-immunoreactive cells did not reveal any differences, neither a silencing nor a selective increase in the proliferation of BLBP-positive cells in Reelin conditioned medium (Table 5.5A). Moreover, we could not detect any significant effect of Reelin on neuronal differentiation and the overall population of precursors (Table 5.5B). Taken together, these data strongly suggest that Reelin positively regulates the BLBP-content in cortical precursors, but not in those from the GE or spinal cord.

Table 5.5 Labelling index (LI) and number of neurons in cultures with conditioned medium

<b>A</b>		
	<b>RC2-only</b>	<b>RC2/BLBP</b>
<b>BrdU 24h: control medium</b>	0.89±0.05	0.96±0.03
<b>BrdU 24h: Reelin-cond.medium</b>	0.93±0.1	0.83±0.04
<b>BrdU 1h: control medium</b>	0.37±0.17	0.45±0.09
<b>BrdU 1h: Reelin-cond.medium</b>	0.47±0.12	0.53±0.17

<b>B</b>		
	<b>2h</b>	<b>24h</b>
<b>Control medium</b>	63%±3	53%±5
<b>Reelin-cond.medium</b>	52%±4	61%±1

Note. Panel A depicts the labelling index (LI) of RC2-only and RC2/BLBP-immunoreactive precursors from E14 mouse cortex cultured in control or Reelin-conditioned medium for 24 hours. The LI was calculated for either cells cultured for 24 hours in the presence of BrdU (BrdU 24h) or for cells cultured for 10 hours without, then 1 hour in the presence of BrdU followed by another 13 hours without BrdU (BrdU 1h). Note, that the LI is not changed between control and Reelin-conditioned medium. Panel B depicts the percentage of neurons in cultures from E14 mouse cortex, cultivated in either control or Reelin-conditioned medium for 2 hours or 24 hours. Note, that the number of neurons is not changed between control or Reelin-conditioned medium. A1: n(CTRL, 24h)=607, n(RIn, 24h)=617, n(CTRL, 1h)=595, n(RIn, 1h)=603; B: n(Ctrl, 2h)=382, n(Ctrl, 24h)=411, n(RIn, 2h)=402, n(RIn, 24h)=425. (n) gives the number of analysed cells. ± standard error of the mean (SEM).

#### 5.7.6.2 Reelin-signalling affects radial glial morphology *in vitro*

Since in the Reelin-deficient cerebral cortex of *reeler* mice as well radial glial process extension is impaired (see Fig. 5.24), we furthermore wanted to analyse whether radial glial morphology is also positively regulated by Reelin. We therefore examined the morphology of RC2-immunoreactive precursor cells from E14 WT and *reeler* cerebral cortex, cultured for 24 hours in Reelin-conditioned or control medium. While after dissociation all cells were round, about 50% of precursor cells had extended processes of at least the length of the diameter of the cell soma after 24 hours *in vitro* (Fig. 5.31A). Notably, the vast majority of these cells had a bipolar morphology and virtually no precursors acquired a multipolar morphology. No significant difference was detected between the morphology of WT and *reeler* cortical precursors (Fig. 5.31B; WT: 53%±4, RIn: 45%±4). Interestingly, the proportion of precursor cells that acquired a bipolar morphology (53%, see Fig. 5.31B) closely resembled the proportion of long cells labelled by Dil from the ventricular surface (57%, see Fig. 5.24). In Reelin-containing medium, however, the number of cells with processes increased significantly to 80-90% ( $p < 0.01$ ) and no difference was detectable between precursors from WT or *reeler* mutant cortex (WT: 83±3, RIn: 71%±2; Fig. 5.31B), suggesting a full rescue of the deficits in radial glial process

extension in the *reeler* cerebral cortex. Taken together, these results show that Reelin regulates BLBP-immunoreactivity and the morphology of radial glial cells.

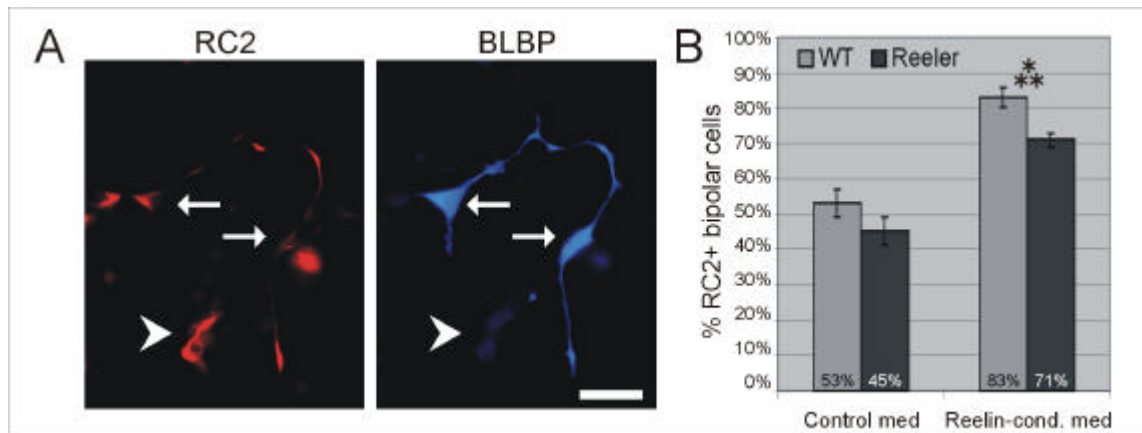


**Figure 5.31 Reelin-signalling affects radial glial morphology *in vitro***

Panel A depicts fluorescent micrographs of two RC2-single positive precursors without processes (arrowhead) and two RC2/BLBP-double-immunoreactive bipolar WT cortical cells (E14) cultured in Reelin-conditioned medium for 24 hours. Panel B depicts the quantitative analysis of the morphology of E14 precursor cells after 24 hours culture in control or Reelin-conditioned medium, respectively. Either WT (light gray) or *reeler* (black) cortical cells were cultured. Cells cultured in the presence of Reelin for 24 hours exhibited significantly more often a bipolar morphology than cells cultured in control medium ( $p < 0.01$ ) concomitant to the increase in BLBP (see Fig. 5.29 and 5.30).  $n(\text{WT})=429$ ,  $n(\text{reeler})=396$ . ( $n$ ) gives the number of analysed cells. Error bars depict the SEM. Scale bar 20 $\mu\text{m}$ .

### 5.7.7 Reelin signals directly to radial glial cells

Since previous work has suggested that signalling from neurons attaching to radial glia influences BLBP-immunoreactivity and their process extension (Feng *et al.* 1994), we examined whether the up-regulation of BLBP by Reelin might also be mediated by direct signalling to radial glia. We therefore used two approaches to reduce the number of neurons in our cultures. First we isolated GFP-negative cells from E14 cortex of Tau::GFP-mice that contain GFP specifically in all neurons (Tucker *et al.* 2001; Heins *et al.* 2002). Selection of GFP-negative cells reduced the proportion of neurons from about 50-60% in unselected cells ( $\beta$ -tubulin-III-immunoreactive cells after 2h *in vitro*: 57% $\pm$ 3,  $n=767$ ) to 25%  $\beta$ -tubulin-III-immunoreactive cells 2 hours after plating ( $n=123$ ). Interestingly, the increase in BLBP-immunoreactive cells after Reelin addition was not reduced but even higher in these cultures despite the reduced number of neurons (Ctrl-med: 41% $\pm$ 7, Rln-cond.med: 77% $\pm$ 5;  $p < 0.04$ ; Fig. 5.32A' compare to Fig. 5.30A). Since, however, still a quarter of all cells were neurons in these cultures, we further decreased their proportion by positively sorting radial glial cells from the hGFAP-GFP(94-4) mouse line that contains GFP in radial glial cells (Zhuo *et al.* 1997; Malatesta *et al.* 2000) as

described before (see Results 5.7.5 and as well Malatesta *et al.* 2000). When only the strongest GFP-positive cells were isolated by FACS, sorted cells were almost all RC2-positive and only  $13\% \pm 7$  were  $\beta$ -tubulin-III-immunoreactive 2 hours after plating (Fig. 5.32B;  $n=197$ ). However, despite the strong reduction of neurons in these cultures BLBP-immunoreactivity could still be significantly increased by Reelin-conditioned medium (Fig. 5.32B; Ctrl-med:  $32\% \pm 1$ , Rln-cond.med:  $57\% \pm 8$ ;  $p < 0.04$ ), strongly suggesting that radial glial cells respond directly to Reelin-signalling by BLBP-upregulation.

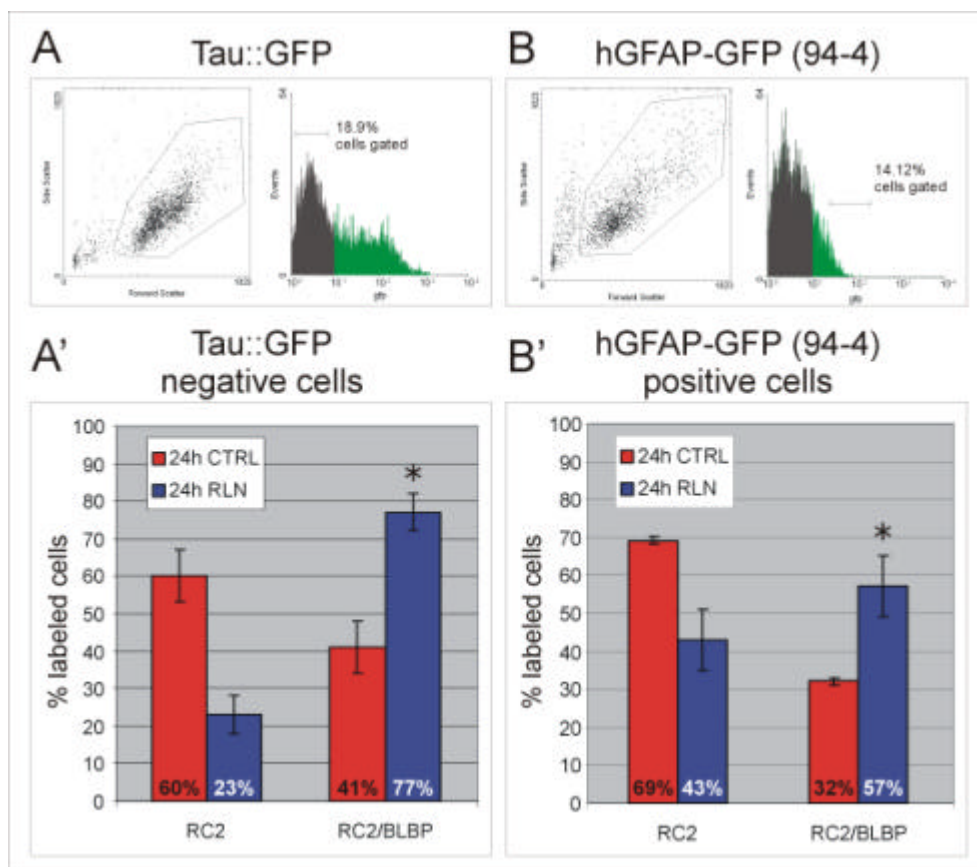


**Figure 5.32 Reelin signals directly to radial glial cells**

Panel A and B show examples of sort profiles of Tau::GFP and hGFAP-GFP (94-4) cortices at E14. Left histograms show the dot plot of cells in forward scatter (FSC; x-axis) and side scatter (SSC; y-axis). The polygonal area is indicating the gated, i.e. analysed, healthy cells. The histograms on the right side show the number of events (x-axis) and the GFP-intensity (y-axis) of the analysed cells. Figure A and A' show the quantitative analysis of E14 FACS-sorted GFP-negative precursor cells from a Tau::GFP-mouse (Tucker *et al.* 2001) cultured in control or Reelin-conditioned medium. A') After 24 hours in the presence of Reelin up to 80% of RC2-immunoreactive cells were as well BLBP-positive ( $p < 0.04$ ). Note that this up-regulation of BLBP in the neuron-depleted cultures even exceeded the BLBP up-regulation in the mixed-cultures (see as well Fig. 5.30), strongly suggesting that neurons are not required for Reelin to up-regulate BLBP in radial glial cells. B shows the quantitative analysis of E14 FACS-sorted GFP-positive precursor cells from a hGFAP-GFP(94-4) mouse (Zhuo *et al.* 1997; Malatesta *et al.* 2000) cultured in control or Reelin-conditioned medium. B') After 24 hours in the presence of Reelin up to 60% of RC2-immunoreactive cells were as well BLBP-positive ( $p < 0.04$ ). Tau::GFP:  $n(\text{CTRL})=237$ ,  $n(\text{Rln})=354$ ; hGFAP-GFP(94-4):  $n(\text{CTRL})=215$ ,  $n(\text{Rln})=367$ . ( $n$ ) gives the number of analysed cells. Error bars depict the SEM.

### 5.7.8 Expression of Reelin-receptors in radial glial cells by real-time RT-PCR

In fact, the Reelin-mediated up-regulation in the neuron-depleted cultures even slightly exceeded the up-regulation in the mixed cultures (compare Fig. 5.30 and Fig. 5.32; WT cortex 21% up-regulation, Tau::GFP negative cells: 36% up-regulation, hGFAP-GFP(94-4) positive cells: 25% up-regulation), strongly suggesting that neurons are not required to mediate Reelin-signalling to radial glial cells. Because of that, radial glial cells might respond directly to Reelin-signalling. Even though the analysis of the Reelin-signalling pathway has been focussed on the signalling cascade in neurons, it has recently been shown that some components are as well expressed in the ventricular zone of the mouse cerebral cortex (Sheldon *et al.* 1997; Trommsdorff *et al.* 1999; Magdaleno *et al.* 2002; Förster *et al.* 2002; Luque *et al.* 2003)). Therefore, we analysed whether radial glial cells express the known Reelin-receptors. We examined the expression of these receptors in radial glial cells by real-time RT-PCR on RNA derived from FACS-sorted radial glial cells (hGFAP-eGFP-mice; Nolte *et al.* 2001) and FACS-sorted neurons (Tau::GFP-mice; Tucker *et al.* 2001). Interestingly, ApoER2- and VLDLR-mRNA was detectable in sorted radial glial cells. Whereas ApoER2 is expressed in comparable amounts in radial glia and neurons, the VLDLR-mRNA level is reduced in radial glia compared to neurons. However, these data indicate that radial glial cells indeed express the known Reelin-receptors ApoER2 and VLDLR (Fig. 5.33), showing that radial glial cells express the prerequisite to perceive direct Reelin-signalling.

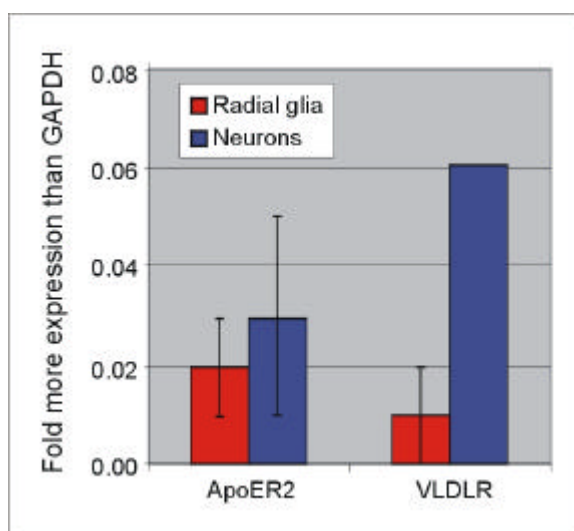


**Figure 5.33 Radial glial cells express the Reelin receptors ApoER2 and VLDLR**

mRNA-levels of ApoER2 and VLDLR in radial glial cells (red) and neurons (blue) sorted from E14 mouse cerebral cortex. Note, that ApoER2 is expressed in a comparable amount in neurons and radial glia. VLDLR is expressed in radial glial cells even if reduced compared to neurons. ApoER2: n(RG)=9, n(neurons)=6; VLDLR: n(RG)=4, n(neurons)=1; (n) is the number of RT-PCR runs; Error bars depict SEM.

## 6. SHORT SUMMARY

### The precursor pool:

- ?? The embryonic mouse precursor pool is a heterogeneous population of proliferating cells consisting of up to 5 subpopulations at a given developmental point of time detectable by the antisera against RC2, GLAST and BLBP.
- ?? Some of the precursor subtypes are correlated to the phase of neurogenesis (RC2-only, RC2/BLBP+, RC2/GLAST+) others to gliogenesis (GLAST/BLBP) others persist during whole development (RC2/GLAST/BLBP+).
- ?? Specific precursor subtypes express basic Helix-Loop-Helix-transcription factors.
- ?? Precursor cells of the SVZ are negative for RC2/BLBP/GLAST-immunoreactivity.
- ?? The precursor subpopulations identified by differential immunoreactivity to RC2, GLAST and BLBP differ in their cell cycle characteristics.

### Radial glial cells:

- ?? The immunocytochemically identified precursor subtypes RC2-only, RC2/GLAST+ and RC2/GLAST/BLBP+ comprise cells with a long radial morphology.
- ?? Radial glial cells constitute the majority of precursor cells of the VZ in the cerebral cortex, the GE and the spinal cord during embryonic development.
- ?? Radial glial cells divide without retracting their processes during M-phase.

### The *reeler* mouse

- ?? The immunocytochemically-identified precursor composition is altered in the *reeler* cerebral cortex but not the GE. The glial antigen BLBP is significantly down-regulated in *reeler* cortical precursor cells.
- ?? The morphology of precursor cells of the VZ is impaired in the *reeler* cerebral cortex but not the GE. The number of long radial glial cells is significantly decreased in the *reeler* cerebral cortex.
- ?? The precursor cell characteristics proliferation, cell fate and neuronal differentiation are not altered in the *reeler* cerebral cortex.
- ?? Notch-pathway components are normally expressed in the developing *reeler* forebrain.
- ?? Reelin-signalling can directly up-regulate BLBP-immunoreactivity and can induce bipolar morphology in precursor cells of the cerebral cortex *in vitro*.
- ?? Radial glial cells of the mouse cerebral cortex express components of the Reelin-signalling pathway.

## 7. DISCUSSION

Our results show, that neither their morphology nor their biochemical characteristics are specific for radial glial cells. Neuroepithelial cells have as well radial processes and cannot be distinguished from radial glia by means of morphology and as well the antisera RC2, BLBP and GLAST are not specific for radial glial cells. RC2 as well labels neuroepithelial cells in the developing cerebral cortex and migrating neuroblasts in the RMS. Furthermore, BLBP and GLAST also mark multipolar cells and mature astrocytes. For this it is important to define what a radial glial cell is in regard of the criteria used in this work. Certainly, one obligatory feature is the radial morphology but likewise required are the glial attributes. Thus, radial glial cells are necessarily characterized by their morphology and the content of GLAST and/or BLBP.

### 7.1 Radial glial cells as a major precursor subtype

#### 7.1.1 Contribution of radial glial cells to the progenitor pool

Our results obtained in sections and by acutely dissociated cell preparations demonstrated radial glial cells as actively dividing precursor cells. This raises the question to which extent radial glial cells contribute to the progenitor pool. The analysis using the antibodies RC2, anti-GLAST and anti-BLBP suggested that almost the entire progenitor pool consists of radial glial cells. However, it was not clear, whether these so-called radial glial markers were specifically labelling cells with long radial processes. We therefore used an alternative approach to discover the real contribution of radial glial cells to the progenitor pool. Labelling of cells with Dil from the ventricular surface and following 3D-reconstruction revealed four distinct subtypes of VZ-precursors by means of morphology. Whereas the majority of precursors of the VZ had processes contacting the pial surface (long cells; 80-60%), only the minority had shorter processes (short cells, growth cone cells and club-shaped cells). Such a high proportion of radial glial precursor cells strongly exceeds the number of glial progenitor cells in the developing cortex during neurogenesis (E12-E17; Grove *et al.* 1993; Williams and Price 1995; Reid *et al.* 1995). Since indeed it has recently been shown that radial glial cells have a broader potential than expected and not only contribute to the generation of neurons, but are the main source for neurons in the cerebral cortex (Malatesta *et al.* 2000; Malatesta *et al.*

2003) the view of radial glial cells has to be changed in two regards. Radial glial cells comprise the majority of precursors during neurogenesis and are precursors for neurons and glial cells (Fig. 7.1).

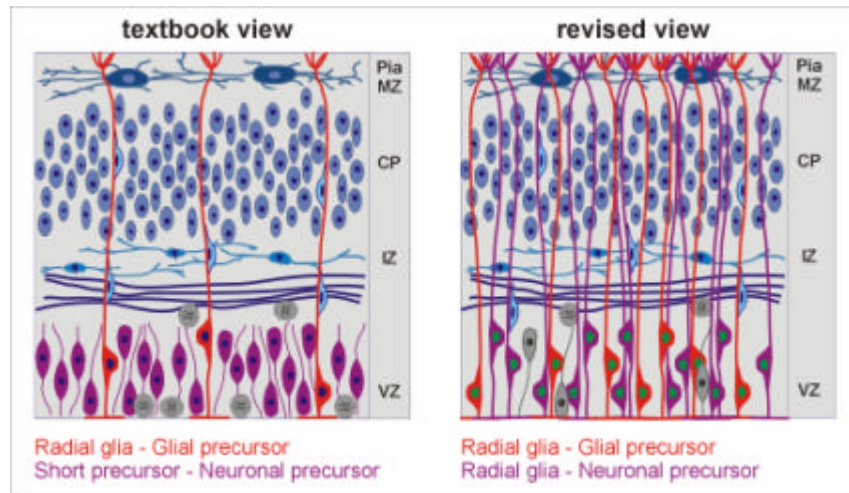


**Figure 7.1 Revised view on the development of the cerebral cortex**

Schematical drawing of the composition and architecture of the cerebral cortex during neurogenesis. The scheme on the left side depicts the previous textbook view (modified from Zigmond *et al.* 1999) whereas the scheme on the right side depicts the revised view with a major contribution of radial glial cells to the progenitor pool and their role as neuronal precursors.

### 7.1.2 Proliferation of precursor cells and radial glia

Moreover, our results demonstrate for the first time that almost all radial glial cells in the rodent cortex are dividing throughout neurogenesis. Most radial glial cells labelled from the pial surface contain the Ki67-antigen and cumulative BrdU-labelling showed that nearly all Ki67-immunoreactive cells in the telencephalon are actively dividing. We therefore conclude that radial glial cells in the rodent cortex do not contain a quiescent subpopulation as observed for primate radial glia (Schmechel and Rakic 1979). It seems likely that these species differences are related to the differences in the thickness of the cortex and the respective length of radial glial processes in rodents and primates. Whereas radial glial cells in primate cortex approach a length of several millimetres, those from rodent cortex cover less than a tenth of this distance (for review see Rakic 1988; Rakic 1995). Since precursor cells are thought to retract their processes during cell division (Hinds and Ruffett 1971), processes of a certain length might restrict the cell cycle progression of precursor cells. However, we could show by combining *in vivo* tracing of radial glial cells from the pial surface with BrdU-pulse labelling that radial glial cells are still in contact with the pial surface 35 hours after S-phase, indicating that they do not retract their

processes during M-phase. These data therefore suggest that process retraction does not necessarily accompany cell division and that radial glial cells might maintain their long radial processes during M-phase of the cell cycle. Recent *in vivo* work on the proliferation of radial glial cells (Noctor *et al.* 2001; Noctor *et al.* 2002; Miyata *et al.* 2001; Tamamaki *et al.* 2001) further confirmed our data. Thus, the thickness of the cortex and therefore the length of the radial process should not necessarily influence proliferative activity.

In support of the idea that radial glial cells proliferate without retraction of their process neurons were also observed to migrate radially by perikaryal translocation as first described by Morest (1970). Recently this mode of cell migration could be visualised *in vivo* by time-lapse video microscopy (Miyata *et al.* 2001; Nadarajah *et al.* 2001). Thereby, the basally oriented neuroblast, generated by an asymmetric cell division, inherits the radial process of the radial glial progenitor and translocates its soma along the process (see also Fig. 5.19A, lowest panel). The basally inherited radial glial process remains connected to the pial surface and thus provides an anchor for somal movement to its final position in the cortical plate.

## 7.2 Heterogeneity of the precursor pool

### 7.2.1 Subtypes of precursor cells

Our results obtained in sections and in morphologically traced acutely dissociated cells showed that precursor cells with a radial morphology are almost all RC2-immunoreactive, but are heterogeneous in their GLAST- and BLBP-content. Thus, only subsets of radial precursor cells express glial characteristics during neurogenesis and hence are radial glial cells. This heterogeneity seems to be lost during development and radial precursors then become homogeneously RC2/GLAST/BLBP-immunopositive. This is concluded from the analysis of radial processes in sections that are in almost all cases triple-labelled at later stages (E18). Moreover, the RC2+ or RC2/GLAST+ subsets are not present anymore after neurogenesis in acutely dissociated cortical cells. It will now be important to further determine the function of these distinct sets of precursor cells. Since it was shown that BLBP is induced by neurons attaching to radial glia (Feng *et al.* 1994), one might e.g. speculate that the BLBP+ radial glia subset is involved in the guidance of migrating neurons. Taken together, these results revise the picture of radial glial cells as a homogeneous cell type throughout the CNS. Their function rather seems to

depend on specific subtypes both within and between distinct brain regions (see also Götz *et al.* 1998; Toresson *et al.* 1999; Heins *et al.* 2002; Campbell and Götz 2002).

### 7.2.2 Molecular markers for distinct sets of precursor cells

We describe here novel subtypes of CNS precursor cells identified by the co-localization of the RC2-antigen, GLAST and BLBP. While these proteins are clearly localized in radial glial cells, they are also contained in morphologically distinct cell populations, e.g. in tangentially oriented cells in the embryonic cortex and GE and in cells of the RMS. Moreover, quantitative differences in the contribution of subtypes identified by this antigenic profile in the overall progenitor pool and the radial glial pool (compare Fig. 5.4 with the composition of morphologically traced radial cells Fig. 5.11 and the composition of morphologically traced subtypes Fig. 5.14) further support the morphological heterogeneity of these novel subtypes. Thus, these antigens are not specific radial glial markers and are not specific for precursor cells with particular morphological characteristics. While the exact function of these novel subtypes remains to be determined, we have promising hints for their functional relevance. First, the distinct subsets identified by their antigenic profile differ in their cell cycle characteristics and second, they express specific transcription factors.

### 7.2.3 Cell cycle differences among the novel precursor subtypes

The novel precursor subtypes differ in their LI, i.e. the proportion of cells labelled by a short BrdU-pulse. Thus, some populations contain more, others less cells in S-phase at the time of labelling. We interpret this result as an indication of differences in the cell cycle since cumulative BrdU-labelling experiments demonstrated that almost all cells are actively dividing and therefore our results cannot be explained by a differential contribution of quiescent cells. We cannot discriminate, however, whether these subsets differ in the length of S-phase (a shorter S-phase would give fewer BrdU-labelled cells, i.e. a lower LI) or in the total cell cycle length (a slower cell cycle would give fewer BrdU-labelled cells). Either way, however, the differences of the novel precursor types in their LI imply functional differences in their cell cycle characteristics. Notably, precursor cells that differ in their LI are also located at different radial positions. For example, the GLAST/BLBP+ cells reside outside the ventricular zone, mostly in the intermediate zone and deep cortical plate, and have the lowest LI of the cortical precursor cells. Likewise in the GE the RC2-negative precursors are located farthest away from the ventricular

surface and have the smallest LI. The distinct alignment of precursor subtypes might therefore explain the discrepancy of our data to the previous reports of a homogeneous cell cycle in the ventricular zone of the developing cortex (Cai *et al.* 1997a; see however: Reznikov and van der Kooy 1995).

#### 7.2.4 Specific precursor subtypes express bHLH transcription factors

While all RC2-positive precursor cells in the cerebral cortex express the homeobox transcription factor Pax6 (Götz *et al.* 1998), only a subset expresses basic Helix-Loop-Helix transcription factors of the proneural gene family. RC2-positive, but GLAST- and BLBP-negative precursor cells contain Mash1 in the GE and Neurogenin in the cortex (this study and M.Götz and F.Guillemot, unpublished observations). This expression profile implies a functional relevance since Mash1 has been suggested to be essential for the progression from the ventricular to the subventricular zone (Torii *et al.* 1999; Casarosa *et al.* 1999). However, we found that precursor cells of the SVZ, detected by the Mphase marker PH3 at abventricular positions, are not RC2-immunoreactive. Since we have shown, that Mash1-immunoreactive cells are as well RC2-positive, SVZ cells should be Mash1-negative too (see Fig. 5.7 and 5.8). Since the quantification however showed that only 10% of RC2-positive precursor cells of the GE were Mash1-positive, it might be conceivable, that we could have missed a very small population of Mash1-positive but RC2-negative cells, which then might constitute a subpopulation of SVZ-precursor (see as well Methods 4.12.2). On the other hand, it might be possible that Mash1 is only necessary for the transition of precursors from the VZ to the SVZ and that it is down-regulated in precursors of the SVZ.

Moreover, the differential expression of Neurogenin and Mash1 in the RC2+ cells of the cortex and GE respectively might have implications for the cell proliferation and be responsible for the differences in the LI between these populations. While RC2+ cells in the cortex exhibit a lower LI than the RC2/GLAST/BLBP+ population, the opposite was observed in the GE where RC2+ cells have the highest LI amongst the GE subtypes.

#### 7.2.5 Precursor subtypes are correlated to distinct progenies

Some precursor subtypes, which we identified by the co-localization analysis of RC2, GLAST and BLBP, seem to be related to the generation of a particular progeny. For example, the RC2+ and RC2/GLAST+ precursor subtypes are restricted to the

phase of neurogenesis in the embryonic cortex and they disappear when gliogenesis starts (around E17). Indeed, the proportion of precursor subtypes restricted to this developmental period (E12: 71%, E14: 58%) closely matches the proportion of neuronal precursors identified in cell lineage experiments *in vivo* and *in vitro* (70%; Grove *et al.* 1993; Williams and Price 1995; Reid *et al.* 1995; Qian *et al.* 1998). Moreover, precursor cells of the RMS in the postnatal telencephalon, a region that still contains neuroblasts, maintain this staining profile (RC2+, but BLBP-negative) at a time when the other areas of the telencephalon have lost these precursor subtypes. These data are consistent with the hypothesis that RC2+, BLBP-negative cells might mostly correspond to neuronal precursor cells (Fig. 7.2).

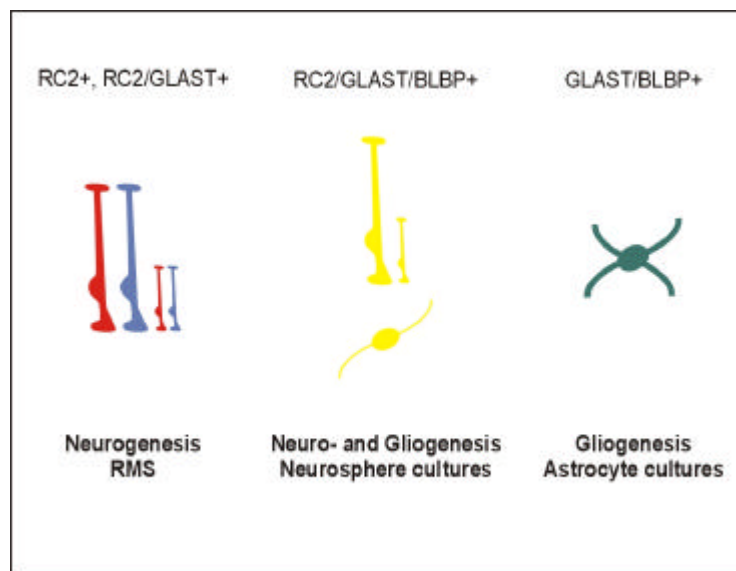


**Figure 7.2 Telencephalic precursor cell subtypes detected by RC2-, BLBP- and GLAST-immunoreactivity**

This schematic drawing depicts the different precursor subtypes identified in the telencephalon by immunostainings with RC2, anti-GLAST and anti-BLBP antibodies. The colour refers to the antigenic profile as depicted on top of the figure and in Fig. 5.4. The morphology of the precursor cells is based on the immunostainings in sections and tracing of radial precursor cells from the pial surface. The cell types that were detected only during neurogenesis are depicted to the left, and those detected only during gliogenesis to the right. Further evidence supporting the correlation between the antigenic profile of the precursor cells and a specific progeny is depicted in the panel.

The correlation between precursor potential and marker expression was further substantiated by the analysis of neurosphere cells purified from embryonic or adult telencephalon. After several passages, neurosphere cells contain mostly multipotent cells (Gritti *et al.* 1996). Interestingly, these cells are homogeneously immunoreactive for RC2, GLAST and BLBP and thus differ from the staining profile of precursors in the RMS. This is in good agreement with the persistence of RC2/GLAST/BLBP+ cells

from neuro- to gliogenesis and led us to hypothesize that precursors with such a marker combination might have a broad potential (Fig. 7.2).

RC2/GLAST/BLBP+ radial glial cells lose the RC2-antigen at the time of transformation in multipolar astrocytes (Misson *et al.* 1988a; Edwards *et al.* 1990) and thereby seemingly give rise to the multipolar GLAST/BLBP+ cells observed in the postnatal cortex. The abundance of GLAST/BLBP+ cells throughout the cortex at postnatal stages and their morphology implicates them as differentiating astrocytes (Fig. 7.2). Indeed, purified astrocytes *in vitro* are GLAST-, BLBP- and GFAP-positive, but RC2-negative. Some of these cells might also be oligodendrocyte precursors since they are AN2-immunoreactive (Niehaus *et al.* 1999). Indeed, the early ventral appearance of tangentially oriented BLBP-positive cells and their apparent dorsal migration correlates well with studies of oligodendrocyte precursors in the telencephalon (Pringle *et al.* 1996; Birling and Price 1998). These data therefore suggest that the precursor subsets discovered by immunohistochemistry with RC2, anti-GLAST and anti-BLBP antisera, might help to identify functionally distinct lineages in the developing CNS.

### 7.3 Role of BLBP in radial glial subsets

#### 7.3.1 Alteration of precursor subtypes in the *reeler* cerebral cortex

To further investigate the function of BLBP and in the search to identify factors regulating radial glial identity we used the *reeler* mutant as a model for cortical malformations and altered radial glial morphology. The analysis of the precursor pool in the absence of Reelin signalling revealed that BLBP-immunoreactivity was greatly reduced in *reeler* neocortical precursor cells. In the WT cerebral cortex BLBP is up-regulated during development. In the *reeler* neocortex however, BLBP-immunoreactivity initially appears at normal levels but is greatly reduced already at E14, the time when the first defects in neuronal migration are apparent (Fig. 5.21 and 5.23). Using acutely dissociated cell preparations, we could quantify that not the cytoplasmic distribution of BLBP is altered in *reeler* precursor cells, but that the total number of BLBP-immunoreactive cells is significantly reduced.

Radial glial endfeet were previously reported as less arborized and disruptions of the glia limitans formed by these endfeet were observed in the *reeler* mutant cortex (Pinto-Lord *et al.* 1982; Hunter-Schaedle 1997). These alterations have been

suggested as premature transformation of radial glia into astrocytes since this transformation involves detachment of radial glial endfeet from the basement membrane and a loss of radial morphology. In contrary, our study showed a decrease of BLBP- and as well GLAST-immunoreactivity, both of which are present in mature astrocytes. Furthermore, we could not detect a premature increase of GFAP-immunoreactivity nor a decrease of RC2-immunoreactivity in *reeler* radial glial cells (data not shown) as described by Hunter-Schaedle (1997). Reports on mouse mutants showing a premature glial differentiation furthermore described multipolar astrocyte precursors leaving the ventricular zone (Nieto *et al.* 2001). However, the population of GLAST/BLBP-immunoreactive precursor cells with multipolar morphology (see as well Fig. 7.2) that we hypothesized as immature astrocytes was not affected by the loss of Reelin in the developing *reeler* cortex (see as well Fig. 5.23). This finding furthermore does not support the hypothesis of a premature glial differentiation in the *reeler* cerebral cortex reported by Hunter-Schaedle (1997). However, consistent with our data, defects of the radial glial transformation to astrocytes and glial differentiation indicated by a reduced level of GLAST have been described in the postnatal cerebellum (Ghandour *et al.* 1981; Benjelloun-Touimi *et al.* 1985; Fukaya *et al.* 1999). Taken together, rather than a premature and increased glial differentiation, these data suggest an impaired astroglial differentiation in the developing *reeler* CNS.

### 7.3.2 Role of BLBP in differentiation and proliferation

Since BLBP is reduced during neurogenesis in the *reeler* cerebral cortex, this allowed testing of the hypothesis, that BLBP is involved in the specification of gliogenic or multipotent precursors (Fig. 7.2). This model would predict a reduction of non-neurogenic precursors supposedly resulting in an increase in neurogenesis in the *reeler* cerebral cortex. We therefore analysed the cell fate of FACS-sorted radial glial cells of WT and *reeler* mutant cortex. Despite the neurochemical defects of radial glial cells in the *reeler* cerebral cortex not even small changes in the number of neurons generated was detectable by quantitative FACS analysis in the *reeler* mutant cortex, suggesting that even if BLBP-immunoreactivity is mainly detectable in cells with glial characteristics it is not implicated in cell fate regulation. Furthermore, preliminary data on the cell fate of BLBP-positive radial glial cells revealed that they also generate neurons (observations by E.Hartfuss, T.Anthony and M.Götz). We isolated GFP-positive radial glial cells from a mouse-line expressing GFP under the

radial glia specific BLBP-promoter RGE by FACS-sorting (Feng and Heintz 1995) and cultured them on a rat feeder layer. The clonal analysis indicated the same neurogenic potential for the BLBP-containing radial glial cells as it has been described for the entire radial glia population (Malatesta *et al.* 2000; Malatesta *et al.* 2003). The functional implication of BLBP in cell fate regulation seems therefore unlikely.

Additionally, we compared the cell cycle characteristics of WT and *reeler* precursor cells to elucidate the potential role of BLBP as cell cycle regulator. Our experiments showed no changes in the cell cycle characteristics between WT and *reeler* mutant cortex precursors. These data therefore suggest that, BLBP seems not to play a major role in the regulation of proliferation or cell fate determination in the developing cerebral cortex, even if it is expressed in precursor cells.

### 7.3.3 Radial glial defects in the *reeler* cerebral cortex

Since the reduction of BLBP in *reeler* precursor cells did not affect their proliferation and cell fate characteristics, we were asking whether the reduction of BLBP in the *reeler* cerebral cortex has any effect at all on the cortical precursor characteristics. Previously BLBP has been implicated in the regulation of radial morphology of radial glial cells. Feng *et al.* (1994) and Anton *et al.* (1997) showed that in postnatal cerebellar cultures cells treated with function-blocking BLBP-antibodies did not exhibit an elongated radial morphology *in vitro*, while cells positive for BLBP did so. We therefore analysed the morphology of ventricular zone precursors in the *reeler* cortex. The morphological 3D-reconstruction analysis revealed that in the *reeler* cortex the number of long cells is significantly decreased (14%) compared to the WT cortex resulting in an increase in precursor cells with a club-shaped morphology. This is consistent and even extends previous reports on radial glial defects in the *reeler* mutant cerebral cortex (Pinto-Lord *et al.* 1982; Hunter-Schaedle 1997). A possible explanation could be that due to the defects of their endfeet and the subsequent disruption of the glia limitans radial glial cells lose their anchorage to the basement membrane and processes are retracted because of the loss of their basal attachment. However, it has been demonstrated in different mouse mutants showing a disrupted pial basement membrane, that the loss of radial glial anchorage leads only to a partial retraction of the processes into the cortical plate but not to a complete loss of their basal processes (Graus-Porta *et al.* 2001;

Halfter *et al.* 2002). If it would be true, that only the loss of basal anchorage of *reeler* radial glia leads to the morphological aberrations, one would have assumed to have an increase in the population of short precursors but not, as we reported, of club-shaped precursors lacking any basal process. However, in the *reeler* cerebral cortex only a partial disruption of the pial basement membrane has been reported, which could explain why only some precursor cells from the VZ lost their basal contacts but some maintained their long radial processes. Interestingly, the contact to the basement membrane and consequently the polarity has been proposed to influence cell fate determination of radial glial cells (Huttner and Brand 1997). However, the disruption of the glia limitans in the *reeler* and several other mouse mutants seems not to affect the proliferation or fate determination of radial glial cells (Georges-Labouesse *et al.* 1998; Arikawa-Hirasawa *et al.* 1999; Costell *et al.* 1999; Graus-Porta *et al.* 2001; Halfter *et al.* 2002).

What else could be the reason for the morphological defects of radial glial cells in the *reeler* cerebral cortex? Various mostly uncharacterised factors have been suggested to act on radial glial process extension and cell migration (Hunter and Hatten 1995; Anton *et al.* 1997; Del Rio *et al.* 1997). Hunter and Hatten (1995) suggested the presence of a soluble factor in the embryonic forebrain to regulate radial glial morphology and transformation into astrocytes. Hasling *et al.* (2003) recently published an analysis about a putative radialisation factor, present in the cortical MZ, which has the potential to restore chemically disrupted radial glial cells *in vitro*. Furthermore, Super *et al.* (2000) could show, that ablation of Reelin-positive Cajal-Retzius cells in the cortical marginal zone of newborn mice results in a decrease of radial glial cells (see as well Soriano *et al.* 1997).

We therefore wanted to examine the radialisation capacity of Reelin itself. We performed 'gain-of-function' experiments by applying Reelin on *reeler* cortical cell cultures to link Reelin-signalling, the down-regulation of BLBP-immunoreactivity and the extension of bipolar processes. In these *in vitro* experiments not only BLBP-immunoreactivity could be up-regulated to its normal level, as well the number of cells with a bipolar morphology could be significantly increased. Since also WT cells further increased the levels of BLBP and exhibited more often a bipolar morphology in the presence of Reelin, it is likely that the amount of endogenous Reelin is limiting *in vivo*. The quantitative analysis of the morphology of VZ precursors revealed about 57% of VZ cells as radial glial cells *in vivo*. *In vitro* 53% of the precursor cells had a

bipolar morphology under control conditions but in the presence of Reelin, the number of cells with bipolar processes was greatly increased (80%). We therefore hypothesize that the high amount of Reelin in the MZ close to radial glial endfeet promotes the growth of long radial processes. This scenario is also consistent with data from Förster *et al.* (2002) showing, that radial glia preferentially extend and settle on Reelin-containing substrate, suggesting a direct link between Reelin and radial morphology.

#### 7.3.4 Reelin signals directly to radial glial cells

Even though already earlier studies described some radial glial abnormalities in the *reeler* cortex (Ghandour *et al.* 1981; Pinto-Lord *et al.* 1982; Benjelloun-Touimi *et al.* 1985; Gadisseux and Evrard 1985; Hunter-Schaedle 1997; Fukaya *et al.* 1999) the analysis of the Reelin-signalling pathway has so far been focused on neurons. We describe here two important additional defects of radial glial cells in the cerebral cortex of Reelin-deficient mice and demonstrate *in vitro* that addition of Reelin to purified radial glia is able to rescue these defects. Two possible scenarios might explain this phenotype. It has been suggested that attachment of granule neurons is necessary for the induction of BLBP in radial glial cells and that BLBP is necessary for the maintenance of a radial morphology (Feng *et al.* 1994). This would lead to the hypothesis that due to the defect in neuronal migration in the *reeler*, neuronal attachment might be reduced on radial glial processes and therefore BLBP is not induced, consequently leading to the morphological radial glial phenotype. However, several reports demonstrated by electron microscopy an increase in neuronal contact to radial glial fibres (Pinto-Lord *et al.* 1982; Gadisseux and Evrard 1985). In fact it has been suggested that a failure of neuronal detachment leads to the migrational defects in the *reeler* mutant cortex. Moreover, it has been proposed that migrating neurons regulate BLBP-content in cortical radial glia via GGF/Neuregulin-signalling via the ErbB2-receptor. However, we have shown that BLBP-immunoreactivity could be induced in the presence of Reelin even in neuron-depleted cultures indicating that besides GGF/Neuregulin-ErbB2R signalling an additional pathway seems to exist. These data presented here therefore suggest a direct signalling of Reelin to radial glial cells independently from neurons. This signalling event is likely to take place in the MZ where radial glial cells are directly neighbouring Reelin-secreting MZ neurons (see Fig. 5.20) such that high levels of Reelin in the MZ might positively regulate BLBP-immunoreactivity and process extension in radial glial cells. The expression

patterns of Reelin and BLBP coincide well, not only in the cerebral cortex (E12) but as well in other CNS regions (E9; Feng *et al.* 1994; Ikeda and Terashima 1997; Alcantara *et al.* 1998). Consistently our data show, that in the absence of Reelin in the *reeler* cerebral cortex radial glia fail to up-regulate BLBP-immunoreactivity. Data from Magdaleno *et al.* (2002) contribute to the idea of a direct Reelin-signalling to radial glial cells. They have shown, that mis-expression of Reelin in nestin-positive precursor cells, most of which are radial glial cells, could rescue some of the defects in the *reeler* cortex. These data suggest, that the position of Reelin in the cortical marginal zone is not important for some *reeler* phenotypes. Furthermore, it could be shown that the Reelin receptors ApoER2 and VLDLR, as well as  $\beta$ 1-class integrins and the adapter protein mDab1 are expressed in radial glial cells, and therefore have the ability to perceive Reelin-signals (this work and Sheldon *et al.* 1997; Trommsdorff *et al.* 1999; Dulabon *et al.* 2000; Graus-Porta *et al.* 2001; Magdaleno *et al.* 2002; Förster *et al.* 2002; Luque *et al.* 2003). Furthermore, we have first results indicating that in the presence of Reelin *in vitro* BLBP-immunoreactivity cannot be induced in both ApoER2/VLDLR- and mDab1-mutant mice, suggesting, that BLBP-regulation in cortical precursor cells by Reelin-signalling involves the same signalling pathway, as shown for neurons (preliminary data by E.Hartfuss, H.Bock and M.Götz). Taken together, these data further support the hypothesis that radial glial cells are directly involved in Reelin-signalling.

In contrast to the cerebral cortex, in other CNS regions radial glial morphology and BLBP-immunoreactivity are not regulated by Reelin. In the GE and in the spinal cord for example, radial glial cells are not altered in the *reeler* mouse consistent with a lack of other defects in both of these regions (for review see e.g. Lambert de Rouvroit and Goffinet 1998). Furthermore, we have shown that precursor cells from the GE and the SC do not up-regulate BLBP in the presence of Reelin *in vitro*. Interestingly, in the WT-situation Reelin-positive cells are present in the GE and the SC. However, it has been demonstrated, that the expression pattern of Reelin and the *reeler* phenotype are not necessarily coherent. Not only regions with high Reelin-expression lack any defects, as well regions without Reelin-expression in the WT show a phenotype in the *reeler*. e.g. the inferior olivary complex and facial nerve nucleus (Goffinet 1983; Goffinet 1984; Blatt and Eisenman 1985; Blatt and Eisenman 1988; for review see e.g. Lambert de Rouvroit and Goffinet 1998). These data therefore imply that besides Reelin-signalling in some brain regions, such as the

cerebral cortex, different mechanisms must exist for regulating radial glial process extension and BLBP-immunoreactivity in other brain regions.

Taken together, Reelin-signalling to radial glial cells might be an important regulator of radial morphology and BLBP-content, both of which are absolutely necessary for radial neuronal migration (Rakic 1972; Feng *et al.* 1994; Anton *et al.* 1997). Indeed it is conceivable, that the defects of neuronal migration in the *reeler* neocortex are not only caused by defects of Reelin-signalling to neurons but also as a result of a significant loss of migration substrate – the radial fiber – which channels the young migrating neurons through the developing cortex to their destined positions in the cortical plate. Furthermore, efficient radial migration via perikaryal translocation depends as well on radial fibre extension. Luque *et al.* (2003) recently provided a model for the migrational defects in the *reeler* cerebral cortex including perikaryal translocation and radial process extension. In this model, neurons translocate to the appropriate position in the WT cortical plate and while the cortex thickens, their basal connections accordingly elongate. In the *reeler* cerebral cortex, however, radial glial process extension is impaired and neurons are continuously pulled up resulting in an inverted layering. Thus radial glial processes and the regulation of process extension by Reelin signalling to radial glial cells might be of crucial importance for all modes of radially migrating neurons.

### 7.3.5 Factors regulating radial glial identity

Essentially, the defects observed in radial glial cells of the *reeler* cerebral cortex are distinct from those observed in other mouse mutants with cortical malformations. As described, we aimed to identify factors regulating radial glial identity. One such factor is the homeobox transcription factor Pax6. The loss of Pax6 has a notably different effect on the alteration of radial glial characteristics than the loss of Reelin in the *reeler*. In the Pax6-deficient cerebral cortex GLAST-, but not BLBP-immunoreactivity is severely reduced and precursor characteristics like cell proliferation and cell fate are changed (Götz *et al.* 1998; Heins *et al.* 2002; Estivill-Torres *et al.* 2002). However, no such defects as proliferation and fate alterations could be detected in the *reeler*. Interestingly, radial glial cell morphology is also affected in the Pax6-mutant cortex, but distinctly different from the changes observed in *reeler* mice (Götz *et al.* 1998). Pax6 is suggested to regulate region specific radial glial identity in the forebrain since it is specifically expressed in radial glial cells of the

cerebral cortex but not in those of the GE. In the Pax6-deficient cerebral cortex, for example, radial glial cells adopt the more wavy morphology of those of the GE (Götz *et al.* 1998) and lose their neurogenic potential, reminiscent of the gliogenic fate of GE radial glia (Heins *et al.* 2002; Malatesta *et al.* 2003).

Taken together these data imply Reelin, besides Pax6, as a key regulator of radial glial identity in the developing cerebral cortex. Whereas Pax6 has been identified as intrinsic regulator of the radial glial precursor functions proliferation and cell fate determination, we could demonstrate here that Reelin acts as extrinsic regulator of radial morphology and BLBP-content, the prerequisites of the radial glial function in regulating radially oriented neuronal migration.

## 8. REFERENCES

- Alcantara, S., Ruiz, M., D'Arcangelo, G., Ezan, F., de Lecea, L., Curran, T., Sotelo, C., and Soriano, E.** (1998). Regional and cellular patterns of reelin mRNA expression in the forebrain of the developing and adult mouse. *J Neurosci* **18**, 7779-7799.
- Angevine, J. B. and Sidman, R. L.** (1961). Autoradiographic study of cell migration during histogenesis of the cerebral cortex in the mouse. *Nature* **192**, 766-768.
- Antanitus, D. S., Choi, B. H., and Lapham, L. W.** (1976). The demonstration of glial fibrillary acidic protein in the cerebrum of the human fetus by indirect immunofluorescence. *Brain Res* **103**, 613-616.
- Anton, E. S., Marchionni, M. A., Lee, K. F., and Rakic, P.** (1997). Role of GGF/neuregulin signaling in interactions between migrating neurons and radial glia in the developing cerebral cortex. *Development* **124**, 3501-3510.
- Arikawa-Hirasawa, E., Watanabe, H., Takami, H., Hassell, J. R., and Yamada, Y.** (1999). Perlecan is essential for cartilage and cephalic development. *Nat Genet* **23**, 354-358.
- Bar, I., Lambert, D. R., Royaux, I., Krizman, D. B., Dernoncourt, C., Ruelle, D., Beckers, M. C., and Goffinet, A. M.** (1995). A YAC contig containing the reeler locus with preliminary characterization of candidate gene fragments. *Genomics* **26**, 543-549.
- Barres, B. A.** (1999). A new role for glia: generation of neurons. *Cell* **97**, 667-670.
- Bayer, S. A. and Altman, J.** (1991). *Neocortical Development*. New York: Raven Press.
- Benjelloun-Touimi, S., Jacque, C. M., Derer, P., De Vitry, F., Maunoury, R., and Dupouey, P.** (1985). Evidence that mouse astrocytes may be derived from the radial glia. An immunohistochemical study of the cerebellum in the normal and reeler mouse. *J Neuroimmunol* **9**, 87-97.
- Berry, M. and Rogers, A. W.** (1965). The migration of neuroblasts in the developing cerebral cortex. *J Anat* **99**, 691-709.
- Bettenhausen, B., Hrabe de Angelis, M., Simon, D., Guenet, J. L., and Gossler, A.** (1995). Transient and restricted expression during mouse embryogenesis of Dll1, a murine gene closely related to *Drosophila* Delta. *Development* **121**, 2407-2418.
- Bhide, P. G.** (1996). Cell cycle kinetics in the embryonic mouse corpus striatum. *J Comp Neurol* **374**, 506-522.
- Bignami, A. and Dahl, D.** (1974). Astrocyte-specific protein and radial glia in the cerebral cortex of newborn rat. *Nature* **252**, 55-56.
- Bignami, A., Eng, L. F., Dahl, D., and Uyeda, C. T.** (1972). Localization of the glial fibrillary acidic protein in astrocytes by immunofluorescence. *Brain Res.* **43**, 429-435.
- Birling, M. C. and Price, J.** (1998). A study of the potential of the embryonic rat telencephalon to generate oligodendrocytes. *Dev Biol* **193**, 100-113.
- Blatt, G. J. and Eisenman, L. M.** (1985). A qualitative and quantitative light microscopic study of the inferior olivary complex of normal, reeler, and weaver mutant mice. *J Comp Neurol* **232**, 117-128.
- Blatt, G. J. and Eisenman, L. M.** (1988). Topographic and zonal organization of the olivocerebellar projection in the reeler mutant mouse. *J Comp Neurol* **267**, 603-615.
- Boulder Committee** (1970). Embryonic vertebrate central nervous system: revised terminology. *Anat Rec* **166**, 257-261.

- Bruckner, K., Perez, L., Clausen, H., and Cohen, S.** (2000). Glycosyltransferase activity of Fringe modulates Notch-Delta interactions. *Nature* **406**, 411-415.
- Cai, L., Hayes, N. L., and Nowakowski, R. S.** (1997a). Local homogeneity of cell cycle length in developing mouse cortex. *J Neurosci* **17**, 2079-2087.
- Cai, X. H., Tomizawa, K., Tang, D., Lu, Y. F., Moriwaki, A., Tokuda, M., Nagahata, S., Hatase, O., and Matsui, H.** (1997b). Changes in the expression of novel Cdk5 activator messenger RNA (p39nck5ai mRNA) during rat brain development. *Neurosci Res* **28**, 355-360.
- Cameron, R. S. and Rakic, P.** (1991). Glial cell lineage in the cerebral cortex: a review and synthesis. *Glia* **4**, 124-137.
- Campbell, K. and Götz, M.** (2002). Radial glia: multi-purpose cells for vertebrate brain development. *Trends Neurosci* **25**, 235-238.
- Casarosa, S., Fode, C., and Guillemot, F.** (1999). Mash1 regulates neurogenesis in the ventral telencephalon. *Development* **126**, 525-534.
- Caviness, V. S., Jr.** (1982). Neocortical histogenesis in normal and reeler mice: a developmental study based upon <sup>3</sup>H-thymidine autoradiography. *Brain Res* **256**, 293-302.
- Caviness, V. S., Jr. and Rakic, P.** (1978). Mechanisms of cortical development: a view from mutations in mice. *Annu Rev Neurosci* **1**, 297-326.
- Caviness, V. S., Jr. and Sidman, R. L.** (1973a). Retrohippocampal, hippocampal and related structures of the forebrain in the reeler mutant mouse. *J Comp Neurol* **147**, 235-254.
- Caviness, V. S., Jr. and Sidman, R. L.** (1973b). Time of origin or corresponding cell classes in the cerebral cortex of normal and reeler mutant mice: an autoradiographic analysis. *J Comp Neurol* **148**, 141-151.
- Caviness, V. S., Jr., Takahashi, T., and Nowakowski, R. S.** (1995). Numbers, time and neocortical neuronogenesis: a general developmental and evolutionary model. *Trends Neurosci* **18**, 379-383.
- Chanas-Sacre, G., Thiry, M., Pirard, S., Rogister, B., Moonen, G., Mbebi, C., Verdiere-Sahuque, M., and Leprince, P.** (2000). A 295-kDA intermediate filament-associated protein in radial glia and developing muscle cells in vivo and in vitro. *Dev Dyn* **219**, 514-525.
- Chapouton, P., Gärtner, A., and Götz, M.** (1999). The role of Pax6 in restricting cell migration between developing cortex and basal ganglia. *Development* **126**, 5569-5579.
- Chaudhry, F. A., Lehre, K. P., van Lookeren, C., Ottersen, O.P., Danbolt, N. C., and Storm-Mathisen, J.** (1995). Glutamate transporters in glial plasma membranes: highly differentiated localizations revealed by quantitative ultrastructural immunocytochemistry. *Neuron* **15**, 711-720.
- Chen, W. J., Goldstein, J. L., and Brown, M. S.** (1990). NPXY, a sequence often found in cytoplasmic tails, is required for coated pit-mediated internalization of the low density lipoprotein receptor. *J Biol Chem* **265**, 3116-3123.
- Chenn, A. and McConnell, S. K.** (1995). Cleavage orientation and the asymmetric inheritance of Notch1 immunoreactivity in mammalian neurogenesis. *Cell* **82**, 631-641.
- Choi, B. H.** (1981). Radial glia of developing human fetal spinal cord: Golgi, immunohistochemical and electron microscopic study. *Brain Res* **227**, 249-267.
- Choi, B. H. and Lapham, L. W.** (1978). Radial glia in the human fetal cerebrum: a combined Golgi, immunofluorescent and electron microscopic study. *Brain Res* **148**, 295-311.
- Choi, D. W.** (1992). Excitotoxic cell death. *J Neurobiol* **23**, 1261-1276.

- Clark, E. A. and Brugge, J. S.** (1995). Integrins and signal transduction pathways: the road taken. *Science* **268**, 233-239.
- Costell, M., Gustafsson, E., Aszodi, A., Morgelin, M., Bloch, W., Hunziker, E., Addicks, K., Timpl, R., and Fässler, R.** (1999). Perlecan maintains the integrity of cartilage and some basement membranes. *J Cell Biol* 1109-1122.
- Crissman, H. A., Oka, M. S., and Steinkamp, J. A.** (1976). Rapid staining methods for analysis of deoxyribonucleic acid and protein in mammalian cells. *J Histochem Cytochem* **24**, 64-71.
- Curran, T. and D'Arcangelo, G.** (1998). Role of reelin in the control of brain development. *Brain Res Rev* **26**, 285-294.
- D'Arcangelo, G., Homayouni, R., Keshvara, L., Rice, D. S., Sheldon, M., and Curran, T.** (1999). Reelin is a ligand for lipoprotein receptors. *Neuron* **24**, 471-479.
- D'Arcangelo, G., Miao, G. G., Chen, S. C., Soares, H. D., Morgan, J. I., and Curran, T.** (1995). A protein related to extracellular matrix proteins deleted in the mouse mutant reeler. *Nature* **374**, 719-723.
- D'Arcangelo, G., Miao, G. G., and Curran, T.** (1996). Detection of the reelin breakpoint in reeler mice. *Brain Res Mol Brain Res* **39**, 234-236.
- de Bergeyck, V., Naerhuyzen, B., Goffinet, A. M., and Lambert de Rouvroit, C.** (1998). A panel of monoclonal antibodies against reelin, the extracellular matrix protein defective in reeler mutant mice. *J Neurosci Methods* **82**, 17-24.
- Del Rio, J. A., Heimrich, B., Borrell, V., Förster, E., Drakew, A., Alcantara, S., Nakajima, K., Miyata, T., Ogawa, M., Mikoshiba, K., Derer, P., Frotscher, M., and Soriano, E.** (1997). A role for Cajal-Retzius cells and reelin in the development of hippocampal connections. *Nature* **385**, 70-74.
- Derer, M.** (1985). Comparative localization of Cajal-Retzius cells in the neocortex of normal and reeler mutant mice fetuses. *Neurosci Lett* **54**, 1-6.
- Doetsch, F. and Alvarez-Buylla, A.** (1996). Network of tangential pathways for neuronal migration in adult mammalian brain. *Proc Natl Acad Sci USA* **93**, 14895-14900.
- Doetsch, F., Caille, I., Lim, D. A., Garcia-Verdugo, J. M., and Alvarez-Buylla, A.** (1999). Subventricular zone astrocytes are neural stem cells in the adult mammalian brain. *Cell* **97**, 703-716.
- Dolle, P., Ruberte, E., Kastner, P., Petkovich, M., Stoner, C. M., Gudas, L. J., and Chambon, P.** (1989). Differential expression of genes encoding alpha, beta and gamma retinoic acid receptors and CRABP in the developing limbs of the mouse. *Nature* **342**, 702-705.
- Don, R. H., Cox, P. T., Wainwright, B. J., Baker, K., and Mattick, J. S.** (1991). 'Touchdown' PCR to circumvent spurious priming during gene amplification. *Nucleic Acids Res* **19**, 4008.
- Dulabon, L., Olson, E. C., Taglienti, M. G., Eisenhuth, S., McGrath, B., Walsh, C. A., Kreidberg, J. A., and Anton, E. S.** (2000). Reelin binds alpha3beta1 integrin and inhibits neuronal migration. *Neuron* **27**, 33-44.
- Dunwoodie, S. L., Henrique, D., Harrison, S. M., and Beddington, R. S.** (1997). Mouse Dll3: a novel divergent Delta gene which may complement the function of other Delta homologues during early pattern formation in the mouse embryo. *Development* **124**, 3065-3076.
- Edwards, M. A., Yamamoto, M., and Caviness, V. S., Jr.** (1990). Organization of radial glia and related cells in the developing murine CNS. An analysis based upon a new monoclonal antibody marker. *Neuroscience* **36**, 121-144.
- Eng, L. F.** (1985). Glial fibrillary acidic protein (GFAP): the major protein of glial intermediate filaments in differentiated astrocytes. *J Neuroimmunol* **8**, 203-214.

- Estivill-Torres, G., Pearson, H., van, H., V, Price, D. J., and Rashbass, P.** (2002). Pax6 is required to regulate the cell cycle and the rate of progression from symmetrical to asymmetrical division in mammalian cortical progenitors. *Development* **129**, 455-466.
- Feng, L., Hatten, M. E., and Heintz, N.** (1994). Brain lipid-binding protein (BLBP): a novel signaling system in the developing mammalian CNS. *Neuron* **12**, 895-908.
- Feng, L. and Heintz, N.** (1995). Differentiating neurons activate transcription of the brain lipid-binding protein gene in radial glia through a novel regulatory element. *Development* **121**, 1719-1730.
- Flügel, A., Willem, M., Berkowicz, T., and Wekerle, H.** (1999). Gene transfer into CD4+ T-lymphocytes: green fluorescent protein - engineered, encephalitogenic T cells illuminate brain autoimmune responses. *Nat Med* **5**, 843-847.
- Förster, E., Tielsch, A., Saum, B., Weiss, K. H., Johanssen, C., Graus-Porta, D., Müller, U., and Frotscher, M.** (2002). Reelin, Disabled 1, and beta 1 integrins are required for the formation of the radial glial scaffold in the hippocampus. *Proc Natl Acad Sci USA* **99**, 13178-13183.
- Frederiksen, K. and McKay, R. D.** (1988). Proliferation and differentiation of rat neuroepithelial precursor cells in vivo. *J Neurosci* **8**, 1144-1151.
- Fukaya, M., Yamada, K., Nagashima, M., Tanaka, K., and Watanabe, M.** (1999). Down-regulated expression of glutamate transporter GLAST in Purkinje cell-associated astrocytes of reeler and weaver mutant cerebella. *Neurosci Res* **34**, 165-175.
- Furuta, A., Rothstein, J. D., and Martin, L. J.** (1997). Glutamate transporter protein subtypes are expressed differentially during rat CNS development. *J Neurosci* **17**, 8363-8375.
- Gadisseux, J. F. and Evrard, P.** (1985). Glial-neuronal relationship in the developing central nervous system. A histochemical-electron microscope study of radial glial cell particulate glycogen in normal and reeler mice and the human fetus. *Dev Neurosci* **7**, 12-32.
- Gaiano, N. and Fishell, G.** (2002). The role of notch in promoting glial and neural stem cell fates. *Annu Rev Neurosci* **25**, 471-490.
- Gaiano, N., Nye, J. S., and Fishell, G.** (2000). Radial glial identity is promoted by Notch1 signaling in the murine forebrain. *Neuron* **26**, 395-404.
- Georges-Labouesse, E., Mark, M., Messaddeq, N., and Gansmuller, A.** (1998). Essential role of alpha 6 integrins in cortical and retinal lamination. *Curr Biol* **8**, 983-986.
- Gerdes, J., Scholzen, T., Gerlach, C., Kubbutat, M., and Zentgraf, H.** (1997). Assessment of cell proliferation in murine tissues with a polyclonal antiserum against the murine Ki-67 protein. *Eur J Cell Biol* **72**, 263.
- Ghandour, M. S., Derer, P., Labourdette, G., Delaunoy, J. P., and Langley, O. K.** (1981). Glial cell markers in the reeler mutant mouse: a biochemical and immunohistological study. *J Neurochem* **36**, 195-200.
- Gilbert, S. F.** (1994). *Developmental Biology*. 4th ed. Sunderland, MA: Sinauer Associates, Inc.
- Gilmore, E. C. and Herrup, K.** (2000). Cortical development: receiving reelin. *Curr Biol* **10**, R162-R166.
- Godina, G.** (1951). Istogenesi e differenziazione dei neuroni e degli elementi gliali della corteccia cerebrale. *Z Zellforsch* **36**, 401-435.
- Goffinet, A. M.** (1979). An early development defect in the cerebral cortex of the reeler mouse. A morphological study leading to a hypothesis concerning the action of the mutant gene. *Anat Embryol (Berl)* **157**, 205-216.

- Goffinet, A. M.** (1983). The embryonic development of the inferior olivary complex in normal and reeler (rlORL) mutant mice. *J Comp Neurol* **219**, 10-24.
- Goffinet, A. M.** (1984). Abnormal development of the facial nerve nucleus in reeler mutant mice. *J Anat* **138**, 207-215.
- Goldowitz, D., Cushing, R. C., Laywell, E., D'Arcangelo, G., Sheldon, M., Sweet, H. O., Davisson, M., Steindler, D., and Curran, T.** (1997). Cerebellar disorganization characteristic of reeler in scrambler mutant mice despite presence of reelin. *J Neurosci* **17**, 8767-8777.
- Golgi, C.** (1885). Sulla fina anatomia degli organi centrali del sistema nervoso. Reggio Emilia: Tipografia di Stefano Calderini e Figlio.
- Gonzalez, J. L., Russo, C. J., Goldowitz, D., Sweet, H. O., Davisson, M. T., and Walsh, C. A.** (1997). Birthdate and cell marker analysis of scrambler: a novel mutation affecting cortical development with a reeler-like phenotype. *J Neurosci* **17**, 9204-9211.
- Götz, M., Stoykova, A., and Gruss, P.** (1998). Pax6 controls radial glia differentiation in the cerebral cortex. *Neuron* **21**, 1031-1044.
- Graus-Porta, D., Blaess, S., Senften, M., Littlewood-Evans, A., Damsky, C., Huang, Z., Orban, P., Klein, R., Schittny, J. C., and Müller, U.** (2001). Beta1-class integrins regulate the development of laminae and folia in the cerebral and cerebellar cortex. *Neuron* **31**, 367-379.
- Gray, G. E. and Sanes, J. R.** (1992). Lineage of radial glia in the chicken optic tectum. *Development* **114**, 271-283.
- Gritti, A., Parati, E. A., Cova, L., Frolichsthal, P., Galli, R., Wanke, E., Faravelli, L., Morassutti, D. J., Roisen, F., Nickel, D. D., and Vescovi, A.L.** (1996). Multipotential stem cells from the adult mouse brain proliferate and self-renew in response to basic fibroblast growth factor. *J Neurosci* **16**, 1091-1100.
- Grove, E. A., Williams, B. P., Li, D. Q., Hajhosseini, M., Friedrich, and Price, J.** (1993). Multiple restricted lineages in the embryonic rat cerebral cortex. *Development* **117**, 553-561.
- Halfter, W., Dong, S., Yip, Y. P., Willem, M., and Mayer, U.** (2002). A critical function of the pial basement membrane in mortical histogenesis. *J Neurosci* **22**, 6029-6040.
- Halliday, A. L. and Cepko, C. L.** (1992). Generation and migration of cells in the developing striatum. *Neuron* **9**, 15-26.
- Hammond, V., Howell, B., Godinho, L., and Tan, S. S.** (2001). Disabled-1 functions cell autonomously during radial migration and cortical layering of pyramidal neurons. *J Neurosci* **21**, 8798-8808.
- Hartfuss, E.** (1998). Immunhistochemische Charakterisierung von Subpopulationen radialer Gliazellen während der Entwicklung des Telencephalons der Maus. *Diploma thesis*.
- Hasling, T. A., Gierdalski, M., Jablonska, B., and Juliano, S. L.** (2003). A radialization factor in normal cortical plate restores disorganized radial glia and disrupted migration in a model of cortical dysplasia. *Eur J Neurosci* **17**, 467-480.
- Hatten, M. E.** (1999). Central nervous system neuronal migration. *Annu Rev Neurosci* **22**, 511-539.
- Heins, N., Cremisi, F., Malatesta, P., Gangemi, R. M., Corte, G., Price, J., Goudreau, G., Gruss, P., and Götz, M.** (2001). Emx2 promotes symmetric cell divisions and a multipotential fate in precursors from the cerebral cortex. *Mol Cell Neurosci* **18**, 485-502.
- Heins, N., Malatesta, P., Cecconi, F., Nakafuku, M., Tucker, K. L., Hack, M. A., Chapouton, P., Barde, Y. A., and Götz, M.** (2002). Glial cells generate neurons: the role of the transcription factor Pax6. *Nat Neurosci* **5**, 308-315.

- Hendzel, M. J., Wei, Y., Mancini, M. A., Van Hooser, A., Ranalli, T., Brinkley, B. R., Bazett-Jones, D. P., and Allis, C. D.** (1997). Mitosis-specific phosphorylation of histone H3 initiates primarily within pericentromeric heterochromatin during G2 and spreads in an ordered fashion coincident with mitotic chromosome condensation. *Chromosoma* **106**, 348-360.
- Hertz, L.** (1979). Functional interactions between neurons and astrocytes I. Turnover and metabolism of putative amino acid transmitters. *Prog Neurobiol* **13**, 277-323.
- Herz, J. and Bock, H. H.** (2002). Lipoprotein receptors in the nervous system. *Annu Rev Biochem* **71**, 405-434.
- Hiesberger, T., Trommsdorff, M., Howell, B. W., Goffinet, A., Mumby, M. C., Cooper, J. A., and Herz, J.** (1999). Direct binding of Reelin to VLDL receptor and ApoE receptor 2 induces tyrosine phosphorylation of disabled-1 and modulates tau phosphorylation. *Neuron* **24**, 481-489.
- Hinds, J. W. and Ruffett, T. L.** (1971). Cell proliferation in the neural tube: an electron microscopic and golgi analysis in the mouse cerebral vesicle. *Z Zellforsch Mikrosk Anat* **115**, 226-264.
- His, W.** (1887). Die Entwicklung der ersten Nervenbahnen beim menschlichen Embryo. Übersichtliche Darstellung. *Arch Anat Physiol Leipzig Anat Abth* **92**, 368-378.
- His, W.** (1888). Zur Geschichte des Gehirns sowie der centralen und peripherischen Nervenbahnen beim menschlichen Embryo. *Abh Kgl sachs Ges Wissensch math phys Kl* **24**, 339-392.
- His, W.** (1889a). Die Formentwicklung des menschlichen Vorderhirns vom Ende des ersten bis zum Beginn des dritten Monats. *Abh Kgl sachs Ges Wissensch math phys Kl* **15**, 673-736.
- His, W.** (1889b). Die Neuroblasten und deren Entstehung im embrionalen Mark. *Abh Kgl sachs Ges Wissensch math phys Kl* **15**, 311-372.
- His, W.** (1904). Die Entwicklung des menschlichen Gehirns während der ersten Monate. Leipzig: Hirzel.
- Hoffarth, R. M., Johnston, J. G., Krushel, L. A., and van der Kooy, D.** (1995). The mouse mutation reeler causes increased adhesion within a subpopulation of early postmitotic cortical neurons. *J Neurosci* **15**, 4838-4850.
- Homayouni, R., Rice, D. S., Sheldon, M., and Curran, T.** (1999). Disabled-1 binds to the cytoplasmic domain of amyloid precursor-like protein 1. *J Neurosci* **19**, 7507-7515.
- Howell, B. W., Hawkes, R., Soriano, P., and Cooper, J. A.** (1997). Neuronal position in the developing brain is regulated by mouse disabled-1. *Nature* **389**, 733-737.
- Howell, B. W., Herrick, T. M., and Cooper, J. A.** (1999). Reelin-induced tyrosine phosphorylation of disabled-1 during neuronal positioning. *Genes Dev* **13**, 643-648.
- Hunter-Schaedle, K. E.** (1997). Radial glial cell development and transformation are disturbed in reeler forebrain. *J Neurobiol* **33**, 459-472.
- Hunter, K. E. and Hatten, M. E.** (1995). Radial glial cell transformation to astrocytes is bidirectional: regulation by a diffusible factor in embryonic forebrain. *Proc Natl Acad Sci USA* **92**, 2061-2065.
- Huttner, W. B. and Brand, M.** (1997). Asymmetric division and polarity of neuroepithelial cells. *Curr Opin Neurobiol* **7**, 29-39.
- Ikeda, Y. and Terashima, T.** (1997). Expression of reelin, the gene responsible for the reeler mutation, in embryonic development and adulthood in the mouse. *Dev Dyn* **210**, 157-172.
- Johnston, S. H., Rauskolb, C., Wilson, R., Prabhakaran, B., Irvine, KD, and Vogt, T. F.** (1997). A family of mammalian Fringe genes implicated in boundary determination and the Notch pathway. *Development* **124**, 2245-2254.

- Kamei, Y., Inagaki, N., Nishizawa, M., Tsutsumi, O., Taketani, Y., and Inagaki, M.** (1998). Visualization of mitotic radial glial lineage cells in the developing rat brain by Cdc2 kinase-phosphorylated vimentin. *Glia* **23**, 191-199.
- Katz, L. C., Burkhalter, A., and Dreyer, W. J.** (1984). Fluorescent latex microspheres as a retrograde neuronal marker for in vivo and in vitro studies of visual cortex. *Nature* **310**, 498-500.
- Keshvara, L., Benhayon, D., Magdaleno, S., and Curran, T.** (2001). Identification of reelin-induced sites of tyrosyl phosphorylation on disabled-1. *J Biol Chem* **276**, 16008-16014.
- Komuro, H. and Rakic, P.** (1998). Orchestration of neuronal migration by activity of ion channels, neurotransmitter receptors, and intracellular Ca<sup>2+</sup> fluctuations. *J Neurobiol* **37**, 110-130.
- Kölliker, A.** (1879). *Entwicklungsgeschichte des Menschen und der höheren Thiere*. Leipzig: Engelmann.
- Kölliker, A.** (1882). *Embryologie ou traité complet du développement de l'homme et des animaux supérieurs*. Paris: Reinwald.
- Kölliker, A.** (1896). *Handbuch der Gewebelehre des Menschen*. 6th ed. Leipzig: Engelmann.
- Kurtz, A., Zimmer, A., Schnutgen, F., Bruning, G., Spener, F., and Müller, T.** (1994). The expression pattern of a novel gene encoding brain-fatty acid binding protein correlates with neuronal and glial cell development. *Development* **120**, 2637-2649.
- Lagenaur, C. and Schachner, M.** (1981). Monoclonal antibody (M2) to glial and neuronal cell surfaces. *J Supramol Struct Cell Biochem* **15**, 335-346.
- Laird, P. W., Zijderveld, A., Linders, K., Rudnicki, M. A., Jaenisch, R., and Berns, A.** (1991). Simplified mammalian DNA isolation procedure. *Nucleic Acids Res* **19**, 4293.
- Lambert de Rouvroit, C. and Goffinet, A. M.** (1998). The reeler mouse as a model of brain development. *Adv Anat Embryol Cell Biol* **150**, 1-106.
- Lee, M. K., Tuttle, J. B., Rebhun, L. I., Cleveland, D. W., and Frankfurter (1990).** The expression and posttranslational modification of a neuron-specific beta-tubulin isotype during chick embryogenesis. *Cell Motil Cytoskeleton* **17**, 118-132.
- Lenhossek, M.** (1893). *Der feinere Bau des Nervensystems in Lichte neuester Forschung*. Berlin: Fischer's Medicinische Buchhandlung. H.Kornfeld.
- Levitt, P., Cooper, M. L., and Rakic, P.** (1981). Coexistence of neuronal and glial precursor cells in the cerebral ventricular zone of the fetal monkey: an ultrastructural immunoperoxidase analysis. *J Neurosci* **1**, 27-39.
- Levitt, P. and Rakic, P.** (1980). Immunoperoxidase localization of glial fibrillary acidic protein in radial glial cells and astrocytes of the developing rhesus monkey brain. *J Comp Neurol* **193**, 815-840.
- Lindsell, C. E., Boulter, J., diSibio, G., Gossler, A., and Weinmaster, G.** (1996). Expression patterns of Jagged, Delta1, Notch1, Notch2 and Notch3 genes identify ligand-receptor pairs that may function in neural development. *Mol Cell Neurosci* **8**, 14-27.
- Lo, L. C., Johnson, J. E., Wuenschell, C. W., Saito, T., and Anderson, D. J.** (1991). Mammalian achaete-scute homolog 1 is transiently expressed by spatially restricted subsets of early neuroepithelial and neural crest cells. *Genes Dev* **9**, 1524-1537.
- Lois, C. and Alvarez-Buylla, A.** (1994). Long-distance neuronal migration in the adult mammalian brain. *Science* **264**, 1145-1148.
- Lois, C., Garcia-Verdugo, J. M., and Alvarez-Buylla, A.** (1996). Chain Migration of Neuronal Precursors. *Science* **271**, 978-981.

- Lund, R. D., Chang, F. L., Hankin, M. H., and Lagenaur, C. F.** (1985). Use of a species-specific antibody for demonstrating mouse neurons transplanted to rat brains. *Neurosci Lett* **61**, 221-226.
- Luque, J. M., Morante-Oria, J., and Fairen, A.** (2003). Localization of ApoER2, VLDLR and Dab1 in radial glia: groundwork for a new model of reelin action during cortical development. *Brain Res Dev Brain Res* **140**, 195-203.
- Luskin, M. B.** (1993). Restricted proliferation and migration of postnatally generated neurons derived from the forebrain subventricular zone. *Neuron* **11**, 173-189.
- Luskin, M. B., Zigova, T., Soteris, B. J., and Stewart, R. R.** (1997). Neuronal progenitor cells derived from the anterior subventricular zone of the neonatal rat forebrain continue to proliferate in vitro and express a neuronal phenotype. *Mol Cell Neurosci* **8**, 351-366.
- Maden, M. and Holder, N.** (1991). The involvement of retinoic acid in the development of the vertebrate central nervous system. *Development Suppl* **2**, 87-94.
- Magdaleno, S., Keshvara, L., and Curran, T.** (2002). Rescue of ataxia and preplate splitting by ectopic expression of Reelin in reeler mice. *Neuron* **33**, 573-586.
- Magdaleno, S. M. and Curran, T.** (2001). Brain development: integrins and the Reelin pathway. *Curr Biol* **11**, R1032-R1035.
- Magini, G.** (1888a). Nevroglia e cellule nervose cerebrali nei feti. pp. 281-291. Pavia: Tipografia Fratelli Fusi.
- Magini, G.** (1888b). Ulteriori ricerche istologiche sul cervello fatale. *Rendiconti della R. Accademia dei Lincei* **4**, 760-763.
- Malatesta, P., Hack, M. A., Hartfuss, E., Kettenmann, H., Klinkert, W., Kirchhoff, F., and Götz, M.** (2003). Neuronal or glial progeny: Regional differences in radial glia fate. *Neuron (in press)*.
- Malatesta, P., Hartfuss, E., and Götz, M.** (2000). Isolation of radial glial cells by fluorescent-activated cell sorting reveals a neuronal lineage. *Development* **127**, 5253-5263.
- Margolis, B.** (1996). The PI/PTB domain: a new protein interaction domain involved in growth factor receptor signaling. *J Lab Clin Med* **128**, 235-241.
- Margotta, V. and Morelli, A.** (1997). Contribution of radial glial cells to neurogenesis and plasticity of the central nervous system in adult vertebrates. *Anim Biol* **6**, 101-108.
- Maric, D., Maric, I., Ma, W., Lahouji, F., Somogyi, R., Wen, X., Sieghart, W., Fritschy, J. M., and Barker, J. L.** (1997). Anatomical gradients in proliferation and differentiation of embryonic rat CNS accessed by buoyant density fractionation: alpha 3, beta 3 and gamma 2 GABAA receptor subunit co-expression by post-mitotic neocortical neurons correlates directly with cell buoyancy. *Eur J Neurosci* **9**, 507-522.
- Marin-Padilla, M.** (1998). Cajal-Retzius cells and the development of the neocortex. *Trends Neurosci* **21**, 64-71.
- Menezes, J. R., Smith, C. M., Nelson, K. C., and Luskin, M. B.** (1995). The division of neuronal progenitor cells during migration in the neonatal mammalian forebrain. *Mol Cell Neurosci* **6**, 496-508.
- Misson, J. P., Austin, C. P., Takahashi, T., Cepko, C. L., and Caviness, V. S., Jr.** (1991). The alignment of migrating neural cells in relation to the murine neopallial radial glial fiber system. *Cereb Cortex* **1**, 221-229.
- Misson, J. P., Edwards, M. A., Yamamoto, M., and Caviness, V. S., Jr.** (1988a). Identification of radial glial cells within the developing murine central nervous system: studies based upon a new immunohistochemical marker. *Brain Res Dev Brain Res* **44**, 95-108.

- Misson, J. P., Edwards, M. A., Yamamoto, M., and Caviness, V. S., Jr.** (1988b). Mitotic cycling of radial glial cells of the fetal murine cerebral wall: a combined autoradiographic and immunohistochemical study. *Brain Res* **466**, 183-190.
- Miyata, T., Kawaguchi, A., Okano, H., and Ogawa, M.** (2001). Asymmetric inheritance of radial glial fibers by cortical neurons. *Neuron* **31**, 727-741.
- Moloney, D. J., Panin, V. M., Johnston, S. H., Chen, J., Shao, L., Wilson, R., Wang, Y., Stanley, P., Irvine, K. D., Haltiwanger, R. S., and Vogt, T.F.** (2000). Fringe is a glycosyltransferase that modifies Notch. *Nature* **406**, 369-375.
- Morest, D. K.** (1970). A study of neurogenesis in the forebrain of opossum pouch young. *Z Anat Entwickl Gesch* **130**, 265-305.
- Mullen, R. J., Buck, C. R., and Smith, A. M.** (1992). NeuN, a neuronal specific nuclear protein in vertebrates. *Development* **116**, 201-211.
- Nadarajah, B., Brunstrom, J. E., Grutzendler, J., Wong, R. O., and Pearlman, A. L.** (2001). Two modes of radial migration in early development of the cerebral cortex. *Nat Neurosci* **4**, 143-150.
- Naimski, P., Bierzynski, A., and Fikus, M.** (1980). Quantitative fluorescent analysis of different conformational forms of DNA bound to the Dye, 4',6-diamidine-2-phenylindole, and separated by gel electrophoresis. *Anal Biochem* **106**, 471-475.
- Niehaus, A., Stegmuller, J., Diers-Fenger, M., and Trotter, J.** (1999). Cell-surface glycoprotein of oligodendrocyte progenitors involved in migration. *J Neurosci* **19**, 4948-4961.
- Nieto, M., Schuurmans, C., Britz, O., and Guillemot, F.** (2001). Neural bHLH genes control the neuronal versus glial fate decision in cortical progenitors. *Neuron* **29**, 401-413.
- Noctor, S. C., Flint, A. C., Weissman, T. A., Dammerman, R. S., and Kriegstein, A. R.** (2001). Neurons derived from radial glial cells establish radial units in neocortex. *Nature* **409**, 714-720.
- Noctor, S. C., Flint, A. C., Weissman, T. A., Wong, W. S., Clinton, B. K., and Kriegstein, A. R.** (2002). Dividing precursor cells of the embryonic cortical ventricular zone have morphological and molecular characteristics of radial glia. *J Neurosci* **22**, 3161-3173.
- Nolte, C., Matyash, M., Pivneva, T., Schipke, C. G., Ohlemeyer, C., Hanisch, U. K., Kirchhoff, F., and Kettenmann, H.** (2001). GFAP promoter-controlled EGFP-expressing transgenic mice: a tool to visualize astrocytes and astrogliosis in living brain tissue. *Glia* **33**, 72-86.
- Nowakowski, R. S., Lewin, S. B., and Miller, M. W.** (1989). Bromodeoxyuridine immunohistochemical determination of the lengths of the cell cycle and the DNA-synthetic phase for an anatomically defined population. *J Neurocytol* **18**, 311-318.
- O'Rourke, N. A., Dailey, M. E., Smith, S. J., and McConnell, S. K.** (1992). Diverse migratory pathways in the developing cerebral cortex. *Science* **258**, 299-302.
- O'Rourke, N. A., Sullivan, D. P., Kaznowski, C. E., Jacobs, A. A., and McConnell, S. K.** (1995). Tangential migration of neurons in the developing cerebral cortex. *Development* **121**, 2165-2176.
- Ogawa, M., Miyata, T., Nakajima, K., Yagy, K., Seike, M., Ikenaka, K., Yamamoto, H., and Mikoshiba, K.** (1995). The reeler gene-associated antigen on Cajal-Retzius neurons is a crucial molecule for laminar organization of cortical neurons. *Neuron* **14**, 899-912.
- Peretto, P., Merighi, A., Fasolo, A., and Bonfanti, L.** (1997). Glial tubes in the rostral migratory stream of the adult rat. *Brain Res Bull* **42**, 9-21.
- Pinto-Lord, M. C., Evrard, P., and Caviness, V. S., Jr.** (1982). Obstructed neuronal migration along radial glial fibers in the neocortex of the reeler mouse: a Golgi-EM analysis. *Brain Res* **256**, 379-393.

- Polleux, F., Dehay, C., and Kennedy, H.** (1997). The timetable of laminar neurogenesis contributes to the specification of cortical areas in mouse isocortex. *J Comp Neurol* **385**, 95-116.
- Price, J., Turner, D., and Cepko, C.** (1987). Lineage analysis in the vertebrate nervous system by retrovirus-mediated gene transfer. *Proc Natl Acad Sci USA* **84**, 156-160.
- Pringle, N. P., Yu, W. P., Guthrie, S., Roelink, H., Lumsden, A., Peterson, A. C., and Richardson, W. D.** (1996). Determination of neuroepithelial cell fate: induction of the oligodendrocyte lineage by ventral midline cells and sonic hedgehog. *Dev Biol* **177**, 30-42.
- Qian, X., Goderie, S. K., Shen, Q., Stern, J. H., and Temple, S.** (1998). Intrinsic programs of patterned cell lineages in isolated vertebrate CNS ventricular zone cells. *Development* **125**, 3143-3152.
- Qian, X., Shen, Q., Goderie, S. K., He, W., Capela, A., Davis, A. A., and Temple, S.** (2000). Timing of CNS cell generation: a programmed sequence of neuron and glial cell production from isolated murine cortical stem cells. *Neuron* **28**, 69-80.
- Rakic, P.** (1971a). Guidance of neurons migrating to the fetal monkey neocortex. *Brain Res* **33**, 471-476.
- Rakic, P.** (1971b). Neuron-glia relationship during granule cell migration in developing cerebellar cortex. A Golgi and electronmicroscopic study in *Macacus Rhesus*. *J Comp Neurol* **141**, 283-312.
- Rakic, P.** (1972). Mode of cell migration to the superficial layers of fetal monkey neocortex. *J Comp Neurol* **145**, 61-83.
- Rakic, P.** (1988). Specification of cerebral cortical areas. *Science* **241**, 170-176.
- Rakic, P.** (1995). A small step for the cell, a giant leap for mankind: a hypothesis of neocortical expansion during evolution. *Trends Neurosci* **18**, 383-388.
- Ramon y Cajal, S.** (1897 Vol.1; 1899 Vol.2; 1904 Vol.3). *Textura del sistema nervioso del hombre y de los vertebrados*. Madrid: Moya.
- Reid, C. B., Liang, I., and Walsh, C.** (1995). Systematic widespread clonal organization in cerebral cortex. *Neuron* **15**, 299-310.
- Reynolds, B. A., Tetzlaff, W., and Weiss, S.** (1992). A multipotent EGF-responsive striatal embryonic progenitor cell produces neurons and astrocytes. *J Neurosci* **12**, 4565-4574.
- Reznikov, K. and van der Kooy, D.** (1995). Variability and partial synchrony of the cell cycle in the germinal zone of the early embryonic cerebral cortex. *J Comp Neurol* **360**, 536-554.
- Rice, D. S. and Curran, T.** (2001). Role of the reelin signaling pathway in central nervous system development. *Annu Rev Neurosci* **24**, 1005-1039.
- Rice, D. S., Sheldon, M., D'Arcangelo, G., Nakajima, K., Goldowitz, D., and Curran, T.** (1998). Disabled-1 acts downstream of Reelin in a signaling pathway that controls laminar organization in the mammalian brain. *Development* **125**, 3719-3729.
- Rothstein, J. D., Martin, L., Levey, A. I., Dykes-Hoberg, M., Jin, L., Wu, D., Nash, N., and Kuncel, R. W.** (1994). Localization of neuronal and glial glutamate transporters. *Neuron* **13**, 713-725.
- Sauer, F. C.** (1935). Mitosis in the neural tube. *J Comp Neurol* **62**, 377-405.
- Schambra, U. B., Lauder, J. M., and Silver, J.** (1992). *Atlas of the prenatal mouse brain*. San Diego, California: Academic Press.
- Schaper, A.** (1897). The earliest differentiation in the central nervous system of vertebrates. *Science* **5**, 430-431.

- Schmechel, D. E. and Rakic, P.** (1979). Arrested proliferation of radial glial cells during midgestation in rhesus monkey. *Nature* **277**, 303-305.
- Senzaki, K., Ogawa, M., and Yagi, T.** (1999). Proteins of the CNR family are multiple receptors for Reelin. *Cell* **99**, 635-647.
- Shawber, C., Boulter, J., Lindsay, C. E., and Weinmaster, G.** (1996). Jagged2: a Serrate-like gene expressed during rat embryogenesis. *Dev Biol* **180**, 370-376.
- Sheldon, M., Rice, D. S., D'Arcangelo, G., Yoneshima, H., Nakajima, K., Mikoshiba, K., Howell, B. W., Cooper, J. A., Goldowitz, D., and Curran, T.** (1997). Scrambler and yotari disrupt the disabled gene and produce a reeler-like phenotype in mice. *Nature* **389**, 730-733.
- Sheppard, A. M. and Pearlman, A. L.** (1997). Abnormal reorganization of preplate neurons and their associated extracellular matrix: an early manifestation of altered neocortical development in the reeler mutant mouse. *J Comp Neurol* **378**, 173-179.
- Shibata, T., Watanabe, M., Tanaka, K., Wada, K., and Inoue, Y.** (1996). Dynamic changes in expression of glutamate transporter mRNAs in developing brain. *Neuroreport* **7**, 705-709.
- Shibata, T., Yamada, K., Watanabe, M., Ikenaka, K., Wada, K., Tanaka, K., and Inoue, Y.** (1997). Glutamate transporter GLAST is expressed in the radial glia-astrocyte lineage of developing mouse spinal cord. *J Neurosci* **17**, 9212-9219.
- Shur, B. D.** (1982). Galactosyltransferase defects in reeler mouse brains. *J Neurochem* **39**, 201-209.
- Smart, I. H.** (1976). A pilot study of cell production by the ganglionic eminences of the developing mouse brain. *J Anat* **121**, 71-84.
- Soriano, E., Alvarado-Mallart, R.M., Dumesnil, N., Del Rio, J.A., and Sotelo, C.** (1997). Cajal-Retzius cells regulate the radial glia phenotype in the adult and developing cerebellum and alter granule cell migration. *Neuron* **18**, 563-577.
- Steiner, H., Duff, K., Capell, A., Romig, H., Grim, M. G., Lincoln, S., Hardy, J., Yu, X., Picciano, M., Fichteler, K., Citron, M., Kopan, R., Pesold, B., Keck, S., Baader, M., Tomita, T., Iwatsubo, T., Baumeister, R., and Haass, C.** (1999). A loss of function mutation of presenilin-2 interferes with amyloid beta-peptide production and notch signaling. *J Biol Chem* **274**, 28669-28673.
- Storck, T., Schulte, S., Hofmann, K., and Stoffel, W.** (1992). Structure, expression, and functional analysis of a Na<sup>+</sup>-dependent glutamate/aspartate transporter from rat brain. *Proc Natl Acad Sci USA* **89**, 10955-10959.
- Super, H., Del Rio, J. A., Martinez, A., Perez-Sust, P., and Soriano, E.** (2000). Disruption of neuronal migration and radial glia in the developing cerebral cortex following ablation of Cajal-Retzius cells. *Cereb Cortex* **10**, 602-613.
- Suzuki, T., Fujikura, K., Higashiyama, T., and Takata, K.** (1997). DNA-staining for fluorescence and laser confocal microscopy. *J Histochem Cytochem* **45**, 49-54.
- Swanson, R. A., Liu, J., Miller, J. W., Rothstein, J. D., Farrell, K., Stein, B. A., and Longuemare, M. C.** (1997). Neuronal regulation of glutamate transporter subtype expression in astrocytes. *J Neurosci* **17**, 932-940.
- Sweet, H. O., Bronson, R. T., Johnson, K. R., Cook, S. A., and Davisson, M. T.** (1996). Scrambler, a new neurological mutation of the mouse with abnormalities of neuronal migration. *Mamm Genome* **7**, 798-802.
- Takahashi, T., Nowakowski, R. S., and Caviness, V. S., Jr.** (1995a). Early ontogeny of the secondary proliferative population of the embryonic murine cerebral wall. *J Neurosci* **15**, 6058-6068.

- Takahashi, T., Nowakowski, R. S., and Caviness, V. S., Jr.** (1995b). The cell cycle of the pseudostratified ventricular epithelium of the embryonic murine cerebral wall. *J Neurosci* **15**, 6046-6057.
- Tamamaki, N., Nakamura, K., Okamoto, K., and Kaneko, T.** (2001). Radial glia is a progenitor of neocortical neurons in the developing cerebral cortex. *Neurosci Res* **41**, 51-60.
- Toresson, H., Mata, d. U., Fagerstrom, C., Perlmann, T., and Campbell, K.** (1999). Retinoids are produced by glia in the lateral ganglionic eminence and regulate striatal neuron differentiation. *Development* **126**, 1317-1326.
- Torii, M., Matsuzaki, F., Osumi, N., Kaibuchi, K., Nakamura, S., Casarosa, S., Guillemot, F., and Nakafuku, M.** (1999). Transcription factors Mash-1 and Prox-1 delineate early steps in differentiation of neural stem cells in the developing central nervous system. *Development* **126**, 443-456.
- Trommsdorff, M., Borg, J. P., Margolis, B., and Herz, J.** (1998). Interaction of cytosolic adaptor proteins with neuronal apolipoprotein E receptors and the amyloid precursor protein. *J Biol Chem* **50**, 33556-33560.
- Trommsdorff, M., Gotthardt, M., Hiesberger, T., Shelton, J., Stockinger, W., Nimpf, J., Hammer, R. E., Richardson, J. A., and Herz, J.** (1999). Reeler/Disabled-like disruption of neuronal migration in knockout mice lacking the VLDL receptor and ApoE receptor 2. *Cell* **97**, 689-701.
- Tsai, L. H., Takahashi, T., Caviness, V. S., and Harlow, E.** (1993). Activity and expression pattern of cyclin-dependent kinase 5 in the embryonic mouse nervous system. *Development* **119**, 1029-1040.
- Tucker, K. L., Meyer, M., and Barde, Y. A.** (2001). Neurotrophins are required for nerve growth during development. *Nat Neurosci* **4**, 29-37.
- Ullensvang, K., Lehre, K. P., Storm-Mathisen, J., and Danbolt, N. C.** (1997). Differential developmental expression of the two rat brain glutamate transporter proteins GLAST and GLT. *Eur J Neurosci* **9**, 1646-1655.
- Uyeda, C. T., Eng, L. F., and Bignami, A.** (1972). Immunological study of the glial fibrillary acidic protein. *Brain Res* **37**, 81-89.
- Vignal, W.** (1888a). Recherches sur le développement de la substance corticale du cerveau et du cervelet. *Arch Physiol Norm Pathol* **20**, 311-338.
- Vignal, W.** (1888b). Recherches sur le développement des éléments des couches corticales du cerveau et du cervelet chez l'homme et les mammifères. *Arch Physiol Norm Pathol* **20**, 228-254.
- Vignoud, L., Albiges-Rizo, C., Frachet, P., and Block, M. R.** (1997). NPXY motifs control the recruitment of the alpha5beta1 integrin in focal adhesions independently of the association of talin with the beta1 chain. *J Cell Sci* **110**, 1421-1430.
- Vignoud, L., Usson, Y., Balzac, F., Tarone, G., and Block, M. R.** (1994). Internalization of the alpha5beta1 integrin does not depend on NPXY signals. *Biochem Biophys Res Commun* **199**, 603-611.
- Voigt, T.** (1989). Development of glial cells in the cerebral wall of ferrets: direct tracing of their transformation from radial glia into astrocytes. *J Comp Neurol* **289**, 74-88.
- Ware, M. L., Fox, J. W., Gonzalez, J. L., Davis, N. M., Lambert, D. R., Russo, C. J., Chua, S. C., Jr., Goffinet, A. M., and Walsh, C. A.** (1997). Aberrant splicing of a mouse disabled homolog, mdab1, in the scrambler mouse. *Neuron* **19**, 239-249.
- Williams, B. P. and Price, J.** (1995). Evidence for multiple precursor cell types in the embryonic rat cerebral cortex. *Neuron* **14**, 1181-1188.

- Williams, B. P., Read, J., and Price, J.** (1991). The generation of neurons and oligodendrocytes from a common precursor cell. *Neuron* **7**, 685-693.
- Wolf, E., Wagner, J. P., Black, I. B., and DiCicco-Bloom, E.** (1997). Cerebellar granule cells elaborate neurites before mitosis. *Brain Res Dev Brain Res* **102**, 305-308.
- Xu, L. Z., Sanchez, R., Sali, A., and Heintz, N.** (1996). Ligand specificity of brain lipid-binding protein. *J Biol Chem* **271**, 24711-24719.
- Yoneshima, H., Nagata, E., Matsumoto, M., Yamada, M., Nakajima, K., Miyata, T., Ogawa, M., and Mikoshiba, K.** (1997). A novel neurological mutant mouse, yotari, which exhibits reeler-like phenotype but expresses CR-50 antigen/reelin. *Neurosci Res* **29**, 217-223.
- Zhuo, L., Sun, B., Zhang, C. L., Fine, A., Chiu, S. Y., and Messing, A.** (1997). Live astrocytes visualized by green fluorescent protein in transgenic mice. *Dev Biol* **187**, 36-42.
- Zigmond, M. J., Bloom, F.E., Landis, S.C., Roberts, J.L., and Squire, L.R.** (1999). *Fundamental Neuroscience*. Academic Press.

## 9. THANKS & ACKNOWLEDGEMENTS

In the first place, I want to thank my 'thesis-mother' Magdalena Götz for her intensive theoretical and practical supervision during the experimental work and the writing of my thesis. I want to thank her for the many helpful discussions, for providing an excellent scientific environment and for her never-ending enthusiasm.

Many thanks as well to Paolo Malatesta, who was an irremissibly help for everyday lab-problems, a great discussant not only for scientific questions but also for career plans. Furthermore, I want to thank Julia von Frowein, Nicole Haubst, Michael Hack, Stefan Stricker, Alexandra Heyden, Nico Heins and Prisca Chapouton, for great help in the lab, many discussions and for providing a great atmosphere in the lab. They are the best colleagues one can imagine. Mucella Öcalan and Parvin Ghahraman I want to thank for their expertise and great help with cell culture, immuno-labelling and molecular biology. I want to thank Tatiana Tomasi for her great help with mouse-genotyping. She was an excellent Hiwi! As well many thanks to Magdalena Pawlas for the many LightCycler-runs. Many thanks as well to Helga Zepter, who was an enormous help with bureaucracy. The EDV-group and especially Robert Streif I want to thank for their help with computer-problems, with software and hardware, deleted files, bugs and so on. Moreover, I want to thank Jim Chalcroft and the Histo&Imaging group for the many excellent 'express' printouts. Wolfgang Klinkert I want to thank for his help with the FACSVantage.

I'm grateful to Eckart Förster, Hans Bock and Todd Anthony for a great and fluent co-laboration and for many interesting and helpful discussions. Furthermore I want to thank my thesis-committee Yves Barde and Georg Dechant for great discussions and helpful comments on my data.

I'm grateful to Magdalena Götz, Paolo Malatesta, Stefan Stricker, Nicola Tobisch, Nicole Haubst, Julia von Frowein, Virginia Flanagan and Hans-Jürgen Hartfuss for proofreading the manuscript and their many helpful comments.

I want to say thank you to Nicola, Cinthia, Claudia, Antje, Harald, Julia, Phillip, Heike, Harry, Robert, Gerhard and Alex for many discussions about science, PhD-student life, plans and their empathy and psychological assistance. Furthermore, I want to thank all my friends inside and outside the institute for their friendship and for a great time. In addition, I want to thank Ingo for his love, his empathy and his ability to make me laugh at any time.

Finally, yet importantly, I want to thank my parents for providing a background, which enabled me to make this PhD-thesis. I'm grateful for their efforts they put into my education, for their financial aid, for their never-ending appreciation for all my problems and their confidence in me.

## 10. CURRICULUM VITAE

### Personal data:

**Eva Hartfuss**

Date and place of birth:

13<sup>th</sup> of July 1972, Bad Nauheim, Germany

### School:

August 1979 – July 1983

Primary school Wessling, Germany

August 1983 – July 1992

Carl-Spitzweg-Gymnasium, Unterpfaffenhofen, Germany

Grade: ‚Allgemeine Hochschulreife‘ (Abitur)

### Scientific education:

January 1999 – February 2003

#### PhD thesis:

Max-Planck-Institute of Neurobiology, Martinsried, Germany;  
Junior Group Neuronal Specification; Magdalena Götz, PhD  
“Characterization of subtypes of precursor cells in the  
developing central nervous system.”

March 1998 - December 1998

#### Diploma thesis:

Max-Planck-Institute of Neurobiology, Martinsried, Germany;  
Junior Group Neuronal Specification; Magdalena Götz, PhD  
“Immunohistochemical characterization of subpopulations of  
radial glial cells during the development of the mouse  
telencephalon”

November 1992 - February 1998

#### Undergraduate student:

Ludwig-Maximilians-University, Munich, Germany  
Major: Neurobiology  
Minors: Zoology, Genetics, Pharmacology&Toxicology

### Publications (parts of this thesis-work are already published):

1. **Hartfuss, E.** (1998). Immunohistochemical characterization of subpopulations of radial glial cells during the development of the mouse telencephalon. *Diploma thesis*.
2. Malatesta, P., **Hartfuss, E.** und Götz, M. (2000). Isolation of radial glia cells by fluorescent-activated cell sorting reveals a neuronal lineage. *Development* **127**, 5253-5263.
3. **Hartfuss, E.**, Galli, R., Heins, N. und Götz, M. (2001). Characterization of CNS precursor subtypes and radial glia. *Dev Bio* **229**, 15-30.
4. Götz, M., **Hartfuss, E.** and Malatesta, P. (2002). Radial glial cells as neuronal precursors: A new perspective on the correlation of morphology and lineage restriction in the developing cerebral cortex of mice. *Brain Res Bull* **57**, 777-778.
5. Malatesta, P., Hack, M.A., **Hartfuss, E.**, Kettenmann, H., Klinkert, W., Kirchhoff, F. and Götz, M. (2003). Neuronal or glial progeny: regional differences in radial glia fate. *Neuron* **37**, 751-764.
6. **Hartfuss, E.**, Förster, E., Bock, H.H., Hack, M.A., Leprince, P., Luque, J.M., Herz, J., Frotscher, M. and Götz, M. (2003). Reelin signalling directly affects radial glia morphology and biochemical maturation. *Development* **130**, 4597-4609.